Title
Control of Excitatory Synaptic Strength by Auxiliary Subunits of AMPA Receptors

Author
Milstein, Aaron David

Publication Date
2009

Peer reviewed|Thesis/dissertation

Control of Excitatory Synaptic Strength by Auxiliary Subunits of AMPA Receptors

by

Aaron D. Milstein

DISSERTATION

Submitted in partial satisfaction of the requirements for the degree of

DOCTOR OF PHILOSOPHY

in

Neuroscience

in the

GRADUATE DIVISION

of the

UNIVERSITY OF CALIFORNIA, SAN FRANCISCO

[redacted]

ACKNOWLEDGEMENTS

I thank Jessica O'Brien and Kirsten Bjorgan for excellent technical assistance, Anastassios Tzingounis and Craig Jahr for helpful discussion regarding kinetic modeling, Susan Voglmaier for providing plasmids, Zhanyan Fu and Doris Fortin for help with cerebellar granule cell culture, and Kaiwen Kam for help with developing custom analysis software. I am also grateful to Alexander Jackson, Geoffrey Kerchner, Anastassios Tzingounis, Avi Priel and all members of the Nicoll Lab for critical support and discussions. This work was made possible by the generous financial support of a Graduate Research Fellowship from the National Science Foundation as well as grants from the National Institutes of Health.

Some of the data presented in this thesis were collected by my two talented collaborators, postdoctoral fellows Dr. Yun Shi (Figures 19 – 23) and Dr. Wei Zhou (Figure 25). I played a critical role in the design and interpretation of these experiments, as well as in the preparation of the manuscripts in which the data is reported (Shi et al., 2009; Milstein et al., 2007). I also constructed mathematical models based on the data that Drs. Shi and Zhou collected as part of my thesis work, yielding important insight into the questions I sought to answer, and so the data is presented here for the sake of completeness.

I would also like to express profound appreciation for all the teachers and mentors who helped shape me into who I am and who inspired me to pursue a lifelong career in uncovering the secrets of how the world works and spreading the word to others who share my passion for learning. Thank you to Sandra Boyer, Charles O'Connor, Pamela Natale, Julia Launer, Nick Evento, Divakar Mithal, Mriganka Sur, Elly Nedivi, Casper Hoogenraad, Morgan Sheng, and Roger Nicoll.

Finally, I express my deepest love and affection for my friends and family who continually and unconditionally support me throughout my every advance and blunder. My mother, Ceseli, teaches me that it is nurture as much as nature. My father, Peter, reminds me that even a bad day skiing is better than a good day in the lab. My sister, Malia, has a work ethic and an independence that I can only hope to one day achieve. My love, Cindy, is my biggest supporter and my harshest critic. Throughout my time in graduate school, she has broadened and enriched my life in more ways than I can describe, and inspires me to be a better person.

ABSTRACT OF THE DISSERTATION

Control of Excitatory Synaptic Strength by

Auxiliary Subunits of AMPA Receptors

by Aaron D. Milstein

Doctor of Philosophy in Neuroscience

University of California, San Francisco, 2009

The majority of excitatory synaptic transmission in the mammalian brain is mediated by the activation of AMPA-type glutamate receptors (AMPARs) by the neurotransmitter glutamate. The number of AMPARs clustered at synapses as well as their functional properties dictates the strength and timing of synaptic transmission. Therefore, determining the factors that control the trafficking and gating of AMPARs is critical to understanding how neurons process and encode information. While it was recently discovered that AMPARs interact with a family of auxiliary subunits called transmembrane AMPAR regulatory proteins (TARPs) that control the trafficking and gating of AMPARs, functional diversity among TARP family members has not been explored. In this thesis, I establish cultured cerebellar granule neurons from *stargazer* mutant mice as a model system to separately determine the effects of each TARP subtype on synaptic AMPAR function. I demonstrate that transfection of any of the TARP subtypes γ-2, γ-3, γ-4, or γ-8 into *stargazer* granule cells "rescues" the synaptic expression of native AMPARs, allowing an assessment of the

roles of each TARP subtype in controlling synaptic AMPAR trafficking and gating (Chapters 1 and 2). I also employ TARP domain truncation and transplantation to determine which domains within TARP proteins mediate their subtype-specific effects on AMPAR trafficking and gating (Chapters 1 and 2). Finally, I exploit changes in the pharmacology of AMPARs induced by TARP binding to determine the stoichiometry of the association between TARPs and AMPARs (Chapter 3) and to infer structural information about which specific conformations of AMPARs are selectively stabilized by TARPs during gating (Chapters 4 and 5).

TABLE OF CONTENTS

LIST OF FIGURES

INTRODUCTION

The encoding and processing of information in the brain depends on the strength and timing of synaptic signaling. The predominant mechanism for fast excitatory synaptic transmission in the mammalian central nervous system is the depolarization of the postsynaptic membrane by the AMPA receptor (AMPAR) family of glutamate-gated ion channels. The size of AMPAR-mediated synaptic currents is primarily determined by the peak concentration of glutamate in the synaptic cleft, the number of postsynaptic AMPARs and their inherent affinity for glutamate (Bredt and Nicoll, 2003; Clements, 1996; Kullmann et al., 1999). In contrast, the shape of synaptic currents is governed by diverse processes, including the rate of glutamate clearance (Barbour and Hausser, 1997; Diamond, 2001; Overstreet et al., 1999; Sargent et al., 2005), the ultrastructure of the surrounding neuropil (Cathala et al., 2005; Xu-Friedman and Regehr, 2003) and the gating kinetics of AMPARs. The biophysical properties of synaptic AMPAR complexes depend on their molecular identity, with contributions from subunit composition, splice variation, RNA editing and posttranslational modification (Jonas, 2000; Koike et al., 2000; Mosbacher et al., 1994; Swanson et al., 1997). The mechanisms that govern the trafficking and gating of synaptic AMPARs are of particular interest given accumulating evidence that activity-dependent regulation of these processes provides a molecular basis for learning and memory (Bredt and Nicoll, 2003; Malinow and Malenka, 2002; Sheng and Kim, 2002)

AMPARs are composed of heterotetrameric combinations of the subunits GluA1-4. In addition to these pore-forming subunits, neuronal AMPAR complexes also contain auxiliary subunits that regulate receptor trafficking and gating (Nicoll et al., 2006; Osten and Stern-Bach, 2006; Ziff, 2007). This family of transmembrane AMPAR regulatory proteins (TARPs) consists of its prototypical member, stargazin (γ-2), and the homologous γ-3, γ-4 and γ-8. Loss of γ-2 in the mutant mouse *stargazer* causes profound deficits in surface and synaptic AMPAR expression in cerebellar granule neurons (Hashimoto et al., 1999) and loss of γ-8 in a gene-targeted knockout mouse impairs AMPAR expression in hippocampal pyramidal neurons (Fukaya et al., 2006; Rouach et al., 2005). It has been hypothesized, but not rigorously tested, that overlapping expression of other TARP subtypes in most neurons functionally compensate for one another (Fukaya et al., 2005; Tomita et al., 2003). TARPs were originally identified and discriminated from the homologous proteins γ-1 and γ-5 based on their ability to rescue the surface expression of native AMPARs in cultured cerebellar granule neurons from *stargazer* mutant mice (Tomita et al., 2003). However, it remains untested whether other TARP subtypes share the roles of γ-2 in targeting AMPARs to synapses and modulating their channel properties (Chen et al., 2000; Tomita et al., 2005).

Until recently, it was thought that the trafficking of AMPARs to the plasma membrane and their localization at synapses could be accounted for entirely by AMPAR subunit-specific interactions between the carboxy terminal domains (C-tails) of AMPARs and various cytoplasmic proteins like PICK1, GRIP1, NSF,

and SAP97 (Bredt and Nicoll, 2003; Malinow and Malenka, 2002; Ziff, 2007). However, it is a family of synaptic scaffolding molecules that does not interact directly with AMPARs at all – membrane-associated guanylate kinase proteins (MAGUKs) like PSD-95 – that has been shown to have the strongest control over the number of AMPARs at synapses (Ehrlich and Malinow, 2004; Elias and Nicoll, 2007; Stein et al., 2003). This discrepancy was resolved with the discovery that AMPARs interact with TARPs, which in turn bind MAGUKs through a C-terminal PDZ-binding domain to control the synaptic targeting of AMPARs (Chen et al., 2000; Nicoll et al., 2006). Accordingly, genetic deletion or acute knockdown of MAGUKs strongly reduces AMPAR-mediated synaptic transmission (Elias et al., 2006), as does expression of a dominant-negative TARP γ-2 lacking a PDZ-binding motif (Bats et al., 2007; Schnell et al., 2002). However, it is not known how this TARP- and MAGUK-dependent mechanism for AMPAR trafficking relates to the previously proposed AMPAR subunit-specific model (see Ziff, 2007), or whether structural differences between TARP subtypes correspond to functional differences in synaptic AMPAR targeting.

Here I establish cultured cerebellar granule neurons from *stargazer* mutant mice as a model system to separately determine the effects of each TARP subtype on synaptic AMPAR function. This model system has two essential features: 1) *stargazer* cerebellar granule neurons lack functional TARPs but contain an intracellular pool of native AMPARs retained in the endoplasmic reticulum that can be recruited to the cell surface by ectopic TARP expression (Chen et al., 2000; Tomita et al., 2003; Vandenberghe et al., 2005); and 2) the

small cell body and electrotonically compact dendritic arbors of cerebellar granule neurons allow for accurate somatic measurement of the time course of synaptic currents (Cathala et al., 2005; Silver et al., 1996). This “clean” background contrasts with hippocampal pyramidal neurons, which contain expansive dendrites that extensively filter synaptic conductances (Magee and Cook, 2000), and which express multiple TARP isoforms (Tomita et al., 2003). Miniature excitatory post-synaptic currents (mEPSCs) are generated by the spontaneous, asynchronous release of single vesicles of glutamate from individual pre-synaptic terminals, causing the activation of AMPARs clustered at individual post-synaptic densities. The amplitude of these currents scales with the number of AMPARs contained at each synapse, and the time course of their decay reflects how quickly AMPARs transition through a range of receptor conformations as their channels close and they unbind glutamate. In this thesis I analyze these properties of mEPSCs to establish that each member of the TARP family of AMPAR auxiliary subunits differentially controls synaptic AMPAR trafficking and gating.

CHAPTER 1

TARP Subtypes Differentially Control Synaptic AMPA Receptor Trafficking

Here I discover heterogeneity in the ability of TARP subtypes to traffic AMPARs to synapses and determine the structural elements that mediate this functional diversity using TARP domain transplantation and truncation. I identify a component of synaptic AMPAR trafficking that is independent of the TARP C-terminal PDZ-binding motif, and establish novel roles for the TARP intracellular N-terminus, loop, and C-terminus in controlling synaptic AMPAR trafficking.

In *stargazer* granule neurons, local perfusion of agonist fails to evoke a significant AMPAR response (Chen et al., 2000; Tomita et al., 2003) (Figure 1). However, neurons transiently transfected with TARPs exhibit robust whole-cell responses to glutamate comparable in amplitude to those in wild-type neurons (Chen et al., 2000; Tomita et al., 2003) (Figure 1). This strongly suggests that TARPs are expressed at saturating levels and that all available AMPARs are being delivered to the surface. In the presence of TTX, brief local applications of hypertonic sucrose solution evoke asynchronous release of single vesicles of glutamate from the presynaptic terminals of nearby granule neurons. Resulting AMPAR miniature excitatory postsynaptic currents (mEPSCs) are readily detected in neurons expressing each of the TARPs γ-2, γ-3, γ-4, and γ-8, but not in untransfected neurons (Figure 2A). This demonstrates that TARP association

Figure 1. TARPs Rescue Surface AMPAR Expression in *Stargazer* Cerebellar Granule Neurons

(A) Representative whole-cell responses to the local application of 500 μM glutamate + 500 μM trichloromethiazide (TCM), which inhibits AMPAR desensitization, demonstrate that ectopic TARP expression rescues surface AMPAR responses in *stg*/*stg* granule neurons.

(B) Whole-cell responses are quantified. All TARP subtypes rescued surface AMPAR responses in *stg*/*stg* granule neurons to wild-type levels ($p<0.0001$, n=15-29). Responses were reduced in +/*stg* neurons compared to +/+ ($p<0.0001$).

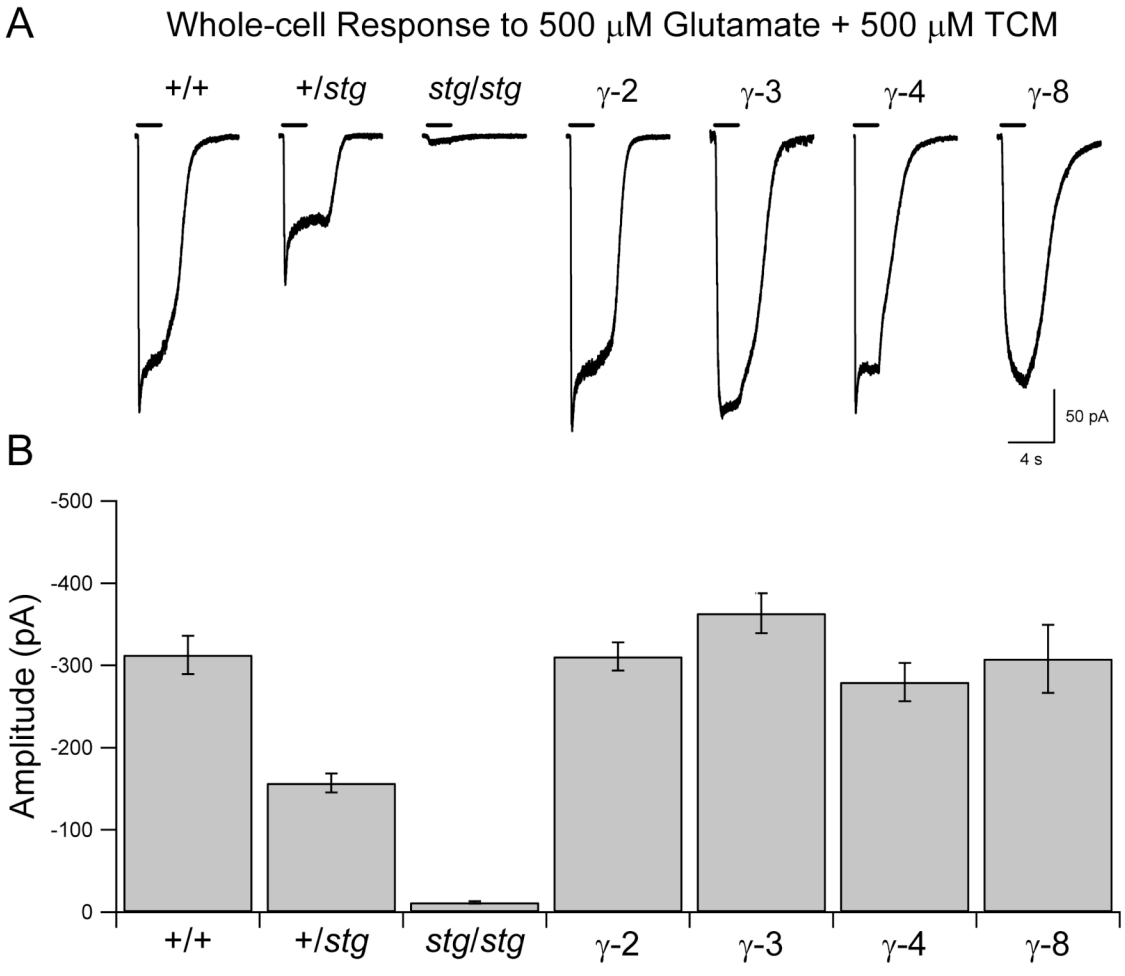
A
Whole-cell Response to 500 μM Glutamate + 500 μM TCM
+/+
+/stg
stg/stg
γ-2
γ-3
γ-4
γ-8
50 pA
4 s
B
Amplitude (pA)
-500
-400
-300
-200
-100
0
+/+
+/stg
stg/stg
γ-2
γ-3
γ-4
γ-8

Figure 2. TARPs Rescue Synaptic AMPAR Targeting in *Stargazer* Cerebellar Granule Neurons

(A) Sample records demonstrate that each TARP subtype is sufficient to restore the synaptic localization of native AMPARs in *stg*/*stg* granule neurons.

(B) mEPSC amplitude depends on TARP subtype. Average mEPSCs are aligned to the peak and superimposed.

(C) mEPSC amplitudes are quantified as cumulative probability distributions, displayed as mean ± SEM (Kolmogorov-Smirnov comparisons to γ-2: n=40; γ-3: n=25, $p<0.007$; γ-4: n=18, n.s.; γ-8: n=14, $p<0.001$).

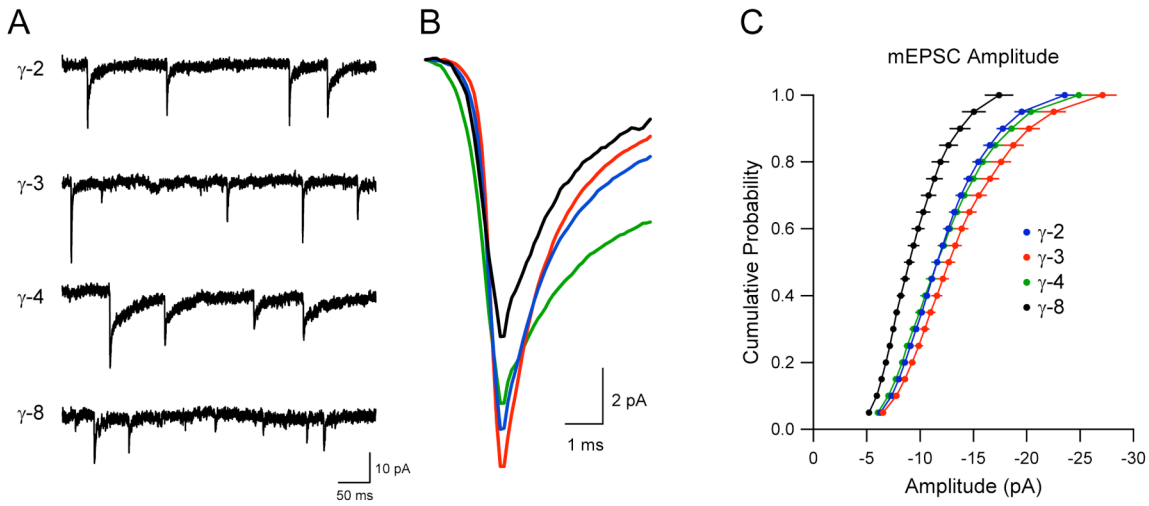
A
γ-2
γ-3
γ-4
γ-8
10 pA
50 ms
B
2 pA
1 ms
C
mEPSC Amplitude
Cumulative Probability
1.0
0.8
0.6
0.4
0.2
0.0
0
-5
-10
-15
-20
-25
-30
Amplitude (pA)
γ-2
γ-3
γ-4
γ-8

is sufficient to localize AMPARs at synapses. Notably, the average peak amplitude of the "rescued" mEPSCs varies among TARP subtypes (γ-3: ~10% increase relative to γ-2; γ-8: ~25% decrease relative to γ-2; see Figures 2B and 2C). Since each TARP rescues surface AMPAR responses to the same extent (Figure 1), these differences in the size of mEPSCs must either reflect differences in gating, or in the ability of different TARPs to target AMPARs to synapses.

Supporting the latter possibility that the reduced mEPSC amplitudes observed with TARP γ-8 reflects less efficient synaptic targeting of AMPARs, the frequency of AMPAR mEPSCs rescued by γ-8 is also strongly reduced relative to γ-2 (Figure 4D). Previous work has established that TARPs target AMPARs to synapses through an intracellular PDZ-binding motif. While the TARP subtypes γ-2, γ-3, γ-4, and γ-8 all contain identical PDZ-binding motifs, and the rest of their intracellular C-termini are largely homologous, the C-terminus of γ-8 contains three unique stretches of amino acids not found in any of the other TARPs (Figure 3), which could underlie the observed difference in mEPSC amplitudes between γ-8 and the other TARPs. Given that γ-8 is the TARP subtype predominantly expressed in the hippocampus (Rouach et al., 2005; Tomita et al., 2003), a model system for studying synaptic AMPAR trafficking and plasticity, differences in function between γ-8 and other TARPs are of particular interest.

In order to determine to what extent TARPs γ-2 and γ-8 rely on their PDZ-binding motif to localize AMPARs at synapses, I transfected *stargazer* granule neurons with mutant TARP constructs in which C-terminal residues are truncated

(Figure 4A). Surprisingly, and contrary to previous work (Chen et al., 2000), AMPAR-mediated miniature excitatory post-synaptic currents (mEPSCs) are still detected, albeit with a strongly reduced frequency, for all truncation mutants expressed (Figures 4B and 4D). The construct γ-2ΔPDZ, lacking only the last four amino acids of the γ-2 C-terminus, delivers AMPARs to the cell surface as effectively as full-length γ-2 (Figure 4C), as reported previously (Chen et al., 2000). The synaptic expression of AMPARs, however, is reduced both in amplitude and in frequency relative to full-length γ-2, but not abolished (Figures 4B, 4D and 4E). While the previous study analyzed spontaneously occurring, action-potential generated EPSCs, and may have failed to detect synaptic events that occur with such low frequency, here I use locally applied sucrose to force asynchronous release of synaptic vesicles in order to increase the number of mEPSCs sampled during the recording period (see Methods).

It is striking that while truncation of the PDZ-binding domain of γ-2 decreases both the amplitude and frequency of mEPSCs relative to full-length γ-2, the corresponding truncation mutant γ-8ΔPDZ results in synaptic events that are reduced only in frequency, but not in amplitude relative to full-length γ-8 (Figures 4B, 4D and 4E). These data indicate that TARPs γ-2 and γ-8 differ in their dependence on PDZ binding to localize AMPARs at synapses, and reveal that a component of synaptic AMPAR trafficking is mediated by a mechanism independent of the direct interaction between TARPs and MAGUKs. This possibility was also hinted at in a recent study in which deletion of MAGUK proteins resulted in a strong reduction in mEPSC frequency, but little reduction in

Figure 3. Sequence Alignment of TARP C-terminal Domains

The C-terminal domain of TARP γ-8 contains three unique stretches of amino acids not found in any of the other TARP subtypes.

```
gamma-2         SANAGDPS--KSDSKKNSYSYGWSFYFGALSFIIAEMVGVLAVHMFIDRHKQLRATARAT
gamma-3         SANAGDPG--QRDSKK-SYSYGWSFYFGAFSFIIAEIVGVVAVHIYIEKHQQLRARSH-S
gamma-4         SSNTGDPSDKRDEDKKNHYNYGWSFYFGALSFIVAETVGVLAVNIYIEKNKELRFKTK-R
gamma-8         SANAGEPGPKRDEEKKNHYSYGWSFYFGGLSFILAEVIGVLAVNIYIERSREAHCQSR-S

gamma-2         DYLQA------------SAITRIPSYRYRYQRRSRSSSR-STEPSHSRDASPVGVKGFNT
gamma-3         ELLKK------------STFARLPPYRYRFRR--RSSSR-STEP-RSRDLSPIS-KGFHT
gamma-4         EFLKA---------SSSSPYSRMPSYRYR-RRRSRSSSR-STEASPSRDASPVGLKITGA
gamma-8         DLLKAGGGAGGSGGSGPSAILRLPSYRFRYRRRSRSSSRGSSEASPSRDASPGGPGG-PG

gamma-2         LPSTEISMYTLSRDPLKAATTPTATY---------------------------NSDRD--
gamma-3         IPSTDISMFTLSRDPSK--LTMGTLL---------------------------NSDRD--
gamma-4         IPMGELSMYTLSREPLK--VTTAASY---------------------------SPDQD--
gamma-8         FASTDISMYTLSRDPSK--GSVAAGLASAGGGGGGAGVGAYGGAAGAAGGGGTGSERDRG

gamma-2         --NSFLQVHNCIQKDSKDSL--------------------------------HANTANR
gamma-3         --HAFLQFHNSTPKEFKESL--------------------------------HNNPANR
gamma-4         --AGFLQMHDFFQQDLKEGF--------------------------------HVSMLNR
gamma-8         SSAGFLTLHNAFPKEAASGVTVTVTGPPAAPAPAPPAPAAPAPGTLSKEAAASNTNTLNR

gamma-2         RTTPV
gamma-3         RTTPV
gamma-4         RTTPV
gamma-8         KTTPV
```

Figure 4. A Component of Synaptic AMPAR Trafficking is Independent of the TARP C-terminus

(A) Intracellular C-terminal domains of TARPs γ-2 and γ-8, with striped regions indicating unique residues in γ-8, and truncation mutants labeled.

(B) Sample records of "rescued" AMPAR mEPSCs in *stg*/*stg* cerebellar granule neurons.

(C) C-terminal truncation of TARPs reduces surface AMPAR expression. Whole-cell responses to 500 μM glutamate + 500 μM TCM are quantified (* $p<0.0001$ relative to γ-2; # $p<0.0001$ relative to γ-8; n=11-39).

(D) C-terminal truncation of TARPs strongly reduces mEPSC frequency, but does not abolish AMPAR mEPSCs (* $p<0.0001$ relative to γ-2; # $p<0.0001$-0.0007 relative to γ-8; n=16-51).

(E) C-terminal truncation of γ-2, but not γ-8, reduces mEPSC amplitude

(* $p<0.0001$ relative to γ-2; n=5-44). 4 pA detection threshold indicated with dashed line. For the conditions γ-2ΔC and γ-8ΔC, each cell contributed too few events to perform meaningful statistical comparisons (see Materials and Methods).

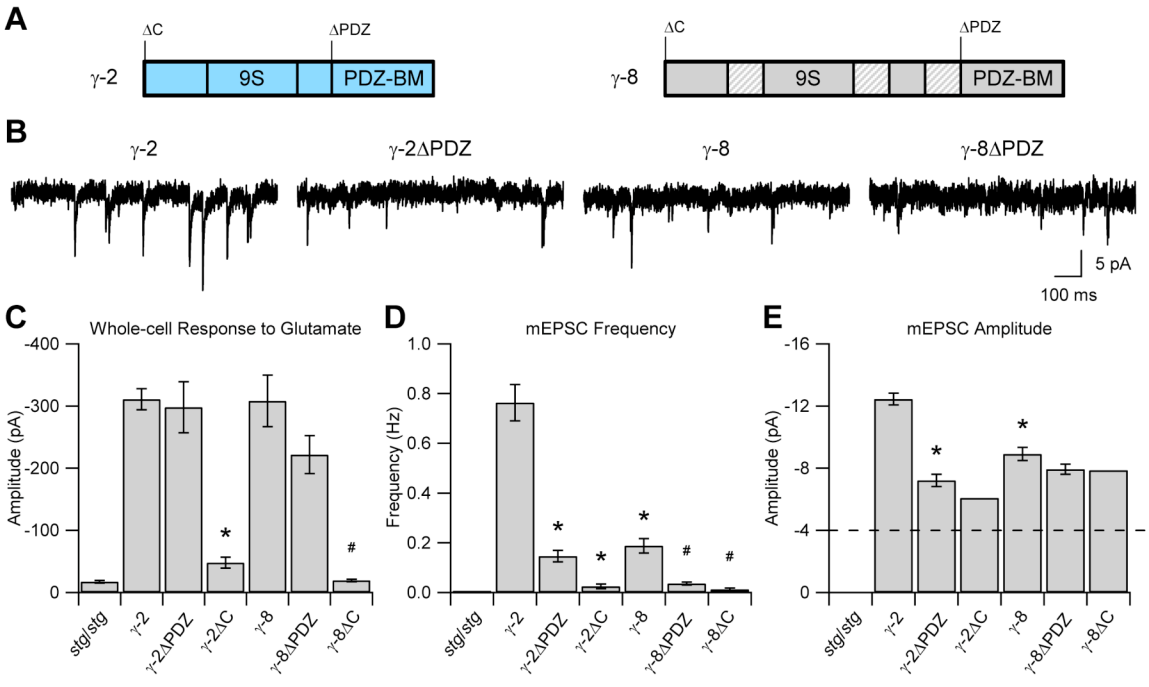
A
ΔC
ΔPDZ
γ-2
9S
PDZ-BM
γ-8
B
γ-2
γ-2ΔPDZ
γ-8
γ-8ΔPDZ
5 pA
100 ms
C
Whole-cell Response to Glutamate
Amplitude (pA)
D
mEPSC Frequency
Frequency (Hz)
E
mEPSC Amplitude
Amplitude (pA)
stg/stg
γ-2
γ-2ΔPDZ
γ-2ΔC
γ-8
γ-8ΔPDZ
γ-8ΔC

mEPSC amplitude (Elias et al., 2006). This PDZ-independent synaptic AMPAR targeting does not appear to require other elements in the TARP C-terminus, as mEPSCs of similar amplitude to γ-2ΔPDZ and γ-8ΔPDZ can be detected even when complete C-terminal truncation severely reduces the surface delivery of AMPARs (γ-2ΔC and γ-8ΔC) (Figures 4C and 4E). It is likely that previously characterized cytoplasmic proteins that interact directly with specific AMPAR subunits mediate this TARP- and MAGUK-independent component of synaptic AMPAR trafficking (Bredt and Nicoll, 2003; Ziff, 2007).

I further investigated the structural basis for the difference in mEPSC amplitudes between TARPs γ-2 and γ-8 by expressing chimeric TARP constructs in which the intracellular domains of the two TARPs were exchanged. In addition to their divergent C-termini, γ-2 and γ-8 also differ in their two other intracellular domains, the N-terminus, and the intracellular loop (see transmembrane structure diagrams in Figure 5A). Each of these chimeric TARP constructs fully rescues whole-cell glutamate responses in *stargazer* granule cells (Figures 5B and 6), indicating that domain transplantation does not impair the expression level of chimeric TARPs, their interaction with AMPARs, their ability to delivery AMPARs to the plasma membrane, or the ability of AMPARs to respond to glutamate. Therefore, I interpret differences in the amplitudes of mEPSCs rescued by these chimeric TARPs to reflect specific differences in their ability to traffic AMPARs to synapses.

I first analyzed mEPSCs rescued by the C-tail swap chimeras γ-2-C-8 and γ-8-C-2. While the chimera γ-8-C-2, containing the backbone of γ-8 and the C-tail

of γ-2, produces AMPAR mEPSCs larger in amplitude than γ-8, the converse is not true – γ-2-C-8 produces mEPSCs that are similar in amplitude to the host γ-2 rather than the donor γ-8 (Figure 7). This demonstrates that while unique residues in the γ-8 C-terminus contribute to the synaptic targeting phenotype of γ-8, they are not sufficient to confer that phenotype to γ-2. Similar results were obtained with the other single domain-swap chimeras (Figure 7), indicating that no individual intracellular domain is sufficient to account for TARP subtype-specific trafficking of AMPARs to synapses. However, all TARP chimeras that have both their N- and C-terminus in common produce mEPSCs with the same amplitude (for example, both γ-2-C-8 and γ-8-N-2 share the N-terminus of γ-2 and the C-terminus of γ-8 and produce mEPSCs similar in amplitude to γ-2, as shown in the chart in Figure 7B). To test the possibility that multiple TARP intracellular domains functionally interact to account for the observed differences in mEPSC amplitude, I constructed chimeras in which all three intracellular domains (N, L, and C) were exchanged. Remarkably, complete intracellular domain transplantation (γ-2-NLC-8 and γ-8-NLC-2) succeeds in fully exchanging the mEPSC amplitude phenotypes of γ-2 and γ-8 (Figures 5A and 5D). These data are the first to assign a function to TARP intracellular domains other than the C-terminus, and uncover an intriguing cooperative interaction among multiple TARP intracellular domains that differs between TARP subtypes and differentially influences synaptic AMPAR targeting.

Figure 5. Multiple TARP Intracellular Domains Contribute to TARP Subtype-Specific Trafficking of AMPARs

(A) Representative average mEPSCs demonstrate that complete TARP intracellular domain transplantation is required to fully exchange the mEPSC amplitude phenotypes of TARPs γ-2 and γ-8. Diagrams depict transmembrane structure of TARPs γ-2, γ-8, and intracellular domain chimeras γ-2-NLC-8 and γ-8-NLC-2. Transmembrane domains are shaded.

(B) TARP intracellular domain transplantation does not impair surface AMPAR expression. Whole-cell responses to 500 μM glutamate + 500 μM TCM are quantified (no significant differences; n=14-29).

(C) mEPSC frequency for all TARP chimeras is quantified (* $p<0.0001$ relative to γ-2; # $p<0.0001$ relative to γ-8; n=20-51).

(D) mEPSC amplitudes for all TARP chimeras are quantified (* $p<0.0005$-0.002 relative to γ-2; # $p<0.0004$ relative to γ-8; n=20-44).

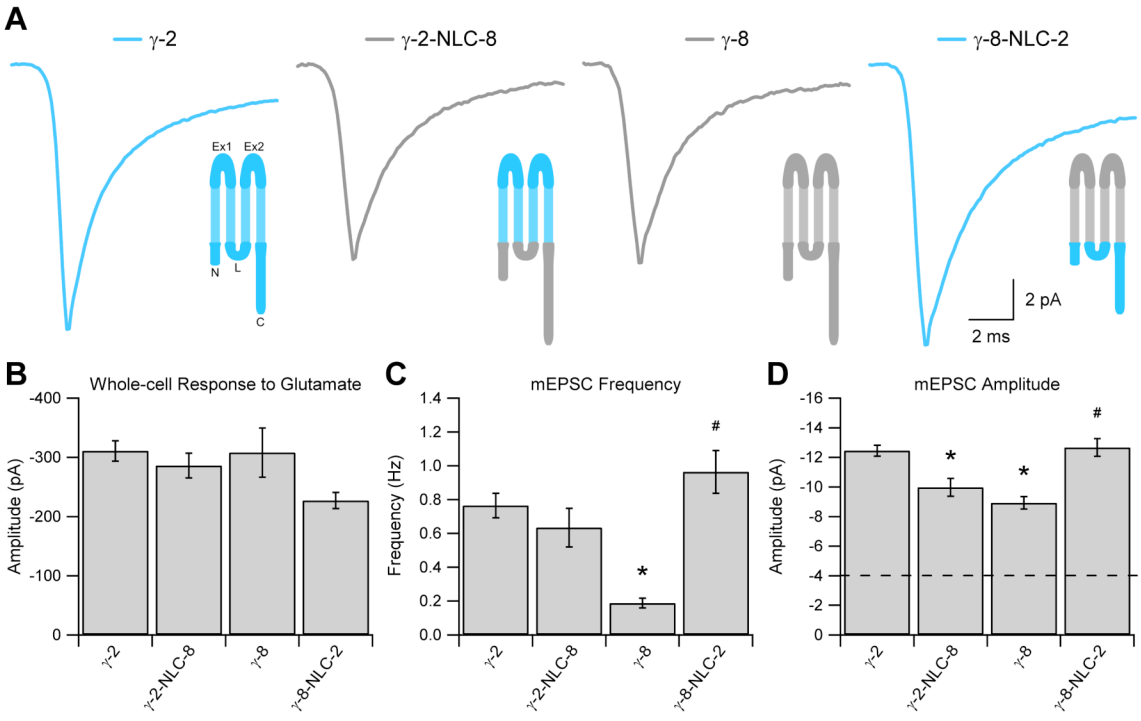
A
γ-2
γ-2-NLC-8
γ-8
γ-8-NLC-2
Ex1
Ex2
N
L
C
2 pA
2 ms
B
Whole-cell Response to Glutamate
Amplitude (pA)
-400
-300
-200
-100
0
γ-2
γ-2-NLC-8
γ-8
γ-8-NLC-2
C
mEPSC Frequency
Frequency (Hz)
1.4
1.2
1.0
0.8
0.6
0.4
0.2
0.0
*
#
D
mEPSC Amplitude
Amplitude (pA)
-16
-14
-12
-10
-8
-6
-4
-2
0
*
*
#

Figure 6. TARP Intracellular Domain Chimeras Rescue Surface AMPAR Expression in *Stargazer* Cerebellar Granule Neurons

Whole-cell responses to 500 μM glutamate + 500 μM TCM are quantified (all conditions differ significantly from *stg*/*stg*; $p<0.0001$; n=14-39).

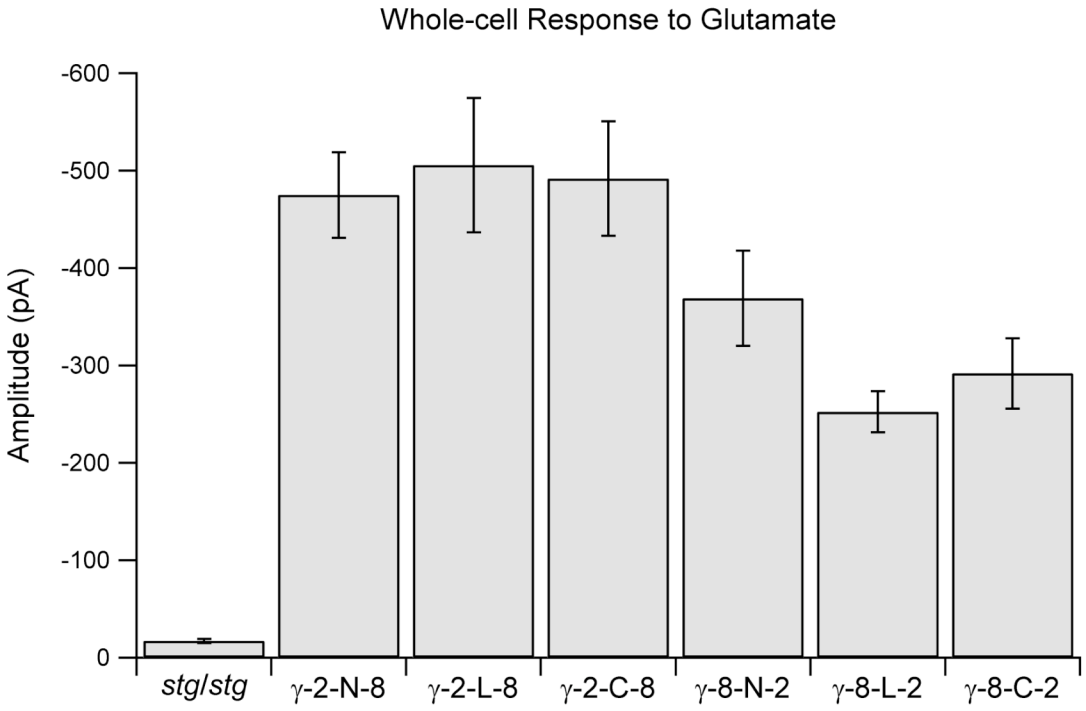
Whole-cell Response to Glutamate
Amplitude (pA)
-600
-500
-400
-300
-200
-100
0
stg/stg
γ-2-N-8
γ-2-L-8
γ-2-C-8
γ-8-N-2
γ-8-L-2
γ-8-C-2

Figure 7. TARP Intracellular Domain Transplantation Influences Synaptic AMPAR Targeting

(A) mEPSC amplitudes for all TARP chimeras are quantified (* $p<0.005$ relative to γ-2; # $p<0.0001$-0.002 relative to γ-8; n=15-45). Dashed lines correspond to mean ± SEM for wild-type γ-2 (blue) and wild-type γ-8 (grey). Bars are shaded with colors that correspond to the chart in (B), demonstrating that groups of TARP chimeras that have both their N- and C-termini in common produce mEPSCs with similar amplitudes.

(B) Chart demonstrates that the specific combination of N- and C-terminal domains contained within a given TARP chimera predicts its AMPAR mEPSC amplitude phenotype, indicating a functional interaction between multiple TARP intracellular domains.

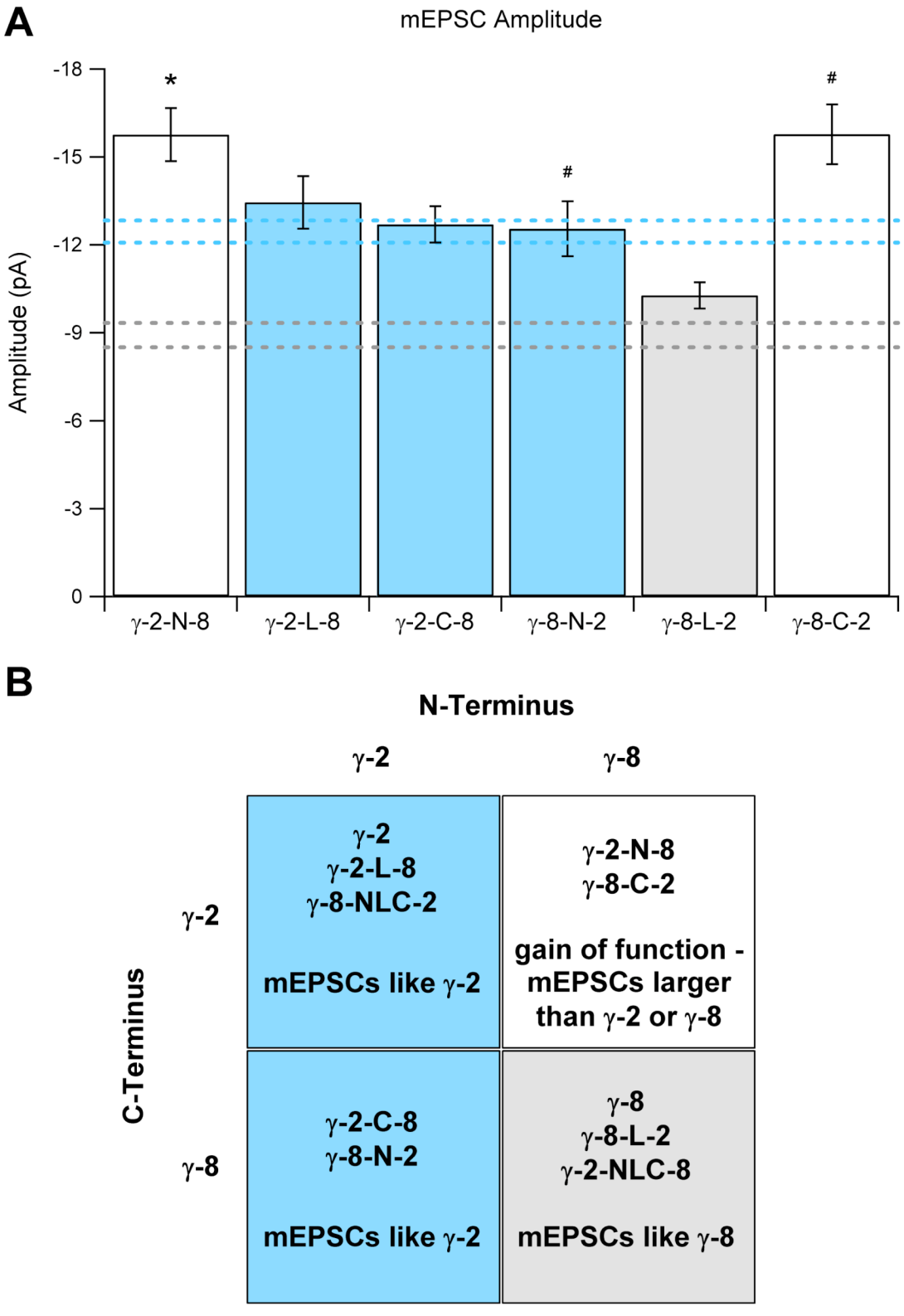
A
mEPSC Amplitude
Amplitude (pA)
-18
-15
-12
-9
-6
-3
0
*
#
#
γ-2-N-8
γ-2-L-8
γ-2-C-8
γ-8-N-2
γ-8-L-2
γ-8-C-2
B
N-Terminus
γ-2
γ-8
C-Terminus
γ-2
γ-8
γ-2
γ-2-L-8
γ-8-NLC-2
mEPSCs like γ-2
γ-2-N-8
γ-8-C-2
gain of function - mEPSCs larger than γ-2 or γ-8
γ-2-C-8
γ-8-N-2
mEPSCs like γ-2
γ-8
γ-8-L-2
γ-2-NLC-8
mEPSCs like γ-8

CHAPTER 2

TARP Subtypes Differentially Control Synaptic AMPA Receptor Gating

Here I examine the effects of each TARP subtype on synaptic AMPAR gating by measuring the kinetics of AMPAR mEPSCs in *stargazer* cerebellar granule neurons. I report a striking heterogeneity in the effects of TARP subtypes on the time course of synaptic transmission. In addition to the slowing of AMPAR current decay previously demonstrated for γ-2, I find that some TARP subtypes dramatically slow AMPAR activation kinetics, which manifests as a prolongation of mEPSC rise times. By using TARP domain transplantation, I determine that, in addition to a previously characterized TARP extracellular domain, multiple TARP intracellular domains contribute to synaptic AMPAR gating. Analysis of quantal synaptic transmission in a TARP γ-4 knockout (KO) mouse corroborates these findings and demonstrates that TARP subtype-specific gating of AMPARs contributes to the kinetics of native AMPARs in the brain.

TARP Subtypes Differentially Control the Shape of Synaptic AMPAR Currents

To determine the effects of each TARP subtype on synaptic AMPAR gating, I measured the rise and decay kinetics of the mEPSCs recorded during the experiments described in Chapter 1. Examination of the sample records (Figures 2A and 2B) clearly shows that the duration of mEPSCs in *stargazer* granule cells varies dramatically depending on the subtype of TARP expressed. This

difference is shown more clearly in the expanded records in Figures 8A and 8B, in which average mEPSCs from individual cells are displayed in grey and the averages of all experiments for each condition are displayed in color. The decay of mEPSCs rescued with γ-3 is slightly, but significantly, faster than γ-2, whereas mEPSCs mediated by γ-8 decay similarly to γ-2. In striking contrast, the mEPSCs rescued with γ-4 are dramatically slower than γ-2 (Figures 8A and 8B). For simplicity, the decay times presented here reflect weighted time constants calculated from the area under the peak-normalized response (Cathala et al., 2005) (see Methods). However, mEPSC decay times were best fit by a sum of two exponential components, and closer analysis reveals that the effect of TARPs on AMPAR channel kinetics is primarily to promote the time course and relative contribution of a slow component of gating (Table 1). In conducting these experiments, I also observed an unexpected effect of some TARP subtypes on AMPAR activation kinetics, which had not been reported for γ-2. TARPs γ-4 and γ-8 considerably prolong the time-to-peak of AMPAR mEPSCs (Figure 8C). These results demonstrate that the kinetic regulation of AMPARs by TARPs depends on TARP subtype.

TARP Subtypes Differentially Control AMPAR Agonist Affinity

To determine the mechanisms by which TARPs differentially modulate AMPAR channel kinetics, I examined the effect of TARP subtype on the apparent affinity for agonist in granule cells. I recorded whole-cell responses to the local application of various concentrations of the nondesensitizing agonist kainate. A

typical experiment is shown in Figure 9A, and the resulting dose-response relationships are shown in Figure 9B. The kainate EC_{50} values for surface AMPARs depends on the subtype of associated TARP (Figure 9B and Table 2). These values correlate closely with the effects of each TARP on mEPSC decay – the faster decay of AMPARs associated with γ-3 is coupled with a higher kainate EC_{50}, while the slower decay mediated by γ-4 is coupled with a lower EC_{50}. Furthermore, TARP γ-4 significantly reduced the Hill coefficient calculated from the shape of the kainate dose-response relationship (Table 2). This effect of TARPs has also been reported in heterologous systems (Priel et al., 2005; Tomita et al., 2005) and may indicate that TARPs reduce the number of agonist molecules that must be bound to effectively open the AMPAR channel.

TARP Subtype-Specific Gating of AMPARs Depends on a TARP Extracellular Domain

Given the differences in kinetics observed with mEPSCs rescued by the various TARPs, I sought to determine the molecular mechanism for TARP subtype-specific control of AMPAR gating. A previous study used chimeras between γ-2 and the presumed inactive homologue γ-5 to show that the first extracellular domain (Ex1) of γ-2 is sufficient to account for its effects on AMPAR gating and pharmacology (Tomita et al., 2005). This mechanism is attractive given that the Ex1 domain is well positioned to interact directly with the AMPAR ligand-binding domain, known to be a critical determinant of agonist efficacy and channel kinetics (Robert et al., 2005; Zhang et al., 2008). However, subsequent work has

Figure 8. TARP Subtypes Differentially Control Synaptic AMPA Receptor Gating

(A) mEPSC decay depends on TARP subtype. Average mEPSCs are normalized and aligned to the peak. Average mEPSCs from individual neurons are displayed in grey, and averages of all experiments for each condition are shown in color. Weighted time constant values calculated from the area under the peak-normalized current are displayed as mean ± SEM (see Methods).

(B) mEPSC decay times are quantified as cumulative probability distributions, displayed as mean ± SEM (Kolmogorov-Smirnov comparisons to γ-2; γ-3: $p<0.001$; γ-4: $p<0.001$; γ-8: n.s.). Average mEPSCs across conditions from (A) are aligned to the peak and superimposed (inset).

(C) mEPSC rise time depends on TARP subtype. mEPSC rise times are quantified as cumulative probability distributions, displayed as mean ± SEM (Kolmogorov-Smirnov comparisons to γ-2; γ-3: $p<0.001$; γ-4: $p<0.001$; γ-8: $p<0.001$). Average mEPSCs across conditions from (A) are aligned to the 10% rise point and superimposed (inset).

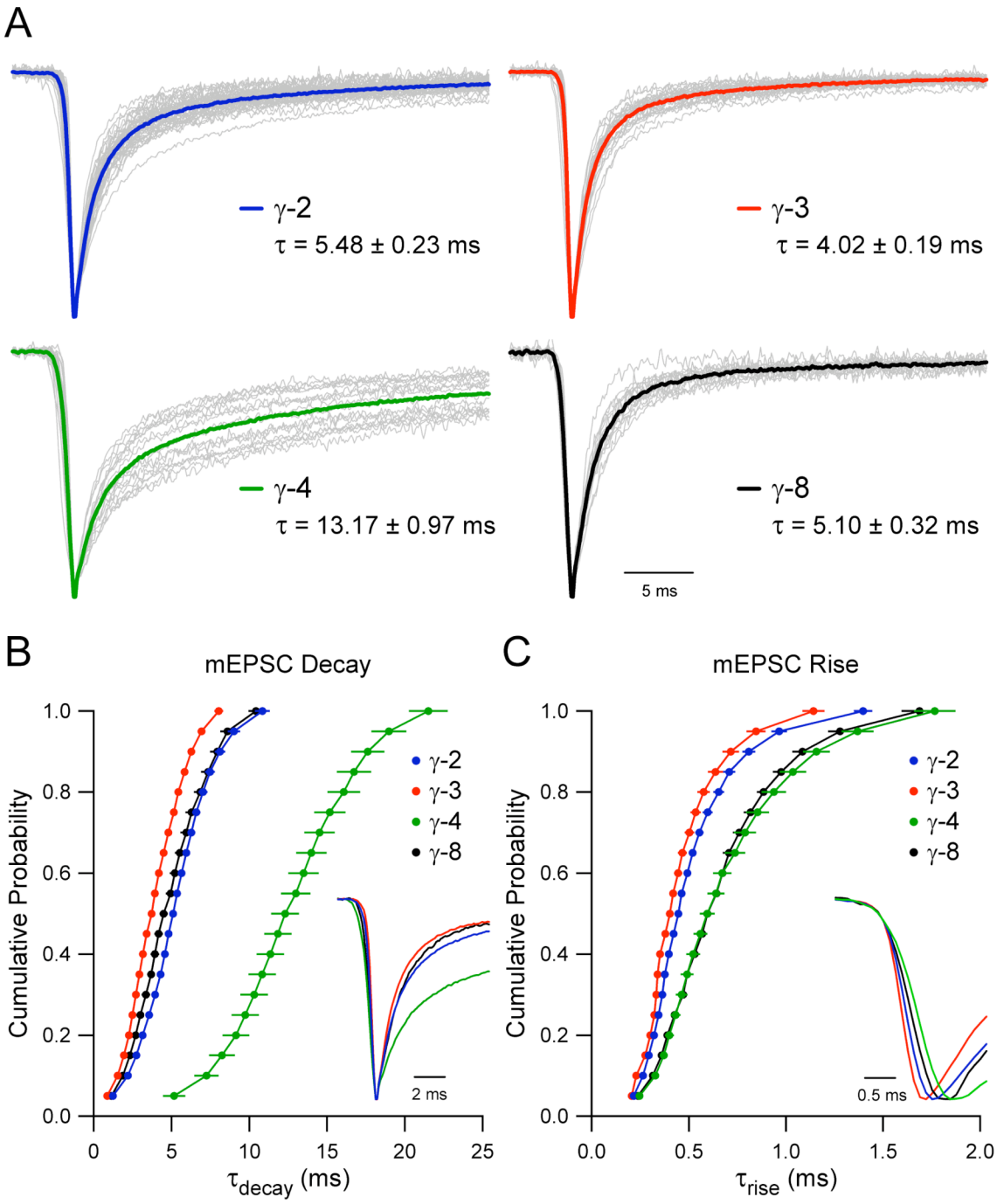
A
γ-2
τ = 5.48 ± 0.23 ms
γ-3
τ = 4.02 ± 0.19 ms
γ-4
τ = 13.17 ± 0.97 ms
γ-8
τ = 5.10 ± 0.32 ms
5 ms
B
mEPSC Decay
Cumulative Probability
τdecay (ms)
2 ms
C
mEPSC Rise
Cumulative Probability
τrise (ms)
0.5 ms

Table 1. Detailed Analysis of mEPSC Decay Kinetics: TARP Subtypes

τ_{fast}, τ_{slow} and A_{slow} are, respectively, the time constants of the fast and slow components of mEPSC decay and the relative amplitude of the slow component of mEPSC decay obtained by fitting the average mEPSC from individual neurons with a double exponential function (see Methods). The measurements are shown as mean ± SEM. Symbols indicate significant difference with respect to TARP γ-2 (* $p<0.001$-0.0001).

Table 1. Detailed Analysis of mEPSC Decay Kinetics: TARP Subtypes

Condition	τ_{fast} (ms)	τ_{slow} (ms)	A_{slow} (%)
γ–2 in *stg*/*stg* (n=40)	1.56 ± 0.05	13.25 ± 0.52	25.76 ± 0.80
γ–3 in *stg*/*stg* (n=25)	1.30 ± 0.05 *	11.41 ± 0.61	20.27 ± 0.74 *
γ–4 in *stg*/*stg* (n=18)	2.87 ± 0.90 *	20.62 ± 1.32 *	43.04 ± 2.23 *
γ–8 in *stg*/*stg* (n=14)	1.69 ± 0.11	17.21 ± 4.88	15.76 ± 1.67 *

Figure 9. AMPAR Agonist Affinity Depends on TARP Subtype

(A) Example of a typical experiment in which varying concentrations of kainate were applied via a local perfusion barrel to an *stg*/*stg* granule neuron expressing γ-2. Saturating concentration (3 mM) was applied at the start and finish of the concentration ladder to exclude the possibility of run-down.

(B) AMPAR affinity for kainate depends on TARP subtype. EC_{50} values are displayed as mean ± SEM for γ-2: n=8; γ-3: n=12; γ-4: n=12; γ-8: n=7. Asterisks indicate statistical significance relative to TARP γ-2 (* $p<0.0001$).

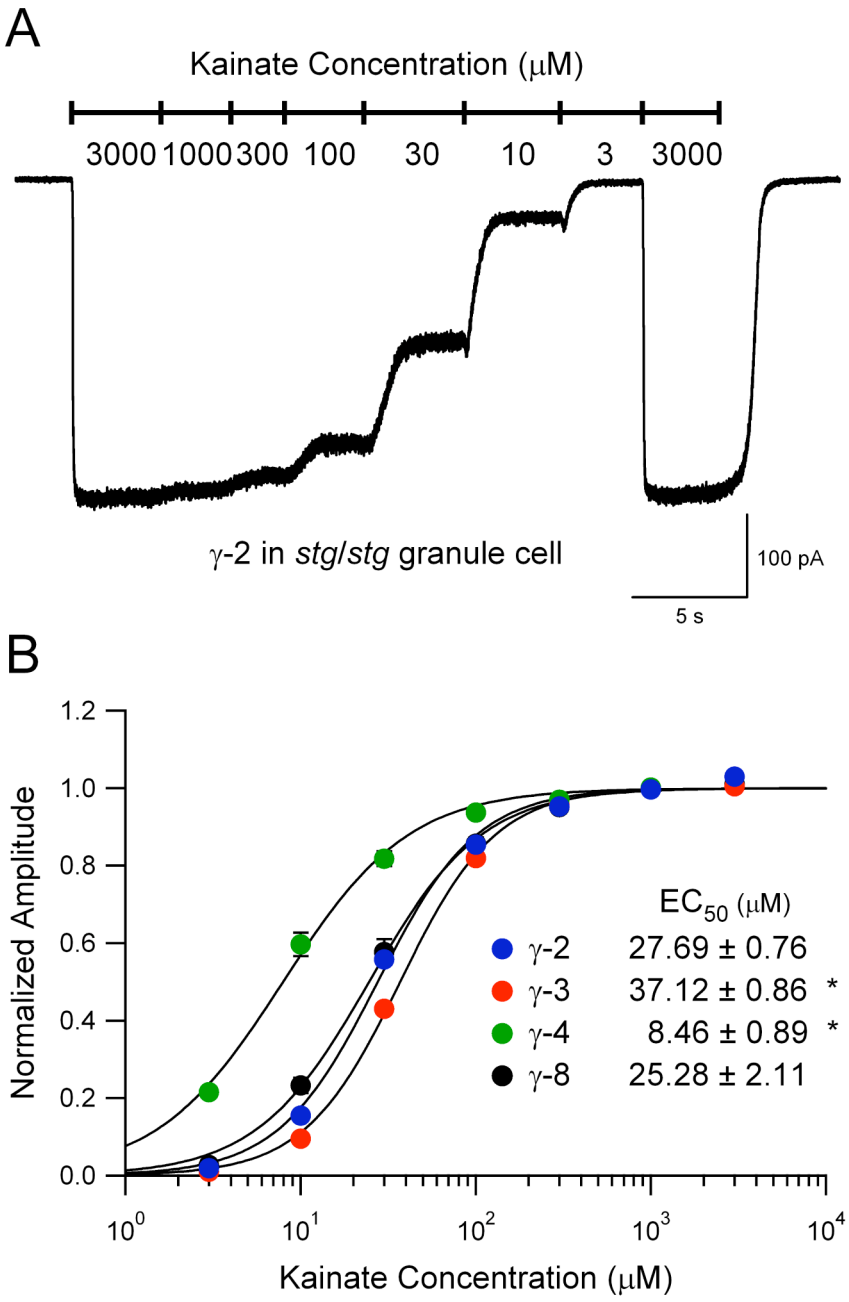
A
Kainate Concentration (μM)
3000 1000 300 100 30 10 3 3000
γ-2 in stg/stg granule cell
100 pA
5 s
B
Normalized Amplitude
1.2
1.0
0.8
0.6
0.4
0.2
0.0
10^0
10^1
10^2
10^3
10^4
Kainate Concentration (μM)
EC50 (μM)
γ-2 27.69 ± 0.76
γ-3 37.12 ± 0.86 *
γ-4 8.46 ± 0.89 *
γ-8 25.28 ± 2.11

Table 2. Analysis of Kainate Dose-Response Relationship

I_{max}, EC_{50}, and n_H are, respectively, the maximum current evoked by local application of 3 mM kainate, the concentration at which the kainate-evoked current is half-maximal, and the Hill coefficient. The latter two values were obtained from a best fit of the data with the logistic equation. The measurements are shown as mean ± SEM. Symbols indicate significant difference with respect to TARP γ-2 (* $p<0.002$-0.0001).

Table 2. Analysis of Kainate Dose-Response Relationship

Condition	I_{max} (pA)	EC_{50} (μM)	n_H
γ–2 in *stg*/*stg* (n=8)	417.83 ± 52.21	27.69 ± 0.76	1.53 ± 0.04
γ–3 in *stg*/*stg* (n=12)	341.35 ± 35.81	37.12 ± 0.86 *	1.59 ± 0.02
γ–4 in *stg*/*stg* (n=12)	251.35 ± 32.06	8.46 ± 0.89 *	1.26 ± 0.04 *
γ–8 in *stg*/*stg* (n=7)	387.48 ± 79.35	25.28 ± 2.11	1.39 ± 0.06

shown that γ-5 can interact with AMPARs and influence their properties in its own right, suggesting that γ-5 may not have been a null source for domain transplantation (Kato et al., 2007; Kato et al., 2008; Soto et al., 2009). Therefore, in order to probe the sufficiency of the TARP Ex1 domain for TARP subtype-specific modulation of AMPARs, I generated a series of chimeras in which the Ex1 domain was exchanged between distinct TARP subtypes. Specifically, I replaced the Ex1 domain of γ-2 with that of γ-4 (γ-2x4) and visa versa (γ-4x2), and replaced the Ex1 domain of γ-3 with that of γ-8 (γ-3x8) and visa versa (γ-8x3).

All four of these chimeric TARPs rescued both the surface and synaptic expression of AMPARs in *stargazer* granule neurons (Figure 10). mEPSCs mediated by γ-2x4 displayed the slow decay kinetics normally associated with γ-4, while γ-4x2 produced the relatively faster decay kinetics associated with γ-2 (Figures 10A and 10B). Remarkably, differences in the rise kinetics of AMPARs imparted by γ-2 and γ-4 were also swapped by exchange of this Ex1 domain (Figure 10C). While the rise phenotypes of TARPs γ-3 and γ-8 were also reversed for the chimeras γ-3x8 and γ-8x3 (Figure 10C), their decay phenotypes were more complicated. mEPSCs rescued by γ-3x8 decayed more slowly than either the host γ-3 or the donor γ-8 (Figures 10A and 10B). These results indicate that while Ex1 is clearly a critical determinant of TARP subtype-specific gating of AMPARs, it is not entirely sufficient to account for the influence of TARPs on AMPAR channel kinetics. Note that although the weighted decay constant is similar for γ-2x4 and γ-3x8 (Figures 10A and 10B), the time course and relative contribution of a slow component of decay are different, suggesting that the Ex1

domains of different TARP subtypes may differ in terms of which specific AMPAR conformations they stabilize during gating.

TARP Subtype-Specific Gating of AMPARs Depends on Multiple TARP Intracellular Domains

Having established that the TARP Ex1 domain does not fully account for TARP subtype-specific control of AMPAR gating, I sought to determine whether the TARP intracellular domains investigated in Chapter 1 for their role in trafficking AMPARs might also influence channel gating. Indeed, analysis of the decay kinetics of mEPSCs rescued by TARP intracellular domain chimeras uncovers a surprising influence of multiple TARP intracellular domains on synaptic AMPAR gating (Figures 11 and 12). Complete exchange of the three intracellular domains of TARPs γ-2 and γ-8 (constructs γ-2-NLC-8 and γ-8-NLC-2) alters mEPSC decay kinetics, with the intracellular domains of γ-2 markedly slowing the kinetics of γ-8 (construct γ-8-NLC-2), and the intracellular domains of γ-8 speeding the kinetics of γ-2 (construct γ-2-NLC-8) (Fig. 11). How is this possible, given that wild-type γ-2 and γ-8 produce mEPSCs that decay similarly? When compared with the aforementioned Ex1 chimeras (γ-3x8 and γ-8x3), it appears that while the Ex1 domain of γ-8 is competent to produce slower AMPAR decay kinetics, it is normally constrained by an inhibitory influence on channel gating exerted by its intracellular domains.

Detailed analysis of mEPSC decay kinetics for each individual intracellular domain-swap chimera reveals that both the TARP intracellular loop and

Figure 10. TARP Subtype-Specific Gating of AMPA Receptors Depends on a TARP Extracellular Domain

(A) Average mEPSCs are normalized and aligned to the peak. Average mEPSCs from individual neurons are displayed in grey, and averages of all experiments for each condition are shown in color. Weighted time constant values calculated from the area under the peak-normalized current are displayed as mean ± SEM (see Methods).

(B) mEPSC decay depends on TARP Ex1. mEPSC decay times are quantified as cumulative probability distributions, displayed as mean ± SEM (Kolmogorov-Smirnov tests, γ-2x4 vs. γ-4x2, $p<0.001$; γ-3x8 vs. γ-8x3, $p<0.001$). Average mEPSCs across conditions from (A) are aligned to the peak and superimposed (inset).

(C) mEPSC rise time depends on TARP Ex1. mEPSC rise times are quantified as cumulative probability distributions, displayed as mean ± SEM (Kolmogorov-Smirnov tests, γ-2x4 vs. γ-4x2, $p<0.001$; γ-3x8 vs. γ-8x3, $p=0.008$). Average mEPSCs across conditions from (A) are aligned to the 10% rise point and superimposed (inset).

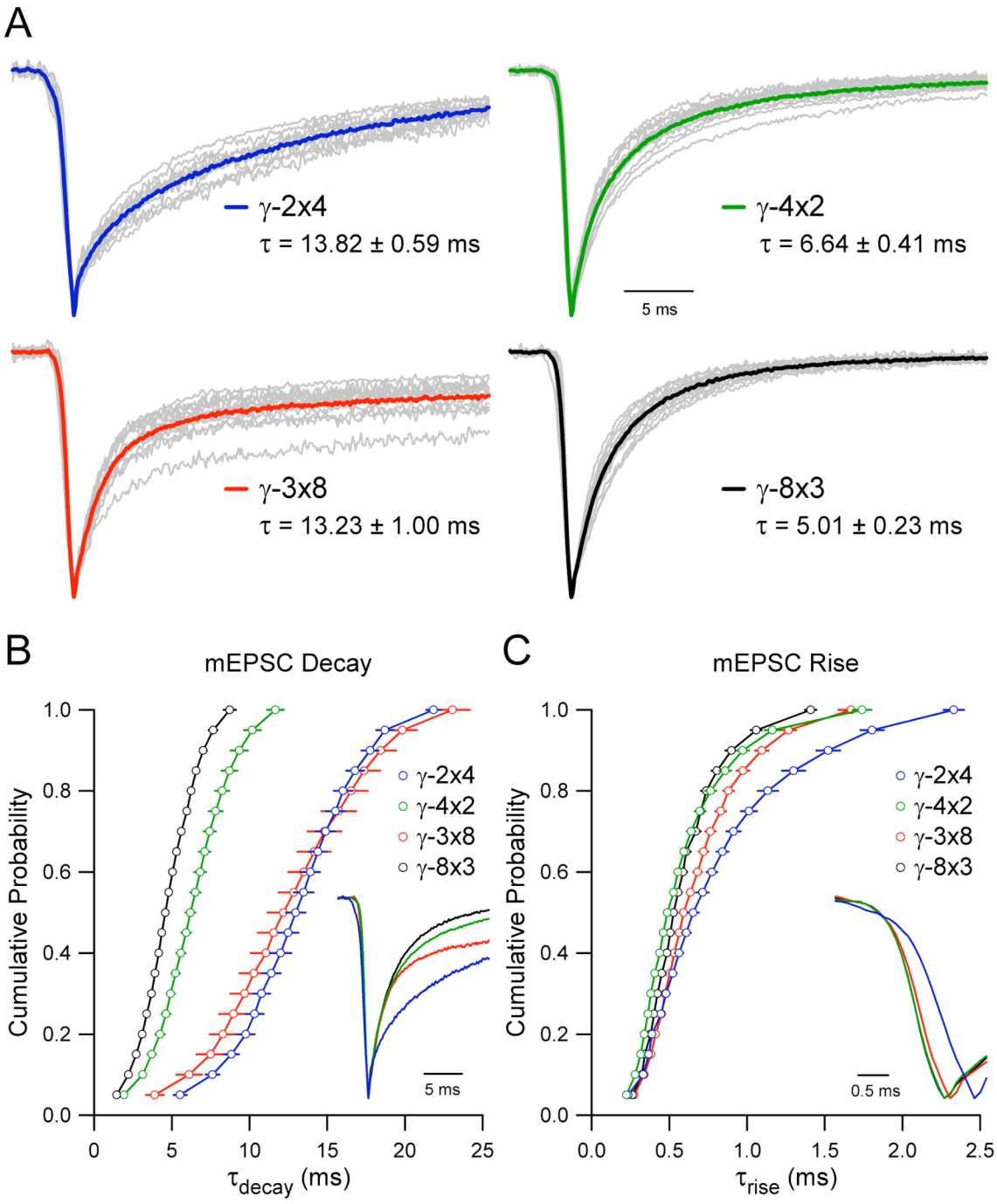
A
γ-2x4
τ = 13.82 ± 0.59 ms
γ-4x2
τ = 6.64 ± 0.41 ms
5 ms
γ-3x8
τ = 13.23 ± 1.00 ms
γ-8x3
τ = 5.01 ± 0.23 ms
B
mEPSC Decay
Cumulative Probability
γ-2x4
γ-4x2
γ-3x8
γ-8x3
5 ms
τdecay (ms)
C
mEPSC Rise
Cumulative Probability
γ-2x4
γ-4x2
γ-3x8
γ-8x3
0.5 ms
τrise (ms)

Figure 11. Multiple TARP Intracellular Domains Contribute to Synaptic AMPAR Gating

(A) Complete TARP intracellular domain transplantation alters mEPSC decay kinetics. Representative average mEPSCs are normalized and aligned to the peak.

(B) mEPSC decay kinetics for all TARP chimeras are quantified (* $p<0.004$ relative to γ-2; $^{\#}$ $p<0.0001$ relative to γ-8 ; n=14-40).

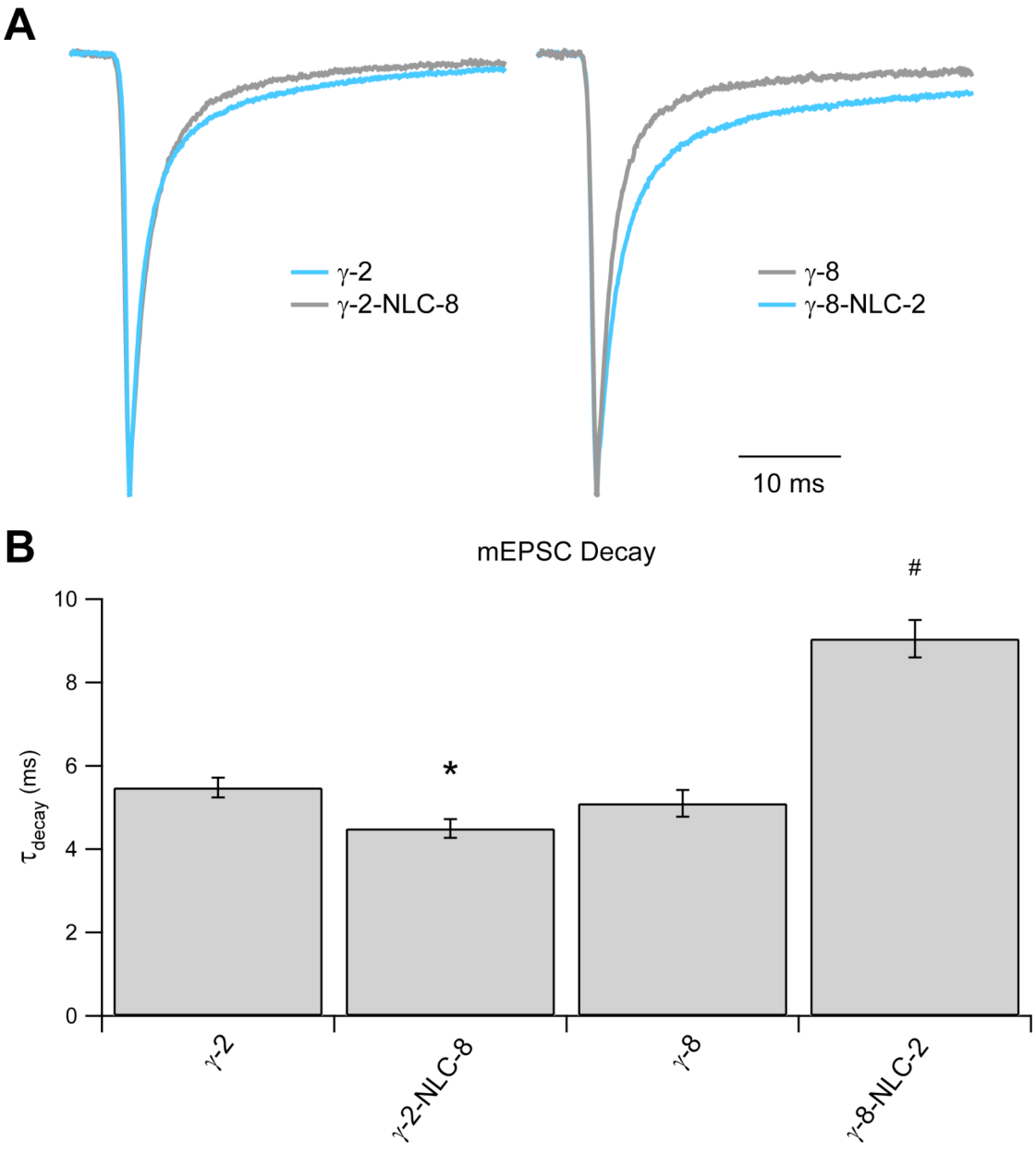
A
γ-2
γ-2-NLC-8
γ-8
γ-8-NLC-2
10 ms
B
mEPSC Decay
τ_{decay} (ms)
10
8
6
4
2
0
*
#
γ-2
γ-2-NLC-8
γ-8
γ-8-NLC-2

Figure 12. Influence of TARP Intracellular Domain Transplantation on mEPSC Decay

mEPSC decay kinetics for all TARP chimeras are quantified (* $p<0.0001$ relative to γ-2; $^{\#}$ $p<0.0002$ relative to γ-8 ; n=14-40). Dashed lines correspond to mean ± SEM for wild-type γ-2 (blue) and wild-type γ-8 (grey).

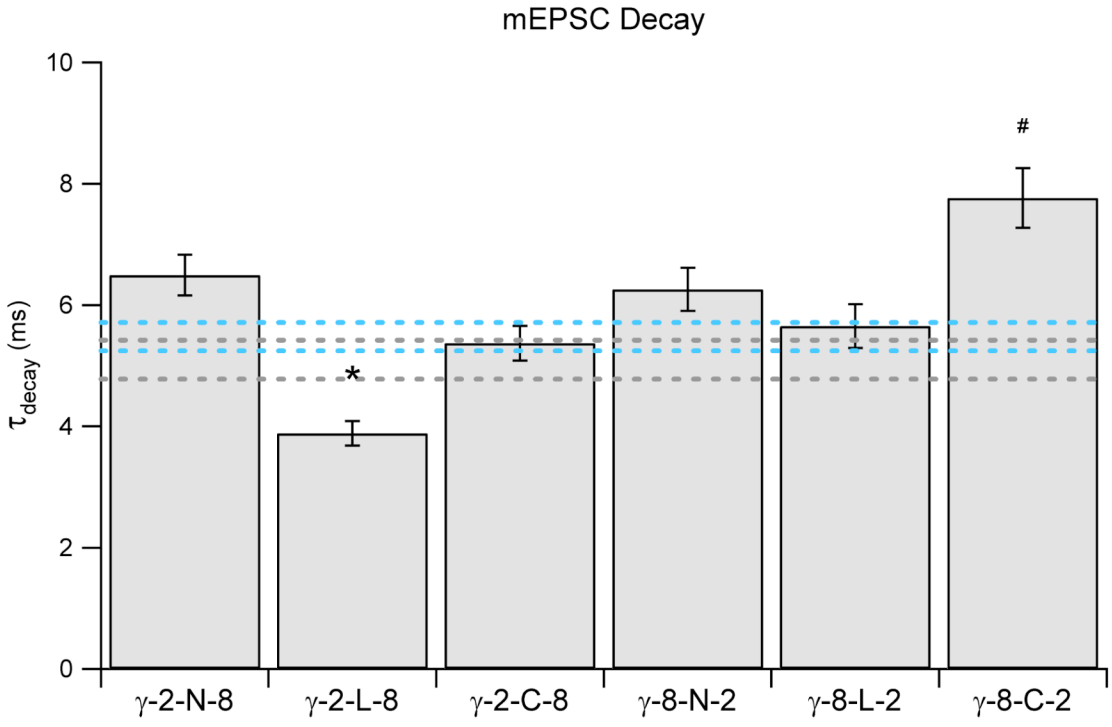
mEPSC Decay
10
8
6
4
2
0
τ_{decay} (ms)
*
#
γ-2-N-8
γ-2-L-8
γ-2-C-8
γ-8-N-2
γ-8-L-2
γ-8-C-2

C-terminus affect synaptic AMPAR kinetics primarily by modulating the time course and relative contribution of a slow component of gating (Figure 12 and Table 3). These results provide new insight into the mechanism by which TARPs influence AMPAR conformation by demonstrating that, in addition to the previously characterized extracellular domain, structural elements on the intracellular side of the receptors also play an important role in synaptic AMPAR gating.

TARP Subtype Specificity Contributes to Kinetics of Native AMPARs

Given the dramatically slow mEPSCs observed in *stargazer* cerebellar granule cells expressing TARP γ-4, I wondered whether endogenous γ-4 confers slow kinetics to synaptic AMPARs in the brain. To address this, I assayed synaptic AMPAR function in a γ-4 knockout (-/-) mouse (Milstein et al., 2007). γ-4 is expressed transiently throughout the developing brain, with especially high levels in the striatum (Fukaya et al., 2005; Tomita et al., 2003). Therefore, I initially recorded quantal synaptic AMPAR currents from medium spiny neurons (MSNs) in the dorsolateral striatum of neonatal animals (P5-P6). mEPSC amplitudes were reduced in γ-4 -/- neurons as compared to wild-type (Figures 13A and 13B), suggesting that this TARP normally participates in the synaptic targeting of AMPARs at this developmental stage. Furthermore, both the decay and rise time of mEPSCs were significantly faster in γ-4 -/- neurons (Figures 13C and 13D). This suggests that the remaining synaptic AMPARs are associated with other TARPs that do not slow the decay or rise of AMPARs to the same extent as γ-4.

The effects of loss of γ-4 on synaptic AMPAR kinetics decline with age in parallel with the decreased expression of γ-4, as mEPSCs recorded from striatal neurons in γ-4 -/- and wild-type mice at P14-P16 were identical (Figure 14). Interestingly, although the loss of γ-4 accelerated mEPSC decay in young animals, mEPSCs in both genotypes slowed with age (compare Figures 13C and 13D with Figures 14C and 14D). This developmental slowing of mEPSCs occurred in parallel with a decreasing input resistance (Figure 15) and likely reflects increased filtering due to the elaboration of the dendritic tree (Magee and Cook, 2000) rather than changes in the channel properties of AMPARs. These results demonstrate that functional heterogeneity in the control of AMPAR gating by TARP subtypes must be considered in order to fully account for the kinetics of AMPARs in populations of neurons that differentially express multiple TARP isoforms.

Table 3. Detailed Analysis of mEPSC Decay Kinetics: TARP Intracellular Domains

Detailed analysis of double exponential fits of the decay phase of AMPAR mEPSCs reveals that the TARP intracellular loop and C-terminus primarily modulate AMPAR channel kinetics by influencing the time course and relative contribution of a slow component of gating. τ_{fast}, τ_{slow}, A_{slow}, and A_{pers} are, respectively, the time constants of the fast and slow components of mEPSC decay, the relative amplitude of the slow component of mEPSC decay, and the relative amplitude of a nonzero persistent current measured 60 ms after the peak of the mEPSC. Symbols indicate statistical significance with respect to either γ-2 (* $p<0.0001$-0.004) or γ-8 ($^{\#}$ $p<0.0001$-0.003); n=14-40.

Table 3. Detailed Analysis of mEPSC Decay Kinetics: TARP Intracellular Domains

	γ-2	γ-2-N-8	γ-2-L-8	γ-2-C-8	γ-2-NLC-8
τ_{fast} (ms)	1.56 ± 0.05	1.79 ± 0.06	1.81 ± 0.11	1.62 ± 0.07	1.88 ± 0.1
τ_{slow} (ms)	13.25 ± 0.52	15.83 ± 0.65	9.27 ± 0.72*	12.92 ± 0.74	10.98 ± 0.83
A_{slow} (%)	25.76 ± 0.8	24.75 ± 0.78	22.18 ± 1.22	22.29 ± 0.93	21.17 ± 1.94*
A_{pers} (%)	2.20 ± 0.18	2.27 ± 0.42	0.81 ± 0.19*	2.16 ± 0.26	1.39 ± 0.14*

	γ-8	γ-8-N-2	γ-8-L-2	γ-8-C-2	γ-8-NLC-2
τ_{fast} (ms)	1.69 ± 0.11	1.93 ± 0.11	1.81 ± 0.07	2.12 ± 0.11	2.29 ± 0.07#
τ_{slow} (ms)	17.21 ± 4.88	14.33 ± 1.32	14.65 ± 1.27	18.49 ± 2.28	19.23 ± 1.10#
A_{slow} (%)	15.76 ± 1.67*	19.02 ± 0.96	15.81 ± 1.28	19.34 ± 1.21	22.01 ± 1.05#
A_{pers} (%)	3.53 ± 0.51*	3.51 ± 0.31	3.09 ± 0.27	4.55 ± 0.47	5.96 ± 0.61#

Figure 13. Deficits in Synaptic AMPAR Function in Striatum of Neonatal TARP γ-4 Knockout Mice

(A) Sample records demonstrate that quantal synaptic AMPAR transmission is altered in MSNs in the neonatal (P5-P6) striatum in γ-4 -/- mice.

(B) mEPSC amplitudes are reduced in neonatal γ-4 -/- mice. mEPSC amplitudes are quantified as cumulative probability distributions, displayed as mean ± SEM (Kolmogorov-Smirnov tests, +/+: n=22 vs. γ-4 -/-: n=22, $p<0.001$). Representative average mEPSCs from (A) are aligned to the peak and superimposed (inset).

(C) Representative average mEPSCs are normalized to the peak (solid lines), and the decay phase is fit with a single exponential function (broken lines). The corresponding decay time constant values are displayed.

(D) mEPSC decay times are accelerated in neonatal γ-4 -/- mice. mEPSC decay times are quantified as cumulative probability distributions, displayed as mean ± SEM (Kolmogorov-Smirnov test, $p<0.001$). Representative average mEPSCs from (C) are aligned to the peak and superimposed (inset).

(E) mEPSCs rise times are accelerated in neonatal γ-4 -/- mice. mEPSC rise times are quantified as cumulative probability distributions, displayed as mean ± SEM (Kolmogorov-Smirnov test, $p<0.001$). Representative average mEPSCs from (C) are aligned to the 10% rise point and superimposed (inset).

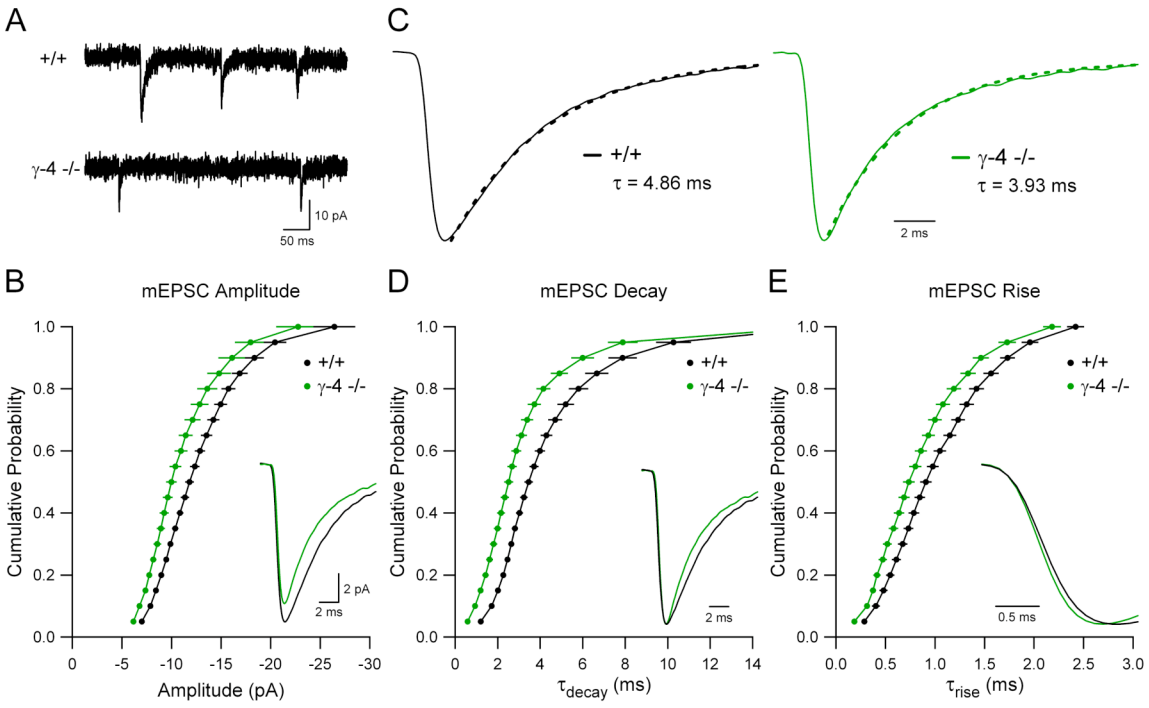
A
+/+
γ-4 -/-
10 pA
50 ms
C
+/+
τ = 4.86 ms
γ-4 -/-
τ = 3.93 ms
2 ms
B
mEPSC Amplitude
Cumulative Probability
+/+
γ-4 -/-
2 pA
2 ms
Amplitude (pA)
D
mEPSC Decay
τdecay (ms)
E
mEPSC Rise
0.5 ms
τrise (ms)

Figure 14. Normal Synaptic AMPAR Function in Striatum of Juvenile TARP γ-4 Knockout Mice

(A) Sample records demonstrate that quantal synaptic AMPAR transmission is normal in MSNs in the striatum of juvenile (P14-P16) γ-4 -/- mice.

(B) mEPSC amplitudes are normal in juvenile γ-4 -/- mice. mEPSC amplitudes are quantified as cumulative probability distributions, displayed as mean ± SEM (Kolmogorov-Smirnov test, +/+: n=21 vs. γ-4 -/-: n=25; n.s.). Representative average mEPSCs are aligned to the peak and superimposed (inset).

(C) Representative average mEPSCs are normalized to the peak (solid lines), and the decay phase is fit with a single exponential function (broken lines). The corresponding decay time constant values are displayed.

(D) mEPSC decay times are normal in juvenile γ-4 -/- mice. mEPSC decay times are quantified as cumulative probability distributions, displayed as mean ± SEM (Kolmogorov-Smirnov test, n.s.). Representative average mEPSCs from (C) are aligned to the peak and superimposed (inset).

(E) mEPSCs rise times are normal in juvenile γ-4 -/- mice. mEPSC rise times are quantified as cumulative probability distributions, displayed as mean ± SEM (Kolmogorov-Smirnov test, n.s.). Representative average mEPSCs from (C) are aligned to the 10% rise point and superimposed (inset).

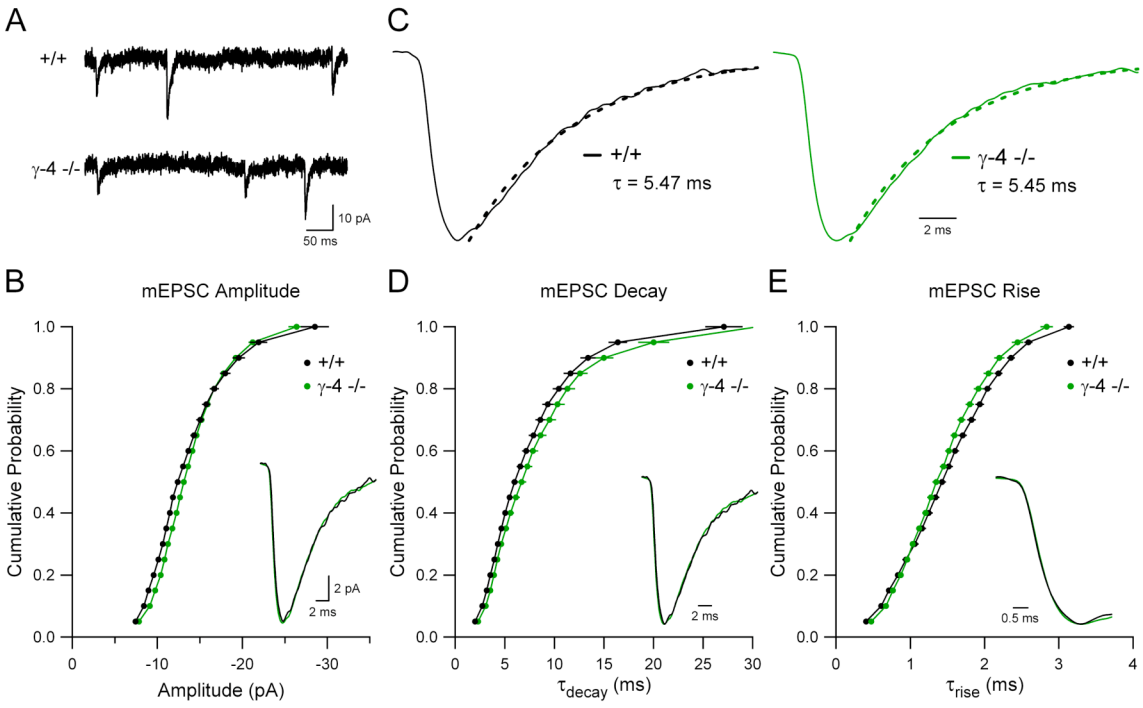
A
+/+
γ-4 -/-
10 pA
50 ms
C
+/+
τ = 5.47 ms
γ-4 -/-
τ = 5.45 ms
2 ms
B
mEPSC Amplitude
Cumulative Probability
+/+
γ-4 -/-
2 pA
2 ms
Amplitude (pA)
D
mEPSC Decay
τdecay (ms)
E
mEPSC Rise
0.5 ms
τrise (ms)

Figure 15. Input Resistance of Striatal MSNs Decreases During Development

In parallel with a slowing of mEPSC decay from P5-P6 to P14-P16, the input resistance of MSNs decreased in both wild-type and γ-4 -/- mice ($p<0.0001$, $n=21-25$).

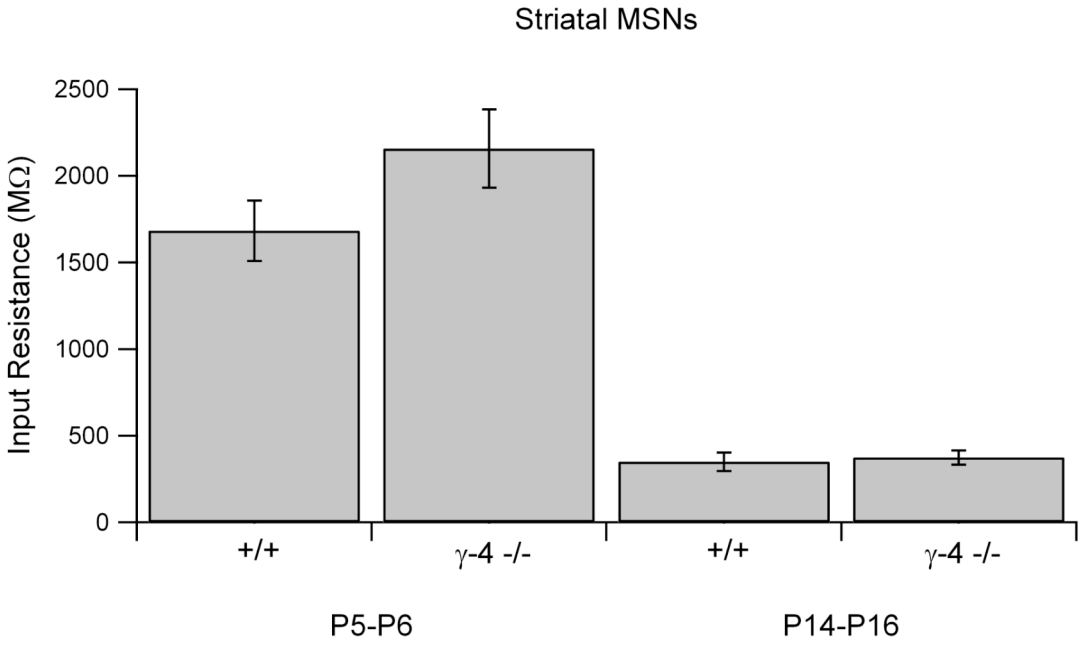
Striatal MSNs
Input Resistance (MΩ)
2500
2000
1500
1000
500
0
+/+
γ-4 -/-
+/+
γ-4 -/-
P5-P6
P14-P16

CHAPTER 3

Variable TARP/AMPA Receptor Stoichiometry Controls Synaptic AMPA Receptor Gating

In conducting the experiments expressing TARPs in *stargazer* cerebellar granule neurons described in Chapters 1 and 2, I also regularly recorded AMPAR mEPSCs in cultures from wild-type (+/+) and *stargazer* heterozygous (+/*stg*) mice. I found that synaptic AMPAR kinetics vary with the expression level of TARP γ-2, suggesting a variable TARP/AMPAR stoichiometry. In order to determine the absolute number of TARP molecules that associate with individual AMPAR channels, I collaborated with postdoctoral fellow Dr. Yun Shi in the design of experiments in HEK cells expressing AMPARs with and without covalently linked TARPs. Dr. Shi collected much of the data presented in this chapter, and I constructed mathematical models critical for the interpretation of the data. We found that AMPARs are functional when associated with either four, two, or zero TARPs, and that the efficacy of the partial agonist kainate varies across these conditions, providing a sensitive assay for TARP/AMPAR stoichiometry. By comparing these results with data obtained from hippocampal neurons, we show that native AMPARs are normally associated with multiple TARP molecules, and that native TARP/AMPAR stoichiometry varies with the expression level of endogenous and exogenous TARPs. Interestingly, AMPARs in hippocampal CA1 pyramidal

neurons are saturated by TARP association (four TARPs per AMPAR), while hippocampal dentate gyrus granule neurons and cerebellar granule neurons are not (less than four TARPs per AMPAR).

TARPs Dose-Dependently Control Synaptic AMPAR Gating

In *stargazer* heterozygote (+/*stg*) neurons, whole-cell AMPAR-mediated responses to glutamate were reduced by half compared to wild-type (Figure 1) and the amplitudes of mEPSCs were also clearly reduced (Figures 16A and 16B), consistent with a model in which the expression level of TARP is limiting for the delivery of AMPARs to the surface and synaptic membranes. Unexpectedly, overexpression of γ-2 in *stg*/*stg* granule neurons resulted in mEPSCs that were dramatically slowed compared to wild-type neurons (Figures 16C and 16D), which only express TARP γ-2. Expression of γ-2 in wild-type neurons also slowed AMPAR mEPSCs to a similar extent (data not shown), ruling out the possibility of some deficit in synapse formation or maintenance in *stg*/*stg* neurons. Furthermore, mEPSCs in +/*stg* neurons were slightly but significantly faster than wild-type (Figures 16C and 16D). These differences are particularly evident when comparing the values obtained from fitting average mEPSCs with a double exponential function (Table 4). Differences in rise time in these experiments were small (Figure 16E).

Given that AMPARs in cerebellar granule neurons absolutely require TARP association for surface and synaptic localization (Chen et al., 2000; Hashimoto et al., 1999), what mediates this dependence of AMPAR kinetics on

TARP expression level? One interesting possibility is that individual AMPAR complexes can associate with more than one TARP molecule, depending on the availability of TARP. Supporting this possibility, a recent single-particle electron microscopy study detected at least two TARP intracellular domains associated with purified native AMPAR complexes (Nakagawa et al., 2005); Nakagawa, personal communication). If the stoichiometry of the association between AMPARs and TARPs is not fixed, varying the number of TARPs associated with single AMPAR could influence synaptic AMPAR kinetics in a dose-dependent manner.

Alternatively, increased expression levels of TARPs could selectively traffic different populations of AMPARs with intrinsically different kinetics. Indeed, a recent report demonstrated that *flop* splice variants of AMPARs contain an ER retention signal that reduces their surface expression compared to *flip* splice variants in heterologous cells (Coleman et al., 2006). In that study, the surface delivery of *flop* AMPAR subunits could be facilitated by co-expression either with *flip* AMPAR subunits, or with TARP γ-2. In order to test the possibility that differences in the relative surface expression levels of *flip* and *flop* AMPAR splice variants mediates the differences in AMPAR gating observed in Figure 16, I conducted a functional assay of AMPAR splice variation using pharmacology. While cyclothiazide (CTZ) reduces desensitization and potentiates peak glutamate responses selectively on *flip* AMPARs, 4-[2-(phenylsulfonylamino)-ethylthio]-2,6-difluoro-phenoxyacetamide (PEPA) acts selectively on *flop* AMPARs. These drugs have previously been used to detect relative differences

Figure 16. TARPs Dose-Dependently Control Synaptic AMPA Receptor Gating

(A) Sample records demonstrate that characteristics of quantal synaptic AMPAR currents vary with the expression level of γ-2.

(B) mEPSC amplitude depends on TARP expression level. mEPSC amplitudes are quantified as cumulative probability distributions, displayed as mean ± SEM (Kolmogorov-Smirnov comparisons to wild-type (+/+): n=22; +/*stg*: n=28, $p<0.001$; γ-2 in *stg*/*stg*: n=40, $p<0.001$). Average mEPSCs are aligned to the peak and superimposed (inset).

(C) Average mEPSCs are normalized and aligned to the peak. Average mEPSCs from individual neurons are displayed in grey, and averages of all experiments for each condition are shown in color (γ-2 in *stg*/*stg* data from Figure 2B is replotted on a different timescale for comparison). Weighted time constant values calculated from the area under the peak-normalized current are displayed as mean ± SEM (see Methods).

(D) mEPSC decay depends on TARP expression level. mEPSC decay times are quantified as cumulative probability distributions, displayed as mean ± SEM (Kolmogorov-Smirnov comparisons to wild-type (+/+); +/*stg*: $p<0.004$; γ-2 in *stg*/*stg*: $p<0.001$). Average mEPSCs across conditions from (C) are aligned to the peak and superimposed (inset).

(E) mEPSC rise is independent of TARP expression level. mEPSC rise times are quantified as cumulative probability distributions, displayed as mean ± SEM (Kolmogorov-Smirnov comparisons to wild-type (+/+); +/*stg*: n.s.; γ-2 in *stg*/*stg*: n.s.). Average mEPSCs across conditions from (C) are aligned to the 10% rise point and superimposed (inset).

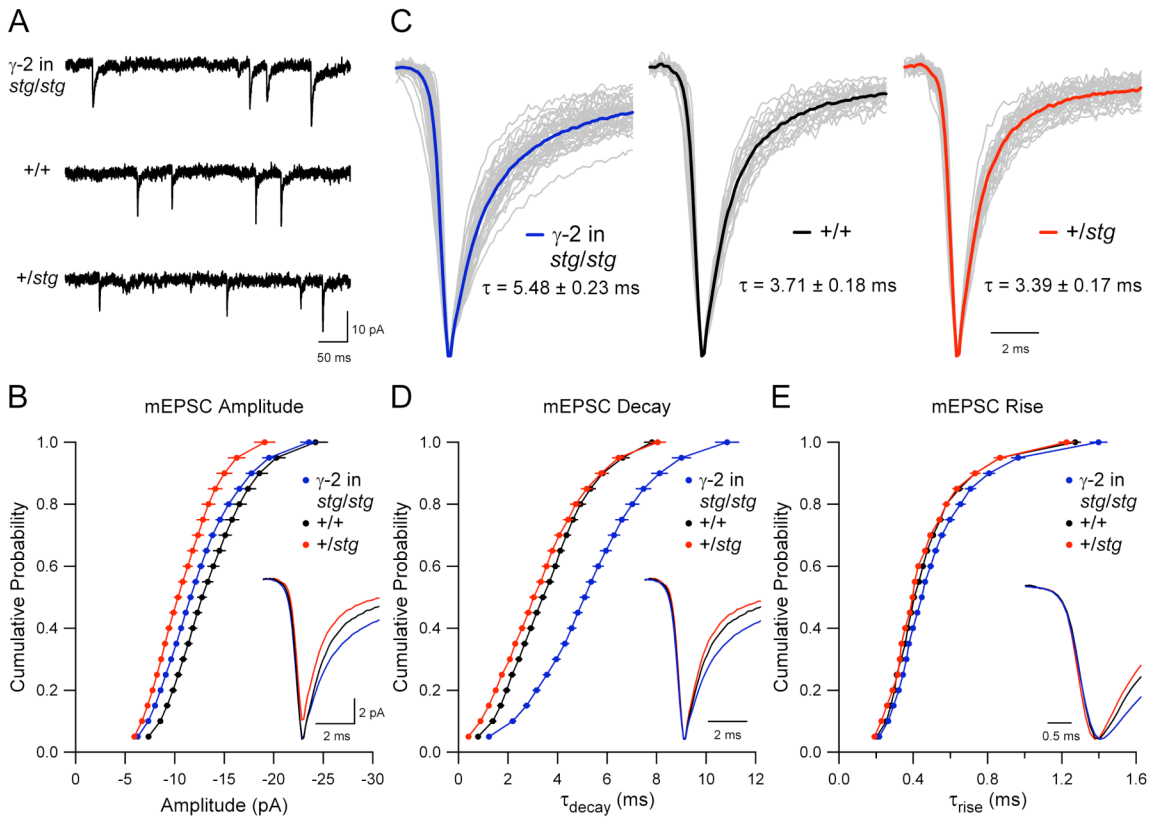
A
γ-2 in stg/stg
+/+
+/stg
10 pA
50 ms
C
γ-2 in stg/stg
τ = 5.48 ± 0.23 ms
+/+
τ = 3.71 ± 0.18 ms
+/stg
τ = 3.39 ± 0.17 ms
2 ms
B
mEPSC Amplitude
Cumulative Probability
Amplitude (pA)
2 pA
2 ms
D
mEPSC Decay
τdecay (ms)
2 ms
E
mEPSC Rise
τrise (ms)
0.5 ms

Table 4. Detailed Analysis of mEPSC Decay Kinetics: TARP Stoichiometry

τ_{fast}, τ_{slow} and A_{slow} are, respectively, the time constants of the fast and slow components of mEPSC decay and the relative amplitude of the slow component of mEPSC decay obtained by fitting the average mEPSC from individual neurons with a double exponential function. The measurements are shown as mean ± SEM. Symbols indicate significant difference with respect to +/+ ($^{\#}$ $p<0.05$-0.0001).

Table 4. Detailed Analysis of mEPSC Decay Kinetics: TARP Stoichiometry

Condition	τ_{fast} (ms)	τ_{slow} (ms)	A_{slow} (%)
+/+ (n=22)	1.21 ± 0.05	9.91 ± 0.58	19.22 ± 1.04
+/*stg* (n=28)	1.02 ± 0.04 #	9.97 ± 0.74	14.80 ± 1.08 #
γ−2 in *stg*/*stg* (n=40)	1.56 ± 0.05 #	13.25 ± 0.52 #	25.76 ± 0.80 #

in the expression of *flip* and *flop* AMPARs in distinct neuronal populations (Sekiguchi et al., 1998). I recorded whole-cell responses to glutamate in cultured granule neurons, first in the presence of CTZ, and then in the presence of PEPA, and calculated PEPA/CTZ ratios from the resulting current amplitudes (Figure 17). This ratio was near unity, indicating substantial contributions from both *flip* and *flop* AMPARs, and did not differ between wild-type, +/*stg*, and γ-2 in *stg*/*stg*. Therefore, the dependence of synaptic AMPAR kinetics on TARP expression level does not reflect differences in the surface expression of distinct AMPAR splice variants. Rather, these data favor the hypothesis that AMPARs associate with TARPs with a variable stoichiometry.

TARPs Dose-Dependently Control AMPAR Agonist Affinity

The apparent affinity of these native AMPARs for agonist also depended on the expression level of TARP γ-2 (Figure 18), with differences in kainate EC_{50} corresponding to differences in mEPSC decay for wild-type, +/*stg*, and *stg*/*stg* neurons expressing γ-2. Notably, overexpression of γ-2 also resulted in a substantial increase in the peak response to saturating kainate relative to wild-type (+/+: 267.51 ± 19.13 vs. γ-2: 417.83 ± 52.21, $p<0.03$), indicating that the efficacy of this partial agonist is also TARP dose-dependent.

Heterologous Expression of AMPARs Covalently Fused to TARPs

While the experiments described above provide the first indication that AMPARs might associate with TARPs with a variable stoichiometry, it is not possible to

determine from the data the exact number of TARPs that associate with individual AMPAR channels. That AMPAR kinetics vary with TARP expression level could result from mixed populations of AMPARs containing anywhere from zero to four associated TARPs. To resolve this question, I collaborated with postdoctoral fellow Dr. Yun Shi to develop a technique that allows the number of TARPs bound to individual AMPARs to be counted unambiguously. We reasoned that by covalently fusing AMPAR subunits to TARPs, we could study the properties of AMPARs with a known TARP stoichiometry. Fusion of the C-terminus of GluA1 to the N-terminus of TARP γ-2 via a short linker sequence (construct A1γ-2) should produce homomeric AMPARs associated with four TARPs (Figure 19A). The following experiments expressing AMPARs with and without fused TARPs in HEK cells were conducted by Dr. Shi.

Outside-out patches from HEK cells expressing the fusion construct A1γ-2 exhibit sizeable currents in response to application of either 1 mM glutamate or 1 mM kainate in the presence of 100 μM CTZ (Figure 19B), demonstrating that these channels fold properly, traffic to the plasma membrane, and appropriately gate in response to agonist. Given that TARP association increases the efficacy of the agonist kainate (Tomita et al., 2005; Turetsky et al., 2005), we measured the ratio of kainate currents to glutamate currents (I_{KA}/I_{Glu}) to determine whether the fused TARP molecules are *functionally* associated with the AMPAR channel. Indeed, A1γ-2 results in I_{KA}/I_{Glu} similar to that produced by co-expression of non-fused GluA1 with TARP γ-2 (Figures 19B and 19C), demonstrating that the fused TARP molecules are capable of modulating the functional properties of the

Figure 17. Dependence of AMPAR Properties on TARP Expression Level Does Not Reflect Changes in Surface Expression of AMPAR Splice Variants

Whole-cell responses to 500 μM Glutamate were first recorded in the presence of 100 μM CTZ and then in the presence of 100 μM PEPA in cultured cerebellar granule neurons. A ratio of current amplitudes was calculated to assay the relative contributions of AMPARs containing *flip* and *flop* isoforms. No difference was observed across the three conditions tested (Kruskal-Wallis Rank Sum Test, +/+, n=10; +/*stg*, n=10; γ-2 in *stg*/*stg*, n=10, n.s.).

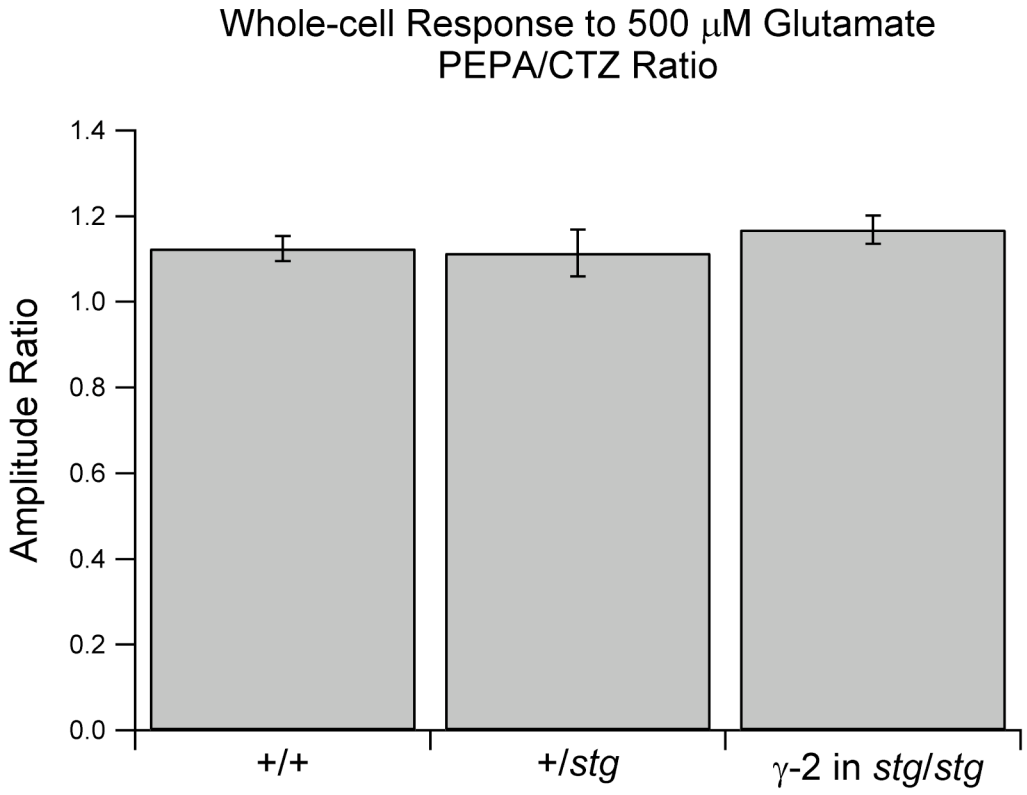
Whole-cell Response to 500 μM Glutamate
PEPA/CTZ Ratio
Amplitude Ratio
1.4
1.2
1.0
0.8
0.6
0.4
0.2
0.0
+/+
+/stg
γ-2 in stg/stg

Figure 18. Variable TARP/AMPAR Stoichiometry Controls AMPAR Agonist Affinity

AMPAR affinity for kainate depends on TARP expression level. EC_{50} values are displayed as mean ± SEM for wild-type (+/+): n=12; +/*stg*: n=12; γ-2 in *stg*/*stg*: n=12. Symbols indicate statistical significance relative to wild-type (+/+) ($^{\#}$ $p<0.03$, $^{\#\#}$ $p<0.001$).

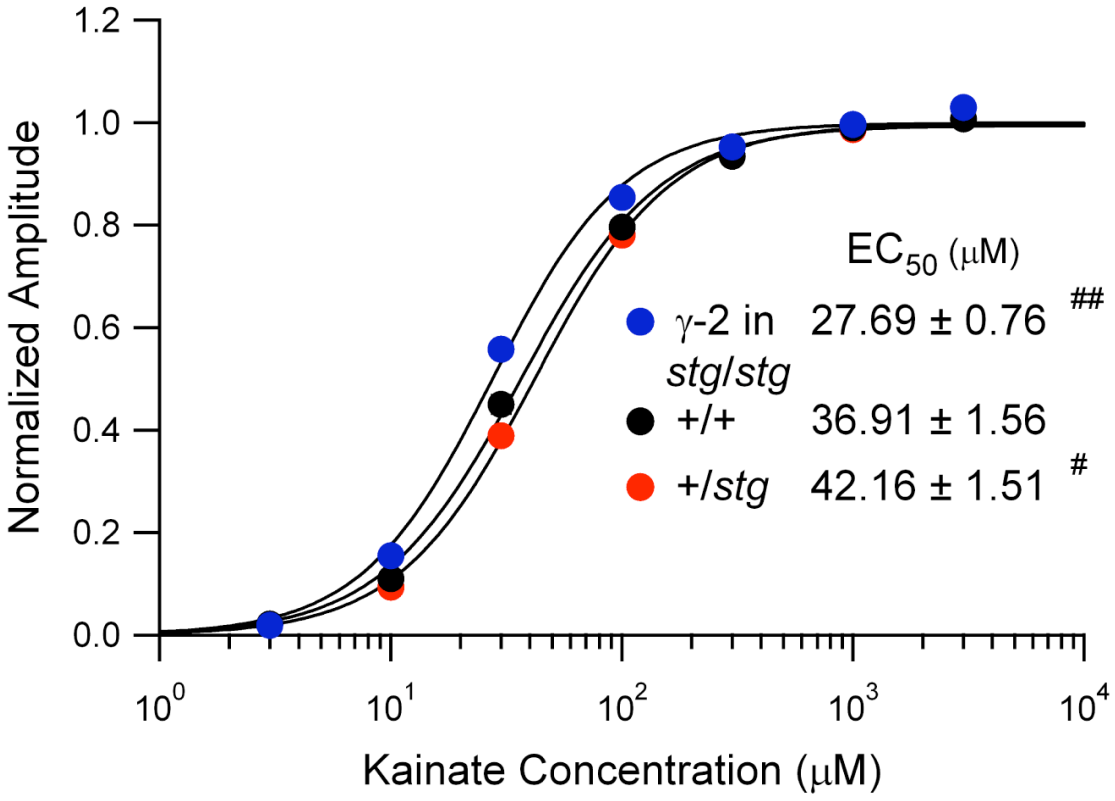
1.2
1.0
0.8
0.6
0.4
0.2
0.0
Normalized Amplitude
10^0
10^1
10^2
10^3
10^4
Kainate Concentration (μM)
EC_{50} (μM)
γ-2 in *stg/stg* 27.69 ± 0.76 ##
+/+ 36.91 ± 1.56
+/*stg* 42.16 ± 1.51 #

Figure 19. Co-Expression or Covalent Fusion of AMPARs with TARPs Similarly Enhances Kainate Efficacy

(A) Diagram illustrates that AMPAR-TARP fusion proteins were constructed by covalently linking the C-terminus of the AMPAR subunit to the N-terminus of the TARP protein via a short stretch of flexible linker sequence.

(B) Sample records show that in outside-out patches from HEK cells transfected with GluA1 fused to TARP γ-2 (A1γ-2), application of either 1 mM glutamate (Glu) or 1 mM kainate (KA) in the presence of 100 μM CTZ results in currents comparable in amplitude to co-expression of non-fused GluA1 with γ-2. The efficacy of kainate relative to glutamate (I_{KA}/I_{Glu}) is enhanced to the same degree by co-expression or fusion of GluA1 with γ-2 (~0.55) relative to GluA1 alone (~0.09). Scale bars: 2 s, 100 pA.

(C) The efficacy of kainate relative to glutamate (I_{KA}/I_{Glu}) for the experiments shown in (B) are quantified as mean ± SEM. Additional experiments quantified here demonstrate that fusion of GluA1 with TARPs γ-3, γ-4, and γ-8 yield similar I_{KA}/I_{Glu} to γ-2.

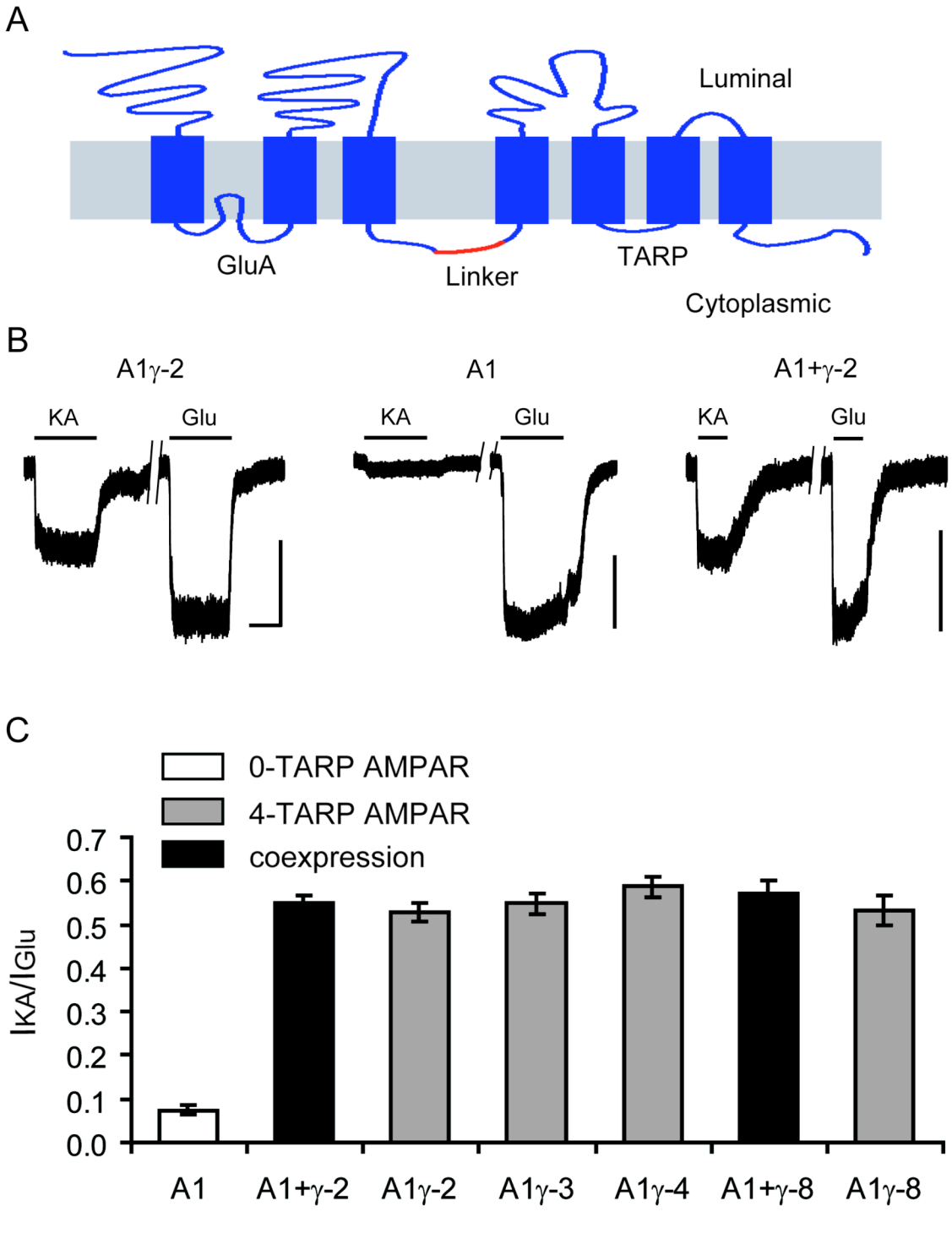
A
Luminal
GluA
Linker
TARP
Cytoplasmic
B
A1γ-2
A1
A1+γ-2
KA
Glu
KA
Glu
KA
Glu
C
0-TARP AMPAR
4-TARP AMPAR
coexpression
IKA/IGlu
0.7
0.6
0.5
0.4
0.3
0.2
0.1
0.0
A1
A1+γ-2
A1γ-2
A1γ-3
A1γ-4
A1+γ-8
A1γ-8

associated AMPAR channels. Similar results were also obtained by fusing GluA1 to the other TARP family members γ-3, γ-4, and γ-8 (Figure 19C).

Kainate Efficacy Co-Varies with TARP/AMPAR Stoichiometry

The observation that fusion of AMPARs and TARPs produces an enhanced kainate efficacy comparable to co-expression of the non-fused proteins raises the possibility that the channels formed in the latter condition normally contain four TARP molecules. However, it is also possible that fewer than four TARPs are sufficient to saturate the effect of TARPs on kainate efficacy. To address this possibility, we devised a method to measure the properties of AMPARs that contain less than four TARP molecules. The polyamine toxin philanthotoxin-433 (PhTx) selectively blocks AMPARs that do not contain the GluA2 subunit. We reasoned that co-expression of A1γ-2 with non-fused GluA2 would produce two populations of channels: homomeric GluA1 receptors containing four TARPs, which could be blocked by PhTx; and GluA1/GluA2 heteromers containing fewer than four TARPs, which would be insensitive to PhTx. This strategy allowed us to measure the kainate efficacy of an isolated population of heteromeric AMPARs that contain fewer than four TARPs.

Co-expression of A1γ-2 with GluA2, as well as the converse, GluA1+A2γ-2, produces kainate efficacies exactly intermediate between that of GluA1+GluA2, which contains no TARPs, and A1γ-2+A2γ-2, which contains four TARPs (Figure 20). Similar results were also obtained with γ-8 as the fused TARP (Figure 20). This establishes unambiguously that AMPAR channels can be

formed that contain fewer than four TARP molecules, and that kainate efficacy co-varies with TARP/AMPAR stoichiometry.

What is the exact stoichiometry of the population containing less than four TARPs? If there is an absolute requirement that heteromeric AMPARs contain two GluA1s and two GluA2s when they are co-expressed *in vitro* (Mansour et al., 2001), then all of the heteromers would contain precisely two TARPs. If, on the other hand, GluA1 and GluA2 assemble randomly (Washburn et al., 1997), then co-expression of equal amounts of A1γ-2 and GluA2 would primarily produce channels that contain two GluA2 subunits, but channels with other stoichiometries would also be present. To distinguish between these possibilities, we varied the ratio of co-expressed A1γ-2 and GluA2 cDNA in order to bias the assembly of AMPARs towards channels that contain either one or three GluA2s, and therefore three or one TARPs, respectively. To verify that altering the ratio of co-transfected cDNAs actually results in surface expression of AMPARs with the expected subunit compositions, we measured the percent block by PhTx of glutamate-evoked currents in outside-out patches. When A1γ-2 is expressed in 20-fold excess of GluA2, PhTx blocks ~90%, while the converse expression ratio produces negligible block by PhTx, as predicted by either model of assembly (Figure 21).

Having confirmed that our co-transfection conditions indeed vary the subunit composition of surface expressed AMPARs, we next isolated the GluA2-containing, heteromeric AMPAR populations with PhTx and determined their kainate efficacies. When expressing 20-fold more A1γ-2 than GluA2, random

Figure 20. Kainate Efficacy of GluA1/GluA2 Heteromers Varies with TARP Stoichiometry

(A) Sample records from experiments co-expressing GluA1 and GluA2 with and without fused TARPs. All experiments were conducted in the presence of PhTx (600 nM-10 μM) to block all GluA1 homomeric AMPARs in order to measure the kainate efficacy of isolated GluA1/GluA2 heteromers. Similar to GluA1 alone (Figure 19B), GluA1/GluA2 heteromers expressed without TARPs (A1+A2) exhibit low I_{KA}/I_{Glu} (~0.09). Either co-expression with γ-2, or fusion of both GluA1 and GluA2 with γ-2 (A1γ-2+A2γ-2) produces channels with enhanced I_{KA}/I_{Glu} (~0.55). When A1γ-2 is co-expressed with non-fused GluA2 (A1γ-2+A2), the measured I_{KA}/I_{Glu} is exactly intermediate between A1+A2 and A1γ-2+A2γ-2. Similar results were obtained for A1+A2γ-2 as well as for analogous experiments with γ-8 as the fused TARP. Scale bars: 2 s, 100 pA.

(B) The efficacy of kainate relative to glutamate (I_{KA}/I_{Glu}) for the experiments shown in (A) are quantified as mean ± SEM.

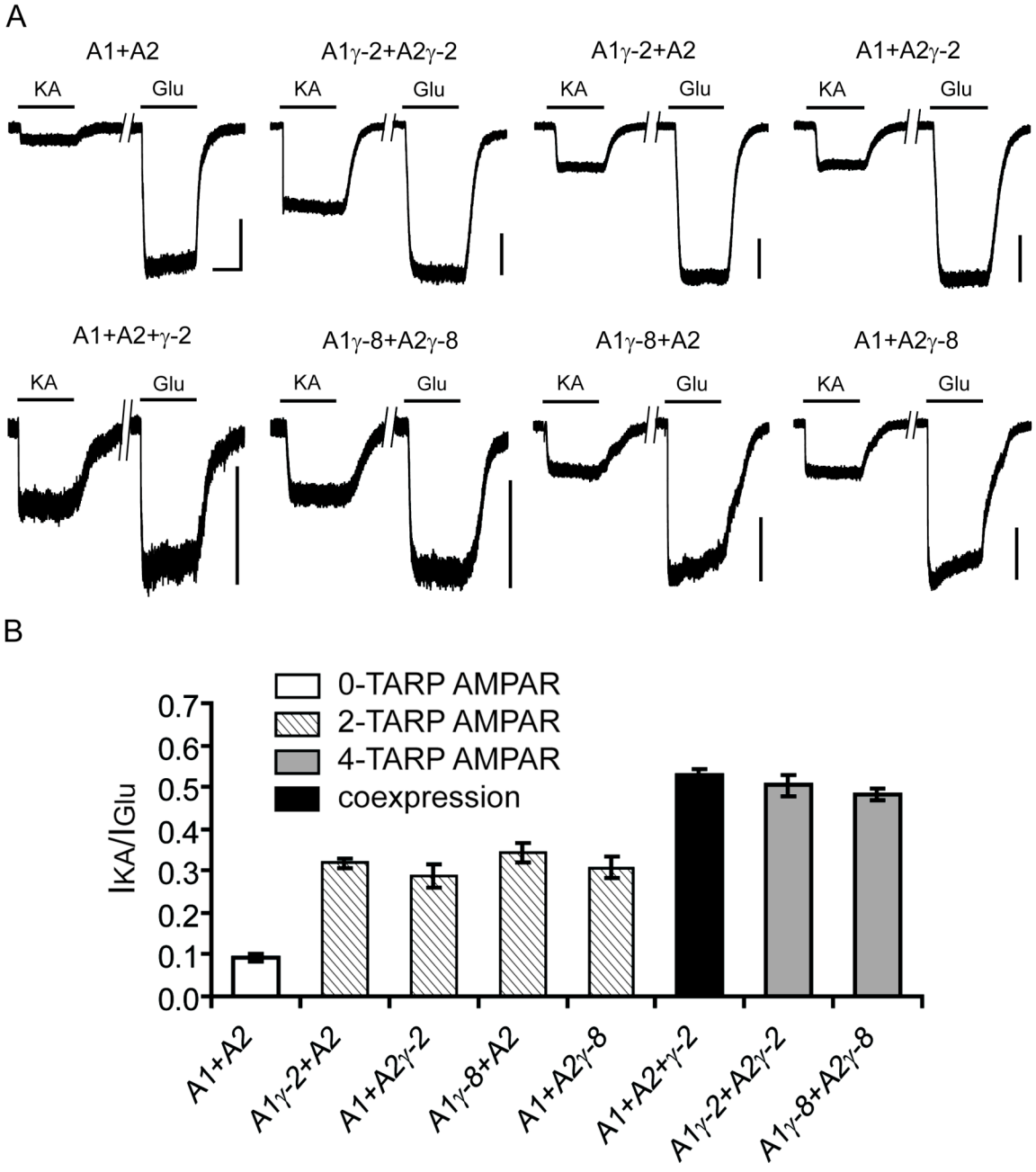
A
A1+A2
A1γ-2+A2γ-2
A1γ-2+A2
A1+A2γ-2
KA
Glu
A1+A2+γ-2
A1γ-8+A2γ-8
A1γ-8+A2
A1+A2γ-8
B
0-TARP AMPAR
2-TARP AMPAR
4-TARP AMPAR
coexpression
IKA/IGlu
0.0
0.1
0.2
0.3
0.4
0.5
0.6
0.7
A1+A2
A1γ-2+A2
A1+A2γ-2
A1γ-8+A2
A1+A2γ-8
A1+A2+γ-2
A1γ-2+A2γ-2
A1γ-8+A2γ-8

Figure 21. Determining the AMPAR Subunit Stoichiometry of GluA1/GluA2 Heteromers

When the ratio of co-transfected A1γ-2 and GluA2 cDNA was varied, the subunit composition of surface expressed AMPARs was assayed by measuring the percent block of glutamate-evoked currents in outside-out patches by PhTx. The experimental data is presented as mean ± SEM, and is compared with values predicted by two alternate models of AMPAR assembly: random assembly, and preferred heterodimer assembly. For the random assembly model, the probability of assembly of each of the following channels was calculated from the binomial distribution: (4)A1γ-2, (3)A1γ-2 + (1)GluA2, (2)A1γ-2 + (2)GluA2, (1)A1γ-2 + (3)GluA2, and (4)GluA2. For the preferred heterodimer model, the ratio of co-transfected cDNA determined the proportion of (2)A1γ-2 + (2)GluA2 heteromers, and the remaining channels where either (4)A1γ-2 or (4)GluA2 homomers. For both models, it was assumed that (4)GluA2 channels do not contribute to the outside-out patch currents due to deficits in trafficking and low single-channel conductance. It was further assumed that only (4)A1γ-2 channels are blocked by PhTx, and that all possible heteromers have the same single-channel conductance. These results demonstrate that the subunit composition of surface expressed AMPARs do indeed vary with the ratio of co-transfected cDNA exactly as predicted by either model.

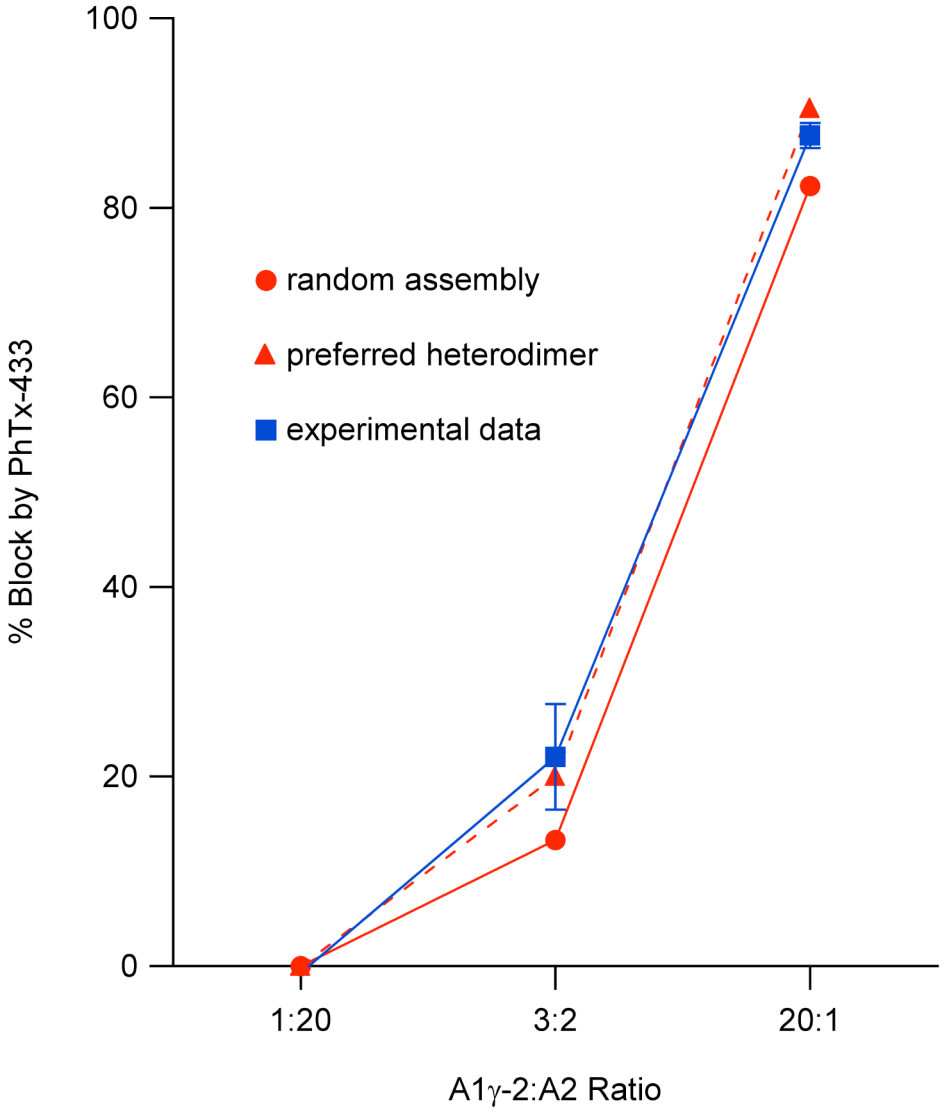
100
80
60
40
20
0
% Block by PhTx-433
random assembly
preferred heterodimer
experimental data
1:20
3:2
20:1
A1γ-2:A2 Ratio

assembly would produce heteromeric channels that contain at most one GluA2 subunit, and therefore three TARPs, while assembly that prefers heterodimers would produce channels that contain exactly two GluA2 subunits, and therefore two TARPs. Consistent with the latter model, we found that the kainate efficacy for this condition is identical to that obtained with a transfection ratio of 3:2 (Figure 22). Similar results were obtained in the converse experiment expressing 20-fold more GluA2 than A1γ-2 (Figure 22). In this case, channels containing four GluA2s and zero TARPs produce negligible currents due to deficits in trafficking and low conductance (Burnashev et al., 1992; Hollmann and Heinemann, 1994). Indeed, in our conditions expression of GluA2 alone in HEK cells generates essentially no current (data not shown). Comparison of the experimental data to values predicted by various assembly models rules out the possibility that kainate efficacy could be saturated by association of AMPARs with fewer than four TARPs (Figure 22). These experiments strongly suggest that, even under conditions that should favor channels with assembly ratios of 1:3 or 3:1, GluA1 and GluA2 preferentially assemble at a ratio of 2:2, and that the intermediate kainate efficacy observed when co-expressing GluAs with and without fused TARPs reflects receptors that predominantly contain two TARPs.

TARP/AMPAR Stoichiometry Differs Between Two Distinct Types of Hippocampal Neurons

We next sought to determine if the above results from HEK cells could be compared with data from neuronal AMPARs in order to read out native TARP/AMPAR stoichiometry. These experiments were also carried out by Dr. Shi. First we measured the kainate efficacy of AMPARs in outside-out patches

from mouse hippocampal CA1 pyramidal neurons. These native AMPARs displayed a high kainate efficacy consistent with incorporation of four TARP molecules per AMPAR complex (Figures 23A and 23C). Since AMPARs in mouse CA1 are predominantly GluA1/2 heteromers (Lu et al., 2009; Zamanillo et al., 1999) associated with TARP γ-8 (Rouach et al., 2005; Tomita et al., 2003), it is that receptor composition expressed in HEK cells that provides the best comparison (Figures 20B and 23C).

We next tested whether TARP/AMPAR stoichiometry in these neurons could be altered by genetic depletion or exogenous overexpression of TARPs, as I had shown for cerebellar granule neurons (Figure 16). Indeed, outside-out patches of neurons from heterozygous (+/-) and homozygous (-/-) TARP γ-8 knockout mice exhibited reduced kainate efficacy relative to wild-type (+/+) (Figures 23A and 23C). However, overexpression of either TARP γ-8 (Figures 23A and 23C) or TARP γ-2 (I_{KA}/I_{Glu} = 0.53±0.03; n = 4, data not shown) did not substantially increase kainate efficacy, supporting the notion that native AMPARs in CA1 pyramidal neurons contain four TARPs per AMPAR complex, and are therefore saturated by TARP expression. The finding that overexpression of TARP γ-2 does not alter kainate efficacy differs from the results of Turetsky et al., 2005. However, these authors specifically used immature neurons in which TARP expression levels are low, likely containing AMPARs with reduced stoichiometry.

These data contrast with those I obtained from cerebellar granule neurons, where the apparent TARP/AMPAR stoichiometry was not saturated in

Figure 22. Determining the TARP Stoichiometry of GluA1/GluA2 Heteromers

In order to determine the stoichiometry of AMPARs produced by co-expression of A1γ-2 and GluA2 in HEK cells, the ratio of co-transfected cDNA was varied and the kainate efficacy of AMPARs in outside-out patches was measured. The experimental data is presented as mean ± SEM, and is compared with values predicted by the same alternate models of AMPAR assembly analyzed in (A). For models assuming that the kainate efficacy of AMPARs saturates at four TARPs, the kainate efficacies of the other channels was assumed to vary linearly between the extreme conditions of zero and four TARPs, producing the following I_{KA}/I_{Glu}: (4)A1γ-2 (0.55), (3)A1γ-2 + (1)GluA2 (0.435), (2)A1γ-2 + (2)GluA2 (0.32), (1)A1γ-2 + (3)GluA2 (0.205), and (4)GluA2 (0.09). For models assuming that kainate efficacy saturates at two TARPs, I_{KA}/I_{Glu} were assigned as follows: (4)A1γ-2 (0.55), (3)A1γ-2 + (1)GluA2 (0.55), (2)A1γ-2 + (2)GluA2 (0.55), (1)A1γ-2 + (3)GluA2 (0.32), and (4)GluA2 (0.09). Kainate efficacy was then calculated from the weighted average of all the channels present on the surface, discluding the (4)A1γ-2 homomers, which were blocked by PhTx. The same assumptions made in (A) were also made here. The experimental data is best fit by the preferred heterodimer model that assumes kainate efficacy saturates at four TARPs. These results demonstrate that heteromeric AMPARs in the presence of TARPs are preferentially formed as heterodimers containing two GluA1 subunits, and two GluA2 subunits. They further show that the intermediate kainate efficacy observed in our experiments primarily reflects AMPARs that contain two TARPs.

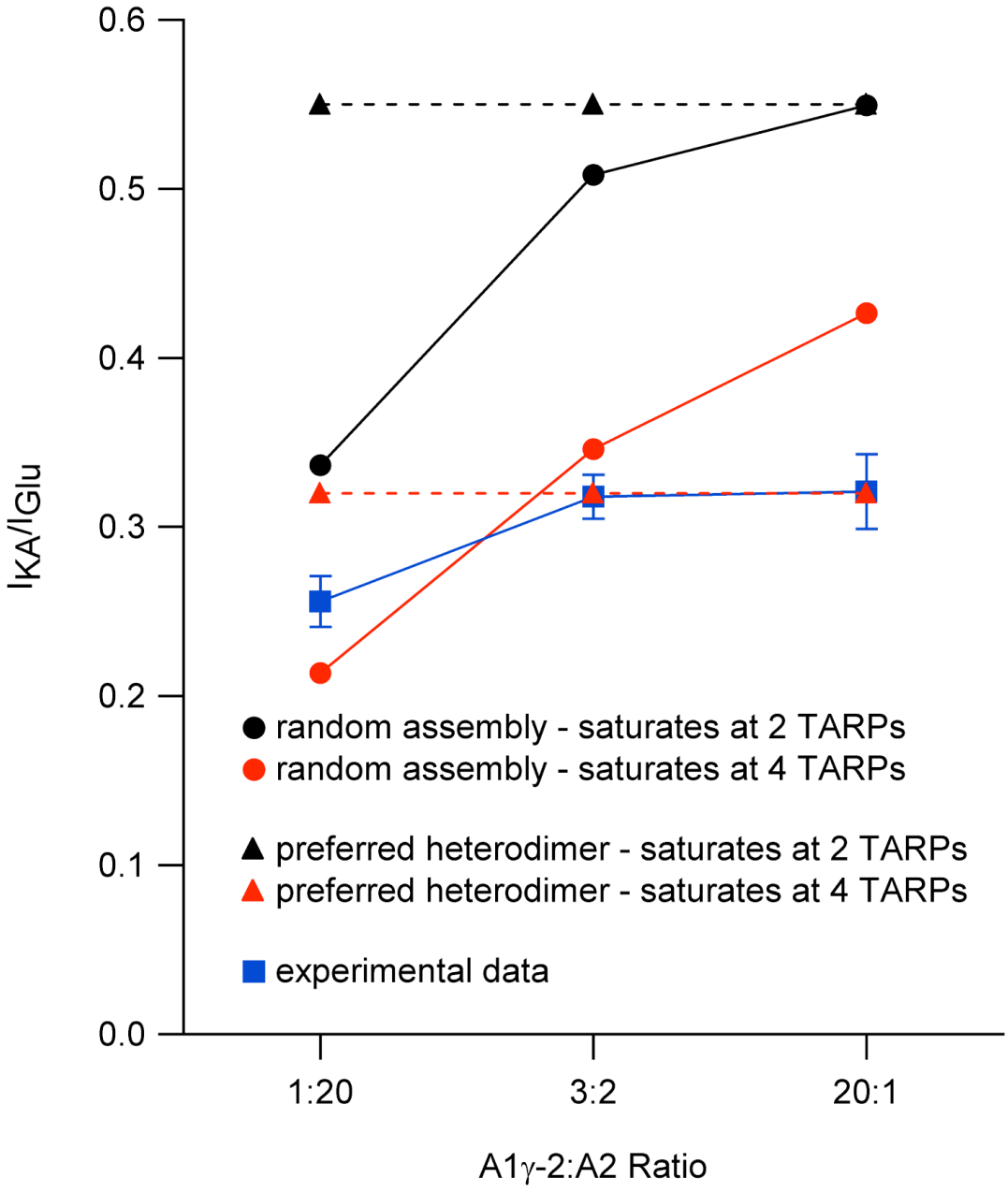
0.6
0.5
0.4
0.3
0.2
0.1
0.0
IKA/IGlu
random assembly - saturates at 2 TARPs
random assembly - saturates at 4 TARPs
preferred heterodimer - saturates at 2 TARPs
preferred heterodimer - saturates at 4 TARPs
experimental data
1:20
3:2
20:1
A1γ-2:A2 Ratio

Figure 23. TARP/AMPAR Stoichiometry Varies By Neuronal Cell Type

(A) Sample traces demonstrate that the kainate efficacy of AMPARs in outside-out patches from mouse hippocampal neurons is comparable to that observed in HEK cells for AMPAR channels associated with multiple TARP molecules. In both CA1 pyramidal neurons and in dentate gyrus granule neurons, kainate efficacy is reduced as TARP expression levels are reduced in TARP γ-8 heterozygous (+/-) and homozygous (-/-) knockout mice. However, overexpression of γ-8 in wild-type (+/+) pyramidal neurons does not increase I_{KA}/I_{Glu}, whereas it does in dentate granule neurons, suggesting that AMPARs are saturated with four TARPs in CA1, but not saturated in granule neurons. Scale bars: 2 s, 50 pA.

(B) The efficacy of kainate relative to glutamate (I_{KA}/I_{Glu}) for the experiments shown in (A) are quantified as mean ± SEM (* $p<0.05$; ** $p<0.01$ relative to +/+).

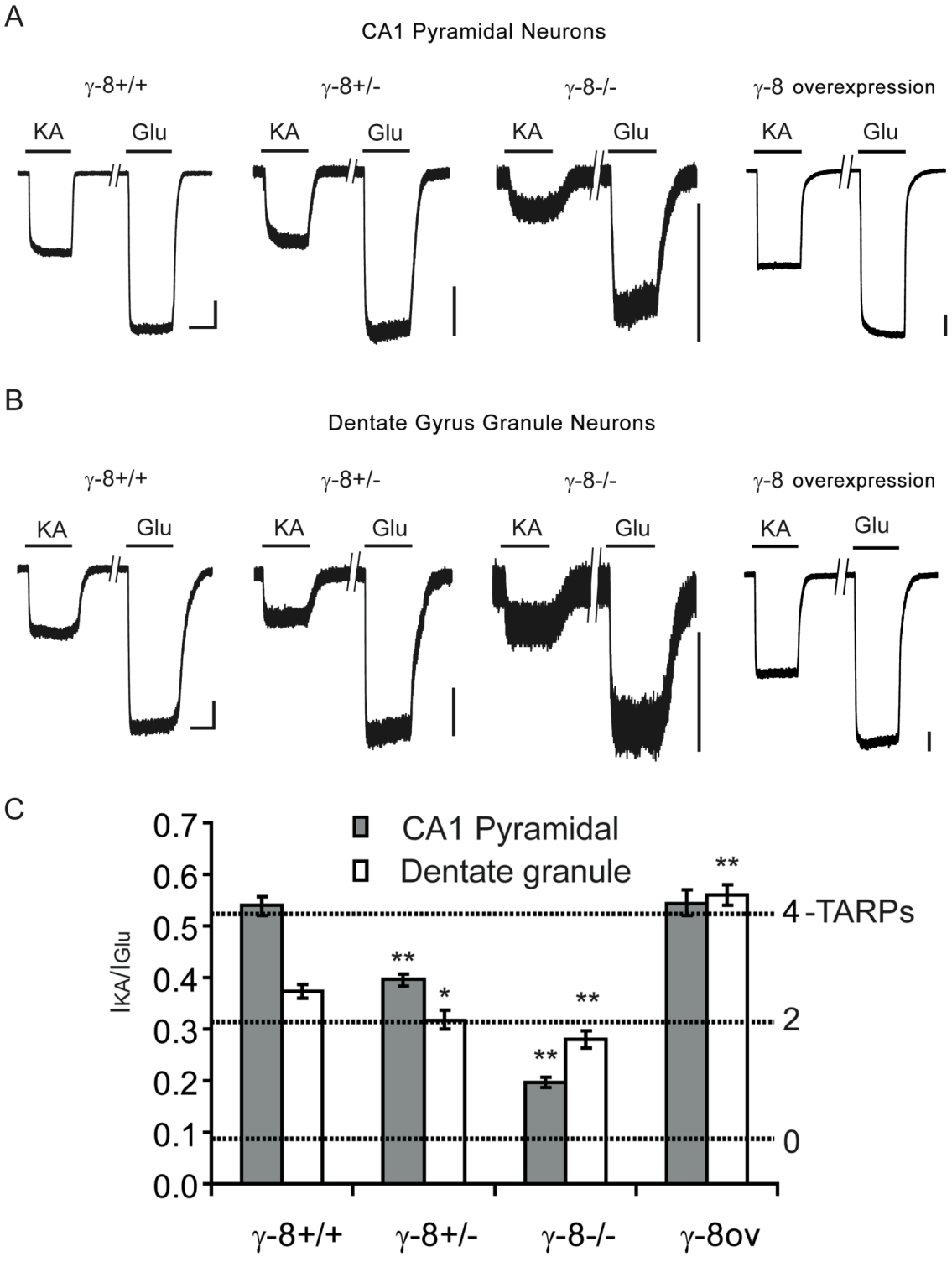
A
CA1 Pyramidal Neurons
γ-8+/+
γ-8+/-
γ-8-/-
γ-8 overexpression
KA
Glu
B
Dentate Gyrus Granule Neurons
C
CA1 Pyramidal
Dentate granule
IKA/IGlu
0.7
0.6
0.5
0.4
0.3
0.2
0.1
0.0
4-TARPs
2
0
**
*
γ-8+/+
γ-8+/-
γ-8-/-
γ-8ov

wild-type neurons, and could be increased by overexpression of TARP γ-2 (Figure 16). This raises the possibility that TARP/AMPAR stoichiometry is a parameter that differs across neuronal cell types. We tested this possibility by measuring kainate efficacy in another neuronal population, hippocampal dentate gyrus granule cells. In situ data suggests that these neurons express lower levels of TARP γ-8 than CA1 pyramidal neurons (Lein et al., 2007), and might be expected to display reduced TARP/AMPAR stoichiometry. Indeed, wild-type granule cells exhibited a lower kainate efficacy than that observed in CA1 pyramidal cells (Figures 23B and 23C). Furthermore, exogenous overexpression of TARP γ-8 substantially increased kainate efficacy in these cells (Figures 23B and 23C), confirming that AMPARs are not saturated with TARPs in this cell type. Importantly, the kainate efficacy observed when TARP γ-8 was overexpressed was identical to that recorded in CA1 pyramidal neurons, demonstrating that, despite possible differences in AMPAR subunit composition, the absolute I_{KA}/I_{Glu} values obtained in these two neuronal cell types can be directly compared to infer relative differences in TARP/AMPAR stoichiometry. Similar to pyramidal neurons, genetic depletion of TARP γ-8 further reduced kainate efficacy, with neurons from γ-8 +/- and γ-8 -/- mice exhibiting reduced kainate efficacy relative to wild-type (Figures 23B and 23C).

At this point we can only speculate as to what the precise TARP/AMPAR stoichiometry is in γ-8 +/- and γ-8 -/- mice. If we assume that at least one TARP must be associated with AMPARs in order for them to be efficiently trafficked to the cell surface, then we would expect all surface receptors to contain at least

one TARP; indeed, the observed kainate efficacy of γ-8 -/- pyramidal neurons is intermediate between that expected for zero and two TARPs, indicating that perhaps it is just one TARP. In this scenario, TARPs γ-2 and γ-3, which are also expressed in pyramidal neurons (Lein et al., 2007; Tomita et al., 2003), are associated with the remaining AMPARs in γ-8 -/- neurons.

CHAPTER 4

Modeling TARP Regulation of AMPA Receptor Gating and Pharmacology

Over a decade of research on AMPAR structure and function has identified binding sites on AMPARs for agonists, antagonists, and allosteric modulators as well as key residues involved in aspects of AMPAR channel gating, with a primary focus on the structure of the isolated ligand-binding domain and heterologous expression of AMPARs. However, the recent discovery that AMPARs are accompanied in the synaptic membrane by TARPs has revealed that the kinetics and pharmacology of neuronal AMPARs differ in many respects from those predicted by classical studies of AMPARs in heterologous systems. Indeed, these effects of TARPs are what truly classify them as auxiliary subunits of AMPARs. Here I summarize recent findings concerning the effects of TARPs on AMPAR gating and pharmacology and construct mathematical and conceptual models to account for the varied functional effects of TARPs on native AMPARs. This work predicts that the changes in conformation that AMPARs undergo during synaptic transmission extend beyond their ligand-binding domains and channel pore, possibly involving rearrangements of structural elements on the cytoplasmic side of the receptors, contained within their auxiliary subunits.

Synaptic AMPAR Gating

When an AMPAR is challenged with a brief (1 ms) pulse of glutamate, the rise time of the resulting current reflects the binding of glutamate to the ligand-binding domains of the AMPAR, followed by a series of conformational changes that lead to opening of the ion channel pore. The current decay time reflects the opposite process, referred to as receptor deactivation, during which the ion channel closes, the receptor changes conformation, and glutamate unbinds (these gating processes are depicted diagrammatically in Figure 24 and example currents are shown in Figure 25). When the glutamate pulse is extended to 100 ms, the persistent rebinding of glutamate and reopening of the channel drives a separate process with a different time course, known as desensitization. While glutamate stays bound during desensitization, AMPARs enter a distinct closed-channel conformation known as the desensitized state (Figure 24). The relative contributions of deactivation and desensitization to the shape of synaptic currents varies across different synapses in the brain and depends on many factors, including the specific geometry of the synapse and the rate of clearance of glutamate by diffusion and active transport (Jonas, 2000). Figure 25 shows examples of outside-out patches from HEK cells expressing the AMPAR subunit GluA1 with and without TARPs in response to either 1 ms or 100 ms pulses of glutamate (data collected by postdoctoral fellow Dr. Wei Zhou). It is also apparent in Figure 25 that TARP subtypes γ-2 and γ-4 differentially modulate each of these parameters of AMPAR gating: activation, deactivation, and

desensitization, corroborating the results I obtained in cerebellar granule neurons analyzing the decay kinetics of AMPAR mEPSCs (Figures 8 and 13).

Modeling the Kinetic Regulation of AMPARs by TARPs

To gain insight into the mechanisms underlying TARP subtype-specific control of AMPAR channel kinetics, I employed a mathematical model. I modified a recently proposed kinetic scheme (Zhang et al., 2006) (depicted in Figure 26A) and used a least square error optimization algorithm to fit the kinetic data obtained from the GluA1 expression data described above (Figure 25). The following experimental observations placed limits on the model's transition rates: 1) TARPs increase agonist affinity, but do not appear to slow agonist unbinding (Turetsky et al., 2005); 2) TARPs increase the rate of recovery from desensitization (Priel et al., 2005; Turetsky et al., 2005); 3) TARPs increase channel opening probability during prolonged agonist application without changing open times (Tomita et al., 2005); and 4) TARPs slow current decay by increasing the relative contribution and time course of a slow component of decay (Zhang et al., 2006) (Chapter 2). The resulting simulated responses to 1 ms or 100 ms square pulses of 1 mM glutamate for GluA1 alone, GluA1 + γ-2, and GluA1 + γ-4 are shown in Figures 26B, 26C, and 26D. The fitted rate constants and calculated time constants of deactivation, desensitization, and rise are provided in Table 5. Comparison to the experimental data in Figure 25 shows that my model predicts well these features of AMPARs and their differential control by TARPs γ-2 and γ-4.

Figure 24. Structural Model of AMPAR Gating

Diagram depicts a simplified model of AMPAR gating. Two AMPAR subunits, each with a ligand-binding domain, and the interaction between the two subunits (dimer interface) are represented. Glutamate binding involves closure of the binding clefts, which places tension on the linker domains. Linker tension can be relieved either by entering an open channel conformation, or by breaking the dimer interface and entering a desensitized conformation.

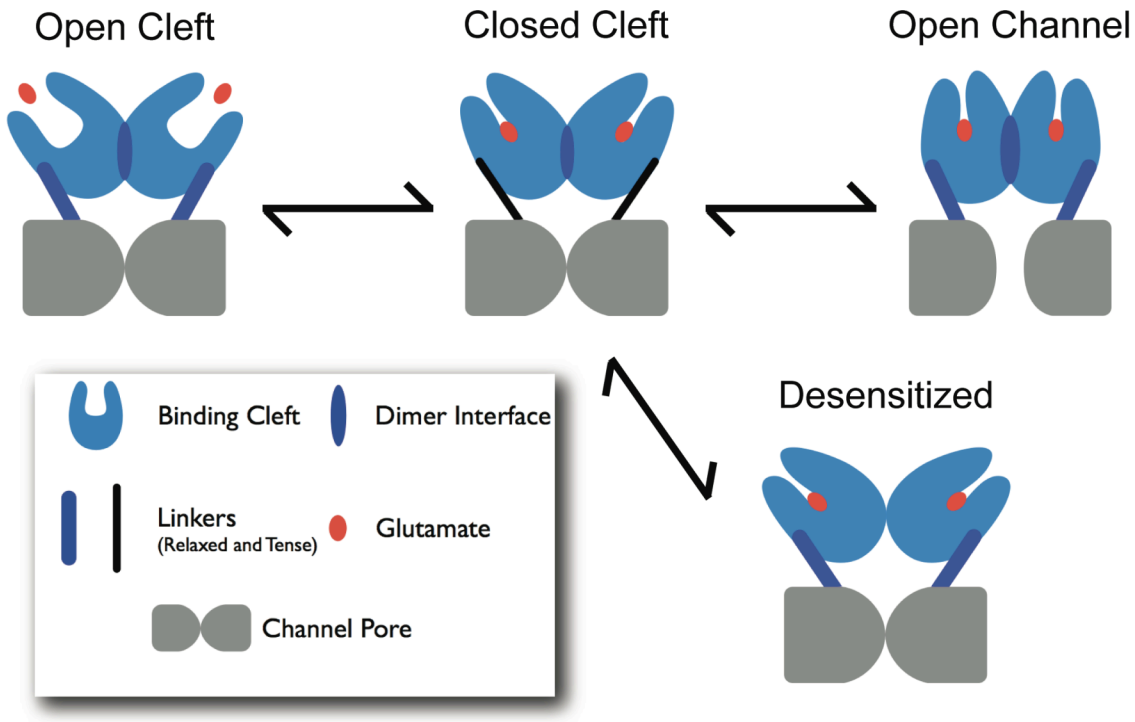
Open Cleft
Closed Cleft
Open Channel
Desensitized
Binding Cleft
Dimer Interface
Linkers
(Relaxed and Tense)
Glutamate
Channel Pore

Figure 25. TARP Subtypes Differentially Modulate AMPAR Activation, Deactivation, and Desensitization

(A-C) 1 mM glutamate was applied for either 1 ms (A and C) or 100 ms (B) to outside-out patches from HEK cells expressing GluA1 with or without TARPs γ-2 and γ-4. The resulting responses are normalized to the peak to illustrate differences in kinetics. Currents in (A) and (B) are aligned to the peak to show that TARPs γ-2 and γ-4 slow the time course of deactivation (A) and desensitization (B) of GluA1. Currents in (C) are aligned to the 10% rise point to show that TARP γ-4 but not γ-2 slows the activation time course of GluA1.

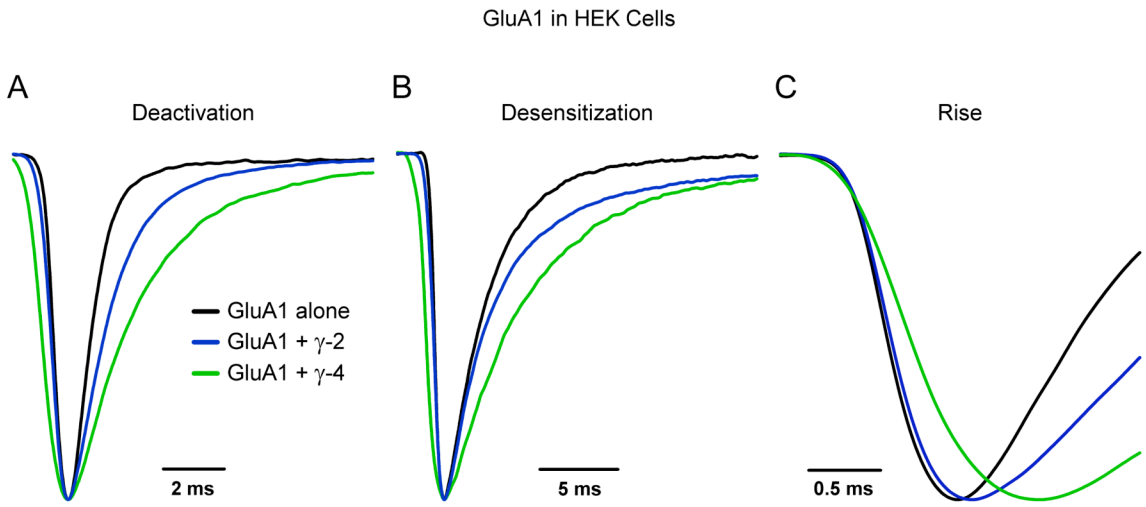
GluA1 in HEK Cells
A
Deactivation
B
Desensitization
C
Rise
GluA1 alone
GluA1 + γ-2
GluA1 + γ-4
2 ms
5 ms
0.5 ms

Figure 26. A Mathematical Model of TARP Control of AMPAR Gating

(A) Diagram illustrating the kinetic scheme used to model the response of AMPAR channels to brief pulses of glutamate.

(B) Simulated responses of GluA1 alone, GluA1 + γ-2 and GluA1 + γ-4 to a 1 ms square pulse of glutamate. Traces are scaled and aligned to the peak to illustrate the time course of deactivation.

(C) Simulated responses of GluA1 alone, GluA1 + γ-2 and GluA1 + γ-4 to a 100 ms square pulse of glutamate. Traces are scaled and aligned to the peak to illustrate the time course of desensitization.

(D) Simulated responses of GluA1 alone, GluA1 + γ-2 and GluA1 + γ-4 to a 1 ms square pulse of glutamate from (B) are aligned to the 10% rise point to illustrate the time course of activation.

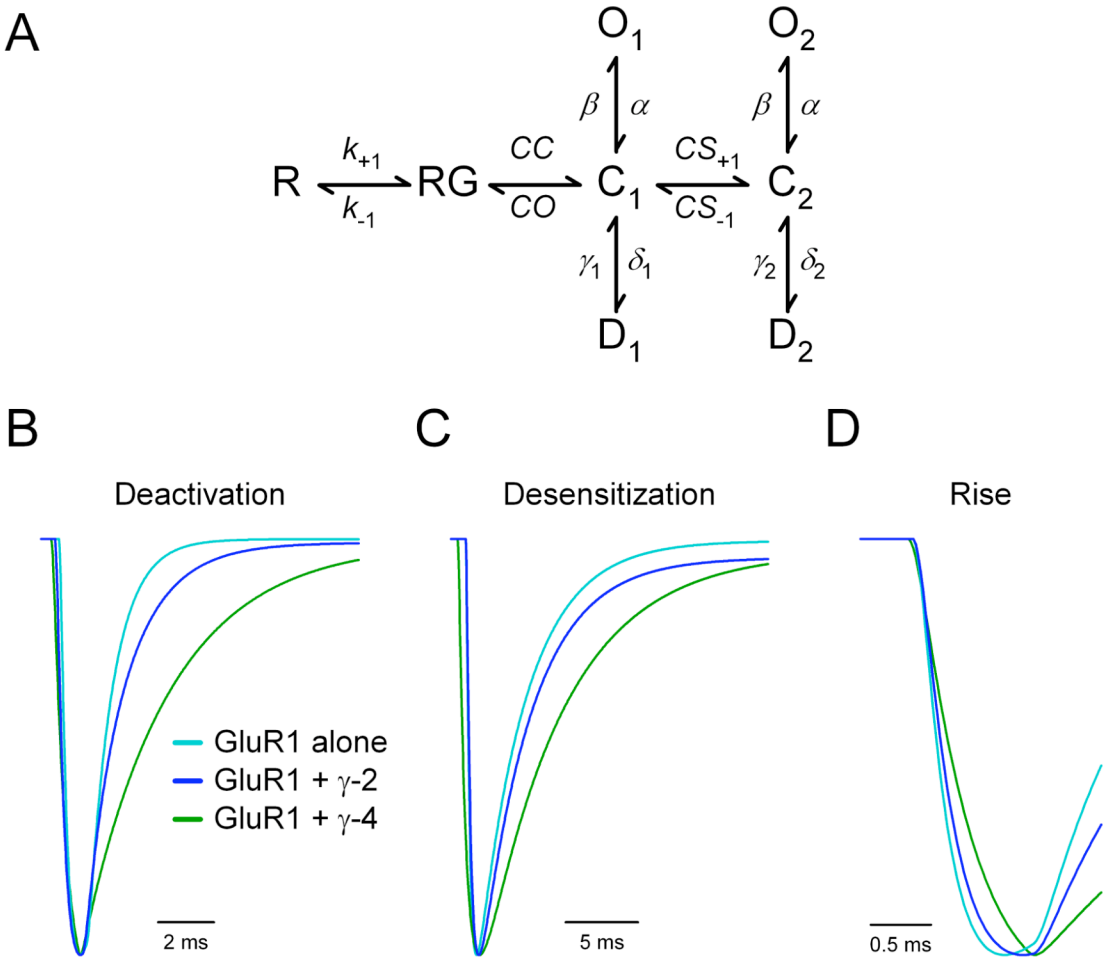
A
O1
O2
β
α
β
α
R
k+1
k-1
RG
CC
CO
C1
CS+1
CS-1
C2
γ1
δ1
γ2
δ2
D1
D2
B
Deactivation
C
Desensitization
D
Rise
GluR1 alone
GluR1 + γ-2
GluR1 + γ-4
2 ms
5 ms
0.5 ms

Table 5. Parameters for Kinetic Model of Regulation of AMPARs by TARPs

The rate constants refer to the model depicted in Figure 26A. When values are omitted in the table, the corresponding value for GluA1 alone was used. $\tau_{deactivation}$ and $\tau_{desensitization}$ were calculated from the simulated current traces shown in Figures 26B and 26C by measuring the area under the peak-normalized curve (see Methods), and τ_{rise} was calculated by measuring the 20%-80% rise time of the simulated traces shown in Figure 26D.

Table 5. Parameters for Kinetic Model of Regulation of AMPARs by TARPs			
	GluA1 alone	GluA1 + γ-2	GluA1 + γ-4
α	6000 s^{-1}		
β	10000 s^{-1}		
k_{+1}	1x10^7 $M^{-1}s^{-1}$		
k_{-1}	5x10^4 s^{-1}		
CC	36500 s^{-1}	25000 s^{-1}	12500 s^{-1}
CO	4550 s^{-1}	2500 s^{-1}	1750 s^{-1}
CS_{+1}	300 s^{-1}	1000 s^{-1}	10000 s^{-1}
CS_{-1}	10000 s^{-1}	3400 s^{-1}	4200 s^{-1}
δ_1	1100 s^{-1}		
γ_1	1 s^{-1}	10 s^{-1}	
δ_2	300 s^{-1}		
γ_2	10 s^{-1}		
$\tau_{deactivation}$	1.15 ms	1.73 ms	3.31 ms
$\tau_{desensitization}$	3.77 ms	6.37 ms	7.71 ms
τ_{rise}	0.26 ms	0.30 ms	0.46 ms

As shown in Figure 26A, before the glutamate-bound receptor, RG, can open, a structural rearrangement of the ligand-binding domain must occur. This "cleft closure" step allows the receptor to "trap" glutamate in a state from which it cannot readily unbind, denoted C_1. Both channel opening and desensitization can occur from this "closed cleft" conformation. To account for the multiple exponential components of decay exhibited by AMPARs when associated with TARPs, this model also includes a second closed state C_2 that results from a presumed conformational shift from C_1. The parameters that result from fitting this model to the data (Table 5) indicate that the primary effect of TARP association is to stabilize the closed-bound conformations C_1 and C_2 by altering the rates in and out of these states. While the closed conformation C_2 is extremely unstable (fast CS_{-1}) and rarely populated (slow CS_{+1}) in the absence of TARPs, association with TARPs stabilizes this conformation of the receptor (decreases CS_{-1}) and increases its relative occupancy (increases CS_{+1}). Accordingly, γ-4 effects these changes to a greater degree than γ-2, which corresponds to their relative difference in slowing AMPAR decay (compare Figures 25 and 26). Furthermore, these simple rate changes also fully account for the effect of γ-4 on AMPAR activation (compare Figures 25C and 26D). By increasing the number of channels that sequentially pass through the closed states C_1 and C_2 before opening, γ-4 prolongs the latency before channels open after binding glutamate, which slows the time to peak response. Although a previous study suggested that a simple increase in the channel opening rate, β, could fully account for the effects of TARPs on AMPAR kinetics (Tomita et al.,

2005), within the current framework, increasing β leads to a speeding of activation kinetics. However, it is important to note that stabilizing the closed state C_2 does increase the probability of opening at steady-state since β is large compared to the other rates away from this state. A simple decrease in the unbinding rate of glutamate, k_{-1}, was also not sufficient to account for the data.

Native AMPAR Pharmacology

Partial Agonist: Kainate

In heterologous systems, AMPARs respond to glutamate with large peak currents and small steady-state currents due to rapid and almost complete desensitization. They also respond to a structurally related compound, kainate, with small non-desensitizing currents (Koike et al., 2000; Partin et al., 1993). TARP association with AMPARs, in expression systems and natively in neurons, increases the efficacy of kainate, resulting in non-desensitizing currents that are similar in amplitude to peak glutamate currents (Patneau and Mayer, 1991; Tomita et al., 2005; Turetsky et al., 2005). This is demonstrated in Figure 27A, which compares the responses of GluA1 in HEK cells to local application of glutamate and kainate with and without TARP γ-2 (Patneau and Mayer, 1991). The effect of TARPs on kainate efficacy manifests both as an increased apparent affinity and an increased maximal response to saturating doses of kainate (Kott et al., 2007; Turetsky et al., 2005) (Figure 9).

Figure 27. TARP Modulation of Native AMPAR Pharmacology

(A) TARP γ-2 increases the efficacy of the partial agonist kainate (KA) on GluA1 expressed in HEK cells and reduces the amount of steady state desensitization induced by glutamate (Glu).

(B) In the presence of TARP γ-2, GluA1 expressed in HEK cells directly responds to the application of the competitive antagonist CNQX with an inward current, demonstrating that TARPs convert CNQX into a partial agonist of AMPARs.

(C) TARP γ-2 reduces voltage-dependent block of GluA4 by spermine in HEK cells.

(D) TARP γ-2 increases the efficacy of cyclothiazide on GluA1 *flip* and GluA1 *flop*, as evidenced by a leftward shift in the dose-response relationships of cyclothiazide on these receptors expressed in ooctyes. Panel (A) is reproduced, with permission, from Turetsky et al., 2005. Panel (B) is reproduced, with permission, from Menuz et al., 2007. Panel (C) is reproduced, with permission, from Soto et al., 2007. Panel (D) is reproduced, with permission, from Tomita et al., 2006.

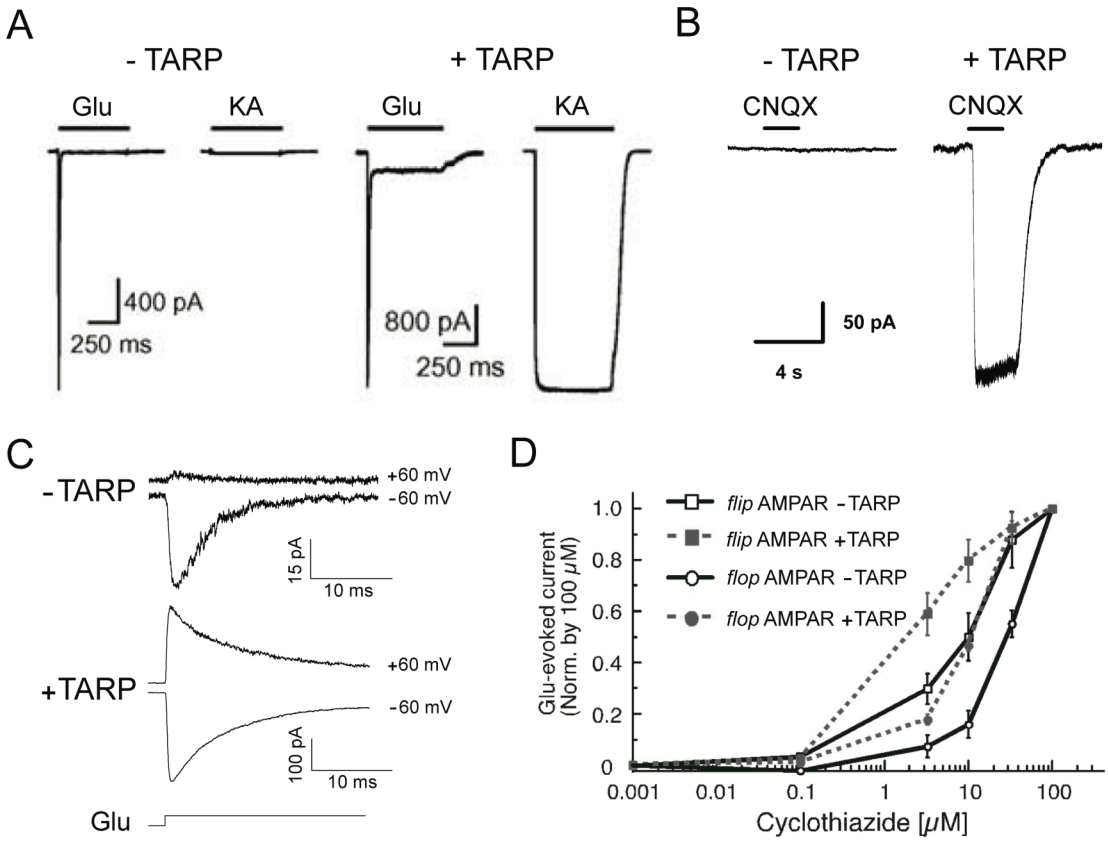
A
- TARP
+ TARP
Glu
KA
Glu
KA
400 pA
250 ms
800 pA
250 ms
B
- TARP
+ TARP
CNQX
CNQX
50 pA
4 s
C
-TARP
+60 mV
-60 mV
15 pA
10 ms
+TARP
+60 mV
-60 mV
100 pA
10 ms
Glu
D
flip AMPAR -TARP
flip AMPAR +TARP
flop AMPAR -TARP
flop AMPAR +TARP
Glu-evoked current
(Norm. by 100 μM)
1.0
0.8
0.6
0.4
0.2
0
0.001
0.01
0.1
1
10
100
Cyclothiazide [μM]

Competitive Antagonist: CNQX

Competitive antagonists, such as CNQX and NBQX, bind AMPARs with high affinity at the glutamate-binding site, thereby precluding their activation by glutamate. Thus, these drugs have been indispensable in elucidating the cell biology and pathophysiology of AMPARs (Bleakman and Lodge, 1998; Shepherd and Huganir, 2007). However, CNQX also has a paradoxical excitatory action on neurons that was presumed to be an off-target effect (Brickley et al., 2001). This discrepancy was resolved by the demonstration that CNQX directly activates AMPAR channels that are associated with TARPs (Menuz et al., 2007) (Figure 27B). Accordingly, CNQX application to brain slices depolarizes a variety of neuronal cell types, particularly when desensitization is pharmacologically inhibited (Menuz et al., 2007). This partial agonist activity of CNQX was not observed with the related compound NBQX, or the non-competitive antagonist GYKI 53655, which remain viable alternatives for chronic blockade of neuronal AMPARs.

Non-competitive Antagonist: Spermine

Neurons express endogenous polyamines such as spermine and spermidine that interact specifically with calcium-permeable AMPARs lacking the GluA2 subunit. These positively charged molecules block open AMPAR channels upon membrane depolarization, conferring inward rectification to the current-voltage relationship of GluA2-lacking AMPARs (Bowie and Mayer, 1995; Kamboj et al., 1995; Koh et al., 1995). Accordingly, measuring rectification of synaptic currents

in the presence of intracellular spermine has become a standard assay for the presence or absence of GluA2-lacking AMPARs in neurons (Hayashi et al., 2000; Isaac et al., 2007). However, recent work has shown that TARP association reduces AMPAR affinity for spermine such that GluA2-lacking AMPARs display only intermediate rather than complete rectification (Cho et al., 2007; Soto et al., 2007; Turetsky et al., 2005) (Figure 27C). This effect is particularly surprising given that TARPs are known to increase the frequency of AMPAR channel openings (Tomita et al., 2005), which would be expected to facilitate block of the open channel. One possible explanation, which I discuss in detail in the next section, is that TARPs disrupt the binding site for spermine by altering the shape of the AMPAR pore itself (Figure 28D).

Allosteric Modulator: Cyclothiazide

As inhibitors of AMPAR desensitization, benzothiadiazines like cyclothiazide and trichloromethiazide are often used to increase steady-state currents in order to facilitate detection of surface AMPARs, measure rectification (see above), or determine the efficacy of novel AMPAR antagonists (Nilsen and England, 2007; Partin et al., 1993; Tomita et al., 2005). Research into the mechanism of action of cyclothiazide has also provided valuable insight into AMPAR structure and function. Cyclothiazide binds AMPARs within an extracellular domain that is regulated by splice variation known as the *flip/flop* cassette (Partin et al., 1995; Sommer et al., 1990; Sun et al., 2002). That *flip* AMPARs desensitize more slowly than *flop* AMPARs immediately suggests a direct role for this domain in

the mechanism of AMPAR desensitization (Koike et al., 2000; Mosbacher et al., 1994; Quirk et al., 2004). Indeed, structural studies have shown that residues contained in the *flip/flop* splice cassette participate in an unstable protein-protein interaction between the ligand-binding domains of adjacent AMPAR subunits (Horning and Mayer, 2004; Sun et al., 2002). During desensitization, AMPARs undergo a conformational change that disrupts this “dimer interface” between AMPAR subunits, decoupling ligand binding from channel opening (Armstrong et al., 2006; Sun et al., 2002) (Figure 24). By interacting at this bridge between AMPAR subunits, cyclothiazide prevents the conformational change required for desensitization (Jin et al., 2005; Sun et al., 2002).

Might TARPs also modulate AMPAR gating by influencing the stability of the dimer interface? This was addressed by taking advantage of the fact that benzothiadiazine binding depends on the intact dimer interface to infer information about the conformation of AMPARs associated with TARPs (Turetsky et al., 2005). TARPs speed the association rate of trichloromethiazide with AMPARs, suggesting that TARPs increase the time AMPARs spend in the non-desensitized conformation. TARPs do not appear to alter the affinity of AMPARs for benzothiadiazines because the dissociation rate of trichloromethiazide does not change (Turetsky et al., 2005). However, TARPs do alter the efficacy of benzothiadiazines, causing a leftward shift in the dose-response relationship for cyclothiazide on AMPARs (Tomita et al., 2006) (Figure 27D). Also, while cyclothiazide is more effective at modulating *flip* AMPARs than *flop* AMPARs (Partin et al., 1994), TARPs substantially increase the potency of cyclothiazide

on *flop* receptors (Tomita et al., 2006). These data demonstrate that, although both TARPs and benzothiadiazines stabilize the non-desensitized state of the AMPAR, TARPs also facilitate that stabilizing action of benzothiadiazines. While it is clear that the influence of TARPs on AMPAR gating depends largely on a TARP extracellular domain (Tomita et al., 2005; Turetsky et al., 2005) (Chapter 2), it is unknown whether that domain interacts directly with the dimer interface (depicted in Figure 28C), or other structural elements of the AMPAR (Figures 28A, 28B, and 28D). Furthermore, whether TARPs act solely by influencing the stability of pre-existing receptor conformations, by fundamentally altering those conformations, or even by forming new conformations, will undoubtedly require high-resolution structural data.

Beyond the Ligand-Binding Domain

Structural and functional studies of AMPARs have shown that ligand binding involves closure of a clamshell-like binding cleft, which exerts tension on the linker domains that connect the binding cleft to the AMPAR pore. This tension can be relieved either by channel opening or by desensitization (see above) (Figure 24) (Armstrong and Gouaux, 2000; Armstrong et al., 2006; Horning and Mayer, 2004; Sun et al., 2002). The degree of cleft closure induced by various ligands corresponds to their relative efficacies, providing a structural basis for partial agonism by kainate and competitive antagonism by DNQX (Armstrong and Gouaux, 2000; Jin et al., 2003). Indeed, recent evidence suggests that the

stability of the closed-cleft conformation is a critical determinant of AMPAR kinetics and agonist efficacy (Robert et al., 2005; Zhang et al., 2008).

One possibility is that TARPs influence AMPAR gating by increasing the amount of cleft closure induced by ligand binding (Figure 28A). The increased tension this would place on the linker domains could well account for the increased efficacy of kainate and partial agonism by CNQX. However, while CNQX does not induce current through AMPARs in the absence of TARPs (Figure 27B), CNQX does induce significant cleft closure in crystals of the isolated AMPAR ligand-binding domain (Menuz et al., 2007). While it cannot be ruled out that TARP association further increases cleft closure, another possibility is that TARPs facilitate the translation of partial cleft closure into channel opening by interacting directly with the linker domains (Figure 28B). Consistent with this model, mutation or transplantation of AMPAR linker domains profoundly alters AMPAR gating and renders CNQX a partial agonist, similarly to TARP association (Klein and Howe, 2004; Schmid et al., 2007; Taverna et al., 2000; Yelshansky et al., 2004). Furthermore, mutation of a transmembrane residue immediately adjacent to a linker domain (known as the lurcher mutation) abolishes the influence of TARPs on both AMPAR gating and trafficking (Tomita et al., 2007).

Interestingly, when AMPAR complexes are purified and imaged by single-particle electron microscopy, the most evident contribution by TARPs to AMPAR structure is not extracellular, but rather transmembrane (Nakagawa et al., 2005). Whether or not TARP transmembrane residues directly contribute to the inner

lining of the AMPAR pore has not been determined. However, that TARPs disrupt the polyamine-binding site inside the AMPAR pore suggests that TARPs at least indirectly alter its conformation (Figure 28D). Further supporting this possibility, TARPs increase the average single-channel conductance of AMPARs (Soto et al., 2007; Tomita et al., 2005). Finally, the data presented in Chapter 2 of this thesis demonstrates that TARP intracellular domains also contribute to the functional modulation of AMPAR channels, highlighting the insufficiency of gating models that focus entirely on the AMPAR ligand-binding domain. The structural models presented here are not necessarily mutually exclusive, and it is likely that some combination of these possible mechanisms underlie the varied influences of TARPs on AMPAR gating.

Figure 28. Structural Models of TARP Control of AMPAR Gating

(A) Increased cleft closure model: diagram depicts TARP extracellular domains interacting directly with the AMPAR ligand-binding clefts, increasing the degree of cleft closure to account for the partial agonist activity of CNQX.

(B) Linker association model: diagram depicts TARP extracellular domains interacting directly with the AMPAR linker domains, facilitating the translation of partial cleft closure into channel opening to account for the partial agonist activity of CNQX.

(C) Dimer interface stabilization model: diagram depicts TARP extracellular domains interacting directly with the AMPAR dimer interface to account for increased stability of the nondesensitized conformation and increased benzothiadiazine efficacy.

(D) Altered pore conformation model: diagram depicts TARP transmembrane domains directly contributing to the shape of the AMPAR pore to account for reduced spermine affinity.

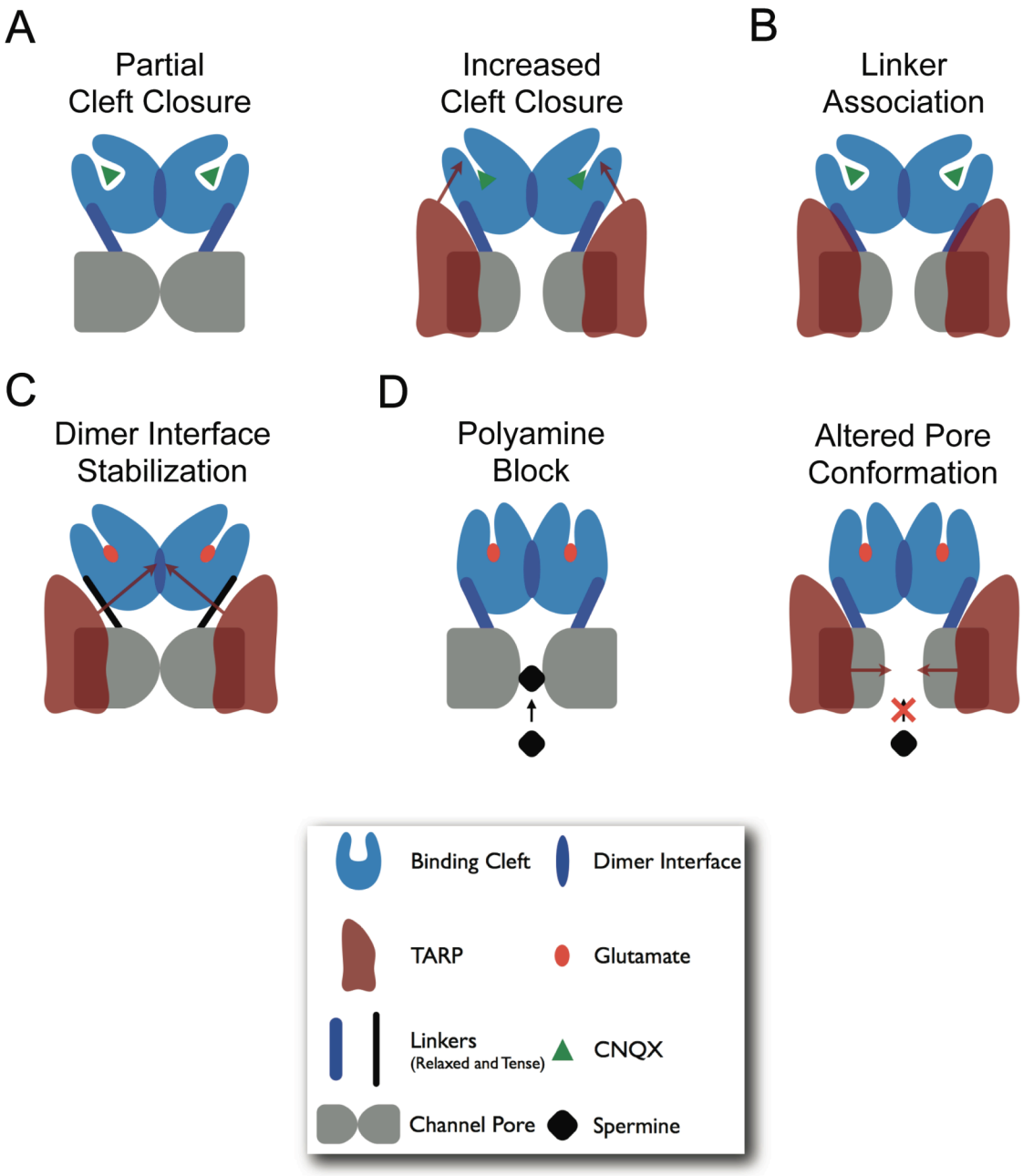
A
Partial
Cleft Closure
Increased
Cleft Closure
B
Linker
Association
C
Dimer Interface
Stabilization
D
Polyamine
Block
Altered Pore
Conformation
Binding Cleft
Dimer Interface
TARP
Glutamate
Linkers
(Relaxed and Tense)
CNQX
Channel Pore
Spermine

CHAPTER 5

Conclusions and Remaining Questions

In this thesis I demonstrate a striking diversity in the regulation of the biophysical properties of AMPARs by TARP auxiliary subunits. I discover unexpected differences in the control of AMPAR activation, deactivation and desensitization by TARP subtypes that were not predicted by previous analyses of steady-state currents in response to prolonged exposure to agonists (Kott et al., 2007; Tomita et al., 2005). I also provide the first demonstration that while all TARP subtypes are sufficient to traffic AMPARs to synapses, their differential regulation of AMPAR trafficking and gating results in remarkable diversity in the shape and size of synaptic responses. I also record AMPAR mEPSCs from a γ-4 knockout mouse to show that developmental regulation of TARP subtype expression contributes to the endogenous kinetics of synaptic AMPARs.

What is the functional relevance of TARP subtype-specific control of AMPAR gating to synaptic transmission? By slowing both the rise and decay phases of AMPAR EPSCs, TARPs maximize the total charge transfer through postsynaptic AMPARs in response to single vesicles of transmitter. These effects were most pronounced for TARP γ-4. Given that this isoform is widely expressed in brain during early development, γ-4 could play a role in the initial formation of synapses, possibly by providing neurons with a highly sensitive reporter of presynaptically released glutamate. However, as neurons mature, recruiting TARP/AMPAR complexes with faster decay kinetics to synapses may allow for

the temporal precision required for neuronal circuit function (Hausser and Clark, 1997). Furthermore, the slow component of decay imparted to AMPARs by TARPs will likely influence the activation of synaptic NMDARs, which depends on local depolarization of the synaptic membrane (Kampa et al., 2004). In this manner, TARP subtypes could potentially influence the degree to which individual synapses can undergo activity-dependent changes in synaptic strength.

The effect of some TARP subtypes on the activation kinetics of AMPARs is unexpected. While a relationship between agonist affinity and rise time is established for NMDA receptors (Lester and Jahr, 1992; Pan et al., 1993), the kinetics of AMPAR activation have received relatively little consideration (but see Clements et al., 1998) due to two confounds: 1) AMPAR activation occurs rapidly, on the same time-scale as solution exchange in fast-application experiments (hundreds of microseconds); and 2) the rise times of mEPSCs recorded at the cell body from neurons with extensive dendrites vary considerably depending on the distance of the activated synapse from the cell body (Magee and Cook, 2000). In that sense, recordings of mEPSCs from cultured cerebellar granule neurons, which have extremely short, electrotonically compact dendrites (Cathala et al., 2005; Silver et al., 1996) provide an ideal model system to detect changes in AMPAR activation kinetics. The observation that TARPs γ-4 and γ-8 slow AMPAR rise times constrained the kinetic model of AMPAR gating presented in Chapter 4, allowing me to infer valuable information

about how TARPs influence the changes in AMPAR conformation that underlie synaptic transmission.

What processes underlie the complex kinetics of AMPARs and their regulation by TARP auxiliary subunits? Structural studies suggest that interactions between adjacent subunits within an AMPAR complex participate in conformational changes that follow agonist binding but precede channel opening (Hansen et al., 2007; Horning and Mayer, 2004; Sun et al., 2002). Accordingly, agonists of varying chemical structure differ in their ability to induce such changes in conformation (Armstrong and Gouaux, 2000). The kinetic model that I extend in Chapter 4 was proposed by Zhang et al. to explain the behavior of four AMPAR agonists of varying affinity that produce profound differences in kinetics (Zhang et al., 2006). This model predicts that differences in the relative stabilities of multiple closed ligand-bound conformations of the receptor produce differences in affinity as well as deactivation and desensitization. Here I demonstrate that these same effects of TARPs on AMPAR gating, as well as the additional effects of slowing activation and speeding recovery from desensitization, are also well accounted for by changes in the rate constants between closed ligand-bound states of the receptor. As with any simple model, mine does not quantitatively describe certain aspects of AMPAR function, and other sets of rate constants could likely fit the data. Ultimately, accounting for multiple glutamate binding sites and multiple open states with varying conductance is needed to fully describe AMPAR single channel activity and the time course of recovery from desensitization (Robert et al., 2005; Robert and

Howe, 2003). Nevertheless, modeling provides a framework to understand how TARPs can allosterically modulate diverse properties of AMPARs.

My experiments in cerebellar granule neurons revealed that neurons expressing low levels of TARPs display mEPSCs with a rapid time course, and neurons expressing saturating levels of TARPs exhibit mEPSCs that decay with a pronounced slow component. This is the first indication that multiple TARP molecules can bind individual AMPAR channels, and that the stoichiometry of the association between TARPs and AMPARs is variable depending on their relative expression levels. Further experiments in HEK cells with AMPAR-TARP fusion proteins demonstrate that at most four TARPs can interact with individual AMPARs. Comparison to data from hippocampal neurons shows that the TARP/AMPAR stoichiometry of native receptors varies by neuronal cell type. While minimal TARP binding appears sufficient to traffic AMPARs to the surface and to the synapse, incorporation of additional TARPs progressively increases agonist affinity and current decay. Interestingly, studies of other ion channels have shown that auxiliary subunits can regulate trafficking and gating separately and with differing dose-dependencies (Canti et al., 2001; Wang et al., 2002). Whether modulation of TARP expression level is a mechanism whereby neurons can acutely regulate synaptic transmission is unknown. However, it has been shown in a number of brain areas that the kinetics of AMPAR EPSCs undergo changes during postnatal development (Takahashi, 2005). Whereas this may reflect diverse mechanisms, ranging from changes in AMPAR subunit composition to changes in the time course of glutamate in the synaptic cleft

(Cathala et al., 2005; Wall et al., 2002), my data suggest that changes in TARP subtype and TARP expression level could also contribute.

Taken together, the results presented here provide a clear demonstration that the TARP family of AMPAR auxiliary subunits confers a remarkable heterogeneity to the channel behavior of native AMPARs. Given that TARP subtypes are differentially expressed throughout the CNS, these functional differences between TARP subtypes will contribute to the known diversity of synaptic AMPAR properties seen in distinct neuronal populations. Interestingly, recent studies have begun to uncover unexpected heterogeneity and synapse-specificity in the localization of the PSD-MAGUK proteins that cluster TARP/AMPAR complexes at synapses through a PDZ interaction (Bats et al., 2007; Beique et al., 2006; Chen et al., 2000; Elias et al., 2006; Schnell et al., 2002). Furthermore, AMPAR subtypes are differentially expressed along the proximal-distal axis of neuronal dendrites (Andrasfalvy et al., 2003; Magee and Cook, 2000). It will be of interest to determine if a similar subcellular specificity is displayed in the localization of individual TARP subtypes within neurons that express multiple TARP isoforms.

METHODS

Molecular Biology

cDNAs encoding rat γ-2, γ-3, γ-4 and γ-8 used in previous studies (Rouach et al., 2005; Tomita et al., 2003) were subcloned by PCR into the EcoR1 and Sal1 restriction sites of the vector pIR2-EGFP (Clontech) to allow for the coexpression of untagged TARP protein and EGFP via an internal ribosome entry site (IRES) under the control of a strong CMV promoter. In order to normalize the expression levels of each TARP subtype, a Kozak translational start sequence was engineered before the start codon in the cDNAs encoding each TARP. TARP chimeras and truncation mutants were constructed using overlap extension PCR. Transfected cells were detected and selected for electrophysiological recording by EGFP fluorescence, which was equivalent for each TARP subtype expressed. No correlations were observed between apparent EGFP fluorescent intensity, whole-cell current amplitude, mEPSC amplitude, or mEPSC decay kinetics for any construct, suggesting that, under these conditions, ectopic TARP expression reflects saturation with respect to the low endogenous expression of AMPARs in cultured cerebellar granule neurons.

Cell Culture

Primary cultures of mouse cerebellar granule neurons were prepared from postnatal day 7 (P7) *stg*/*stg* mouse cerebella and plated at a density of 2.5 x 10^5 cells/cm^2 on glass coverslips precoated with poly-D-lysine in 24-well dishes (BD

Biosciences). Cultures were maintained in a BME-based medium containing 25 mM KCl, 10% FBS, 2 mM L-Glutamine, 2% B27 and 60 µg/mL gentamicin (all Invitrogen) until DIV3 (day in vitro) when the medium was replaced with an MEM-based medium (Invitrogen) containing 5 mM KCl and supplemented with 5 mg/mL D-glucose (Sigma), 2 mM L-glutamine (Invitrogen), 1% insulin-transferrin-sodium selenite (Sigma), 20 µg/mL gentamicin (Invitrogen), and 4 µM Cytosine β-D-arabinofuranoside hydrochloride (Sigma). Each coverslip was transfected with 1 µg cDNA on DIV4 by calcium phosphate, as described previously (Losi et al., 2003).

Electrophysiology

Whole-cell patch-clamp recordings from cultured cerebellar granule neurons were performed on DIV8-10 in an extracellular solution containing 145 mM NaCl, 5 mM KCl, 1 mM $CaCl_2$, 1 mM $MgCl_2$, 5 mM D-Glucose, 25 mM Sucrose, and 5 mM HEPES (all Sigma), pH 7.3. 100 µM picrotoxin (Sigma) and sometimes 10 µM gabazine (Ascent Scientific) were added to the extracellular solution to block GABAergic IPSCs, 0.5 mM TTX (Ascent Scientific, Tocris or Sigma) to prevent action potential-evoked EPSCs, and 100 mM D-APV (Tocris) to block NMDARs. Pipettes with resistances typically ~5-7 MΩ were filled with an internal solution containing 140 mM CsCl, 2 mM $MgCl_2$, 5 mM EGTA, 10 mM HEPES, 0.3 mM NaGTP, and 4 mM Na_2ATP (all Sigma), pH 7.3. Series resistances for these experiments were typically ~35 MΩ. Only recording epochs in which series and input resistances varied less than 10% were analyzed.

Recordings from striatal MSNs in acute coronal slices were performed with an external solution containing 119 mM NaCl, 2.5 mM KCl, 2.5 mM $CaCl_2$, 1.3 mM $MgSO_4$, 1 mM NaH_2PO_4, 26.2 mM $NaHCO_3$, and 11 mM D-glucose (all Sigma) with identical pharmacology as for cultured granule cells. Pipettes with resistances typically ~3-5 MΩ were filled with an internal solution containing 115 mM $CsMeSO_4$, 20 mM $CsCl_2$, 10 mM HEPES, 2.5 mM $MgCl_2$, 4 mM NaATP, 0.4 mM NaGTP, and mM 0.6 EGTA (all Sigma) (pH 7.2). Series resistances for these experiments were typically ~15-20 MΩ.

Recordings were collected using an Axopatch 1D amplifier (Axon Instruments), filtered at 2 kHz, digitized using hardware from National Instruments, sampled at 10 kHz, and analyzed online using custom software in Igor Pro (Wavemetrics).

For agonist application, either kainate (Ascent Scientific) or glutamate (Sigma) was dissolved in extracellular solution and applied via a local perfusion barrel using a system acquired from Automate Scientific. When TCM (500 μM; Sigma), CTZ (100 μM; Ascent Scientific), or PEPA (500 μM; Sigma) were included in the agonist solution to inhibit AMPAR desensitization, they were also added to the locally applied control solution and cells were pre-equilibrated for 1 min before agonist application. For antagonist application, either 1 mM γ-DGG (Tocris), 100 nM – 10 μM PhTx-433 (Chiralix), or 100 μM – 300 μM PhTx-74 (Tocris or Chiralix) was dissolved in agonist solution. mEPSCs were evoked by the local application of 200 mM – 250 mM sucrose (Sigma) dissolved in extracellular solution.

Data Analysis

Individual mEPSCs were detected automatically using custom software in Igor Pro (Wavemetrics) and then manually screened for events that did not contain "contaminating" noise or additional mEPSCs during the 60 ms after the peak, and analysis of mEPSC decay was limited to these "clean" events. To increase the number of mEPSCs recorded from individual neurons, hyperosmotic sucrose solution was locally applied for 10 seconds every 30 seconds. Under these conditions, each recording period contained epochs of both low and high spontaneous release rate, skewing the distribution of inter-event intervals and complicating quantification of mEPSC frequency. Nonetheless, order-of-magnitude differences in the number of mEPSCs detected per neuron were observed across some TARP constructs, and these differences were quantified simply by dividing the total number of mEPSCs detected for each neuron by the total length of the recording period. While all recorded neurons were included in this mEPSC frequency analysis, only neurons from which between 20 and 200 synaptic events were collected were included in the analyses of mEPSC amplitude and decay to avoid skewing the mean towards data collected from neurons that were incompletely sampled.

Average mEPSCs from granule cells expressing TARPs were well fit by a double exponential function with the form

$$I(t) = I_0 + A_{fast} e\left(\frac{t}{\tau_{fast}}\right) + A_{slow} e\left(\frac{t}{\tau_{slow}}\right),$$

whereas mEPSCs from striatal neurons were best fit by a single exponential function of similar form. Very low background noise was present in recordings from cultured granule cells, allowing exponential fits of average mEPSCs to be obtained without further filtering. However, recordings from striatal neurons from acute slices contained considerably more noise, so a binomial smoothing filter was applied to those average mEPSCs prior to analysis to improve the quality of exponential fits. To simplify the comparison of the multi-exponential mEPSC decay times recorded from granule cells, a single weighted decay parameter was calculated from the area under the peak-normalized current (Cathala et al., 2005), according to

$$\tau_{decay} = \frac{1}{I_{peak}} \int_{t_{peak}}^{t_0} I(t)dt ,$$

where t_0 was 60 ms after the peak of the mEPSC. mEPSC rise kinetics were calculated by measuring the 10%-90% rise time measured from individual mEPSCs.

Statistics

For comparisons of cumulative probability distributions, statistics were computed with a Kolmogorov-Smirnov test with a threshold of p=0.05. For comparisons of mean values across multiple conditions, statistics were computed first with a Kruskal-Wallis test with a threshold of p=0.05, and experiments containing significant differences were further evaluated using Wilcoxon posthoc tests

where the threshold α=0.05 was adjusted by dividing α by the number of pairwise comparisons. All data is reported as mean ± SEM.

Computer Modeling

The kinetic model of AMPAR gating presented here is based on a model proposed in a recent report (Zhang et al., 2006). The functions describing the model were implemented using SCoP, a software package by Simulation Resource, Inc. Initial parameters were based on those reported by (Zhang et al., 2006) for GluA2, with some modifications based on a similar model of GluA1 (Robert and Howe, 2003). A least-square optimization algorithm was then performed in SCoP to fit the various parameters to the deactivation and desensitization data obtained by my collaborator, Dr. Wei Zhou, from outside-out patch recordings containing GluA1 with or without TARPs γ-2 and γ-4 (Milstein et al., 2007).

References

Andrasfalvy, B.K., Smith, M.A., Borchardt, T., Sprengel, R., and Magee, J.C. (2003). Impaired regulation of synaptic strength in hippocampal neurons from GluR1-deficient mice. J Physiol *552*, 35-45.

Armstrong, N., and Gouaux, E. (2000). Mechanisms for activation and antagonism of an AMPA-sensitive glutamate receptor: crystal structures of the GluR2 ligand binding core. Neuron *28*, 165-181.

Armstrong, N., Jasti, J., Beich-Frandsen, M., and Gouaux, E. (2006). Measurement of conformational changes accompanying desensitization in an ionotropic glutamate receptor. Cell *127*, 85-97.

Barbour, B., and Hausser, M. (1997). Intersynaptic diffusion of neurotransmitter. Trends Neurosci *20*, 377-384.

Bats, C., Groc, L., and Choquet, D. (2007). The interaction between Stargazin and PSD-95 regulates AMPA receptor surface trafficking. Neuron *53*, 719-734.

Beique, J.C., Lin, D.T., Kang, M.G., Aizawa, H., Takamiya, K., and Huganir, R.L. (2006). Synapse-specific regulation of AMPA receptor function by PSD-95. Proc Natl Acad Sci U S A *103*, 19535-19540.

Bleakman, D., and Lodge, D. (1998). Neuropharmacology of AMPA and kainate receptors. Neuropharmacology *37*, 1187-1204.

Bowie, D., and Mayer, M.L. (1995). Inward rectification of both AMPA and kainate subtype glutamate receptors generated by polyamine-mediated ion channel block. Neuron *15*, 453-462.

Bredt, D.S., and Nicoll, R.A. (2003). AMPA receptor trafficking at excitatory synapses. Neuron *40*, 361-379.

Brickley, S.G., Farrant, M., Swanson, G.T., and Cull-Candy, S.G. (2001). CNQX increases GABA-mediated synaptic transmission in the cerebellum by an AMPA/kainate receptor-independent mechanism. Neuropharmacology *41*, 730-736.

Burnashev, N., Monyer, H., Seeburg, P.H., and Sakmann, B. (1992). Divalent ion permeability of AMPA receptor channels is dominated by the edited form of a single subunit. Neuron *8*, 189-198.

Canti, C., Davies, A., Berrow, N.S., Butcher, A.J., Page, K.M., and Dolphin, A.C. (2001). Evidence for two concentration-dependent processes for beta-subunit effects on alpha1B calcium channels. Biophys J *81*, 1439-1451.

Cathala, L., Holderith, N.B., Nusser, Z., DiGregorio, D.A., and Cull-Candy, S.G. (2005). Changes in synaptic structure underlie the developmental speeding of AMPA receptor-mediated EPSCs. Nat Neurosci *8*, 1310-1318.

Chen, L., Chetkovich, D.M., Petralia, R.S., Sweeney, N.T., Kawasaki, Y., Wenthold, R.J., Bredt, D.S., and Nicoll, R.A. (2000). Stargazin regulates synaptic targeting of AMPA receptors by two distinct mechanisms. Nature *408*, 936-943.

Cho, C.H., St-Gelais, F., Zhang, W., Tomita, S., and Howe, J.R. (2007). Two families of TARP isoforms that have distinct effects on the kinetic properties of AMPA receptors and synaptic currents. Neuron *55*, 890-904.

Clements, J.D. (1996). Transmitter timecourse in the synaptic cleft: its role in central synaptic function. Trends Neurosci *19*, 163-171.

Clements, J.D., Feltz, A., Sahara, Y., and Westbrook, G.L. (1998). Activation kinetics of AMPA receptor channels reveal the number of functional agonist binding sites. J Neurosci *18*, 119-127.

Coleman, S.K., Moykkynen, T., Cai, C., von Ossowski, L., Kuismanen, E., Korpi, E.R., and Keinanen, K. (2006). Isoform-specific early trafficking of AMPA receptor flip and flop variants. J Neurosci *26*, 11220-11229.

Diamond, J.S. (2001). Neuronal glutamate transporters limit activation of NMDA receptors by neurotransmitter spillover on CA1 pyramidal cells. J Neurosci *21*, 8328-8338.

Ehrlich, I., and Malinow, R. (2004). Postsynaptic density 95 controls AMPA receptor incorporation during long-term potentiation and experience-driven synaptic plasticity. J Neurosci *24*, 916-927.

Elias, G.M., Funke, L., Stein, V., Grant, S.G., Bredt, D.S., and Nicoll, R.A. (2006). Synapse-Specific and Developmentally Regulated Targeting of AMPA Receptors by a Family of MAGUK Scaffolding Proteins. Neuron *52*, 307-320.

Elias, G.M., and Nicoll, R.A. (2007). Synaptic trafficking of glutamate receptors by MAGUK scaffolding proteins. Trends Cell Biol *17*, 343-352.

Fukaya, M., Tsujita, M., Yamazaki, M., Kushiya, E., Abe, M., Akashi, K., Natsume, R., Kano, M., Kamiya, H., Watanabe, M., and Sakimura, K. (2006). Abundant distribution of TARP gamma-8 in synaptic and extrasynaptic surface of hippocampal neurons and its major role in AMPA receptor expression on spines and dendrites. Eur J Neurosci *24*, 2177-2190.

Fukaya, M., Yamazaki, M., Sakimura, K., and Watanabe, M. (2005). Spatial diversity in gene expression for VDCCgamma subunit family in developing and adult mouse brains. Neurosci Res.

Hansen, K.B., Yuan, H., and Traynelis, S.F. (2007). Structural aspects of AMPA receptor activation, desensitization and deactivation. Curr Opin Neurobiol.

Hashimoto, K., Fukaya, M., Qiao, X., Sakimura, K., Watanabe, M., and Kano, M. (1999). Impairment of AMPA receptor function in cerebellar granule cells of ataxic mutant mouse stargazer. J Neurosci *19*, 6027-6036.

Hausser, M., and Clark, B.A. (1997). Tonic synaptic inhibition modulates neuronal output pattern and spatiotemporal synaptic integration. Neuron *19*, 665-678.

Hayashi, Y., Shi, S.H., Esteban, J.A., Piccini, A., Poncer, J.C., and Malinow, R. (2000). Driving AMPA receptors into synapses by LTP and CaMKII: requirement for GluR1 and PDZ domain interaction. Science *287*, 2262-2267.

Hollmann, M., and Heinemann, S. (1994). Cloned glutamate receptors. Annu Rev Neurosci *17*, 31-108.

Horning, M.S., and Mayer, M.L. (2004). Regulation of AMPA receptor gating by ligand binding core dimers. Neuron *41*, 379-388.

Isaac, J.T., Ashby, M., and McBain, C.J. (2007). The role of the GluR2 subunit in AMPA receptor function and synaptic plasticity. Neuron *54*, 859-871.

Jin, R., Banke, T.G., Mayer, M.L., Traynelis, S.F., and Gouaux, E. (2003). Structural basis for partial agonist action at ionotropic glutamate receptors. Nat Neurosci *6*, 803-810.

Jin, R., Clark, S., Weeks, A.M., Dudman, J.T., Gouaux, E., and Partin, K.M. (2005). Mechanism of positive allosteric modulators acting on AMPA receptors. J Neurosci *25*, 9027-9036.

Jonas, P. (2000). The Time Course of Signaling at Central Glutamatergic Synapses. News Physiol Sci *15*, 83-89.

Kamboj, S.K., Swanson, G.T., and Cull-Candy, S.G. (1995). Intracellular spermine confers rectification on rat calcium-permeable AMPA and kainate receptors. J Physiol *486 (Pt 2)*, 297-303.

Kampa, B.M., Clements, J., Jonas, P., and Stuart, G.J. (2004). Kinetics of Mg2+ unblock of NMDA receptors: implications for spike-timing dependent synaptic plasticity. J Physiol *556*, 337-345.

Kato, A.S., Siuda, E.R., Nisenbaum, E.S., and Bredt, D.S. (2008). AMPA receptor subunit-specific regulation by a distinct family of type II TARPs. Neuron *59*, 986-996.

Kato, A.S., Zhou, W., Milstein, A.D., Knierman, M.D., Siuda, E.R., Dotzlaf, J.E., Yu, H., Hale, J.E., Nisenbaum, E.S., Nicoll, R.A., and Bredt, D.S. (2007). New transmembrane AMPA receptor regulatory protein isoform, gamma-7, differentially regulates AMPA receptors. J Neurosci *27*, 4969-4977.

Klein, R.M., and Howe, J.R. (2004). Effects of the lurcher mutation on GluR1 desensitization and activation kinetics. J Neurosci *24*, 4941-4951.

Koh, D.S., Burnashev, N., and Jonas, P. (1995). Block of native Ca(2+)-permeable AMPA receptors in rat brain by intracellular polyamines generates double rectification. J Physiol *486 (Pt 2)*, 305-312.

Koike, M., Tsukada, S., Tsuzuki, K., Kijima, H., and Ozawa, S. (2000). Regulation of kinetic properties of GluR2 AMPA receptor channels by alternative splicing. J Neurosci *20*, 2166-2174.

Kott, S., Werner, M., Korber, C., and Hollmann, M. (2007). Electrophysiological properties of AMPA receptors are differentially modulated depending on the associated member of the TARP family. J Neurosci *27*, 3780-3789.

Kullmann, D.M., Min, M.Y., Asztely, F., and Rusakov, D.A. (1999). Extracellular glutamate diffusion determines the occupancy of glutamate receptors at CA1 synapses in the hippocampus. Philos Trans R Soc Lond B Biol Sci *354*, 395-402.

Lein, E.S., Hawrylycz, M.J., Ao, N., Ayres, M., Bensinger, A., Bernard, A., Boe, A.F., Boguski, M.S., Brockway, K.S., Byrnes, E.J.*, et al.* (2007). Genome-wide atlas of gene expression in the adult mouse brain. Nature *445*, 168-176.

Lester, R.A., and Jahr, C.E. (1992). NMDA channel behavior depends on agonist affinity. J Neurosci *12*, 635-643.

Losi, G., Prybylowski, K., Fu, Z., Luo, J., Wenthold, R.J., and Vicini, S. (2003). PSD-95 regulates NMDA receptors in developing cerebellar granule neurons of the rat. J Physiol *548*, 21-29.

Lu, W., Shi, Y., Jackson, A.C., Bjorgan, K., During, M.J., Spregel, R., Seeburg, P.H., and Nicoll, R.A. (2009). Subunit composition of synaptic AMPA receptors revealed by a single cell genetic approach. Neuron, *in press*.

Magee, J.C., and Cook, E.P. (2000). Somatic EPSP amplitude is independent of synapse location in hippocampal pyramidal neurons. Nat Neurosci *3*, 895-903.

Malinow, R., and Malenka, R.C. (2002). AMPA receptor trafficking and synaptic plasticity. Annu Rev Neurosci *25*, 103-126.

Mansour, M., Nagarajan, N., Nehring, R.B., Clements, J.D., and Rosenmund, C. (2001). Heteromeric AMPA receptors assemble with a preferred subunit stoichiometry and spatial arrangement. Neuron *32*, 841-853.

Menuz, K., Stroud, R.M., Nicoll, R.A., and Hays, F.A. (2007). TARP auxiliary subunits switch AMPA receptor antagonists into partial agonists. Science *318*, 815-817.

Milstein, A.D., Zhou, W., Karimzadegan, S., Bredt, D.S., and Nicoll, R.A. (2007). TARP subtypes differentially and dose-dependently control synaptic AMPA receptor gating. Neuron *55*, 905-918.

Mosbacher, J., Schoepfer, R., Monyer, H., Burnashev, N., Seeburg, P.H., and Ruppersberg, J.P. (1994). A molecular determinant for submillisecond desensitization in glutamate receptors. Science *266*, 1059-1062.

Nakagawa, T., Cheng, Y., Ramm, E., Sheng, M., and Walz, T. (2005). Structure and different conformational states of native AMPA receptor complexes. Nature *433*, 545-549.

Nicoll, R.A., Tomita, S., and Bredt, D.S. (2006). Auxiliary subunits assist AMPA-type glutamate receptors. Science *311*, 1253-1256.

Nilsen, A., and England, P.M. (2007). A subtype-selective, use-dependent inhibitor of native AMPA receptors. J Am Chem Soc *129*, 4902-4903.

Osten, P., and Stern-Bach, Y. (2006). Learning from stargazin: the mouse, the phenotype and the unexpected. Curr Opin Neurobiol *16*, 275-280.

Overstreet, L.S., Kinney, G.A., Liu, Y.B., Billups, D., and Slater, N.T. (1999). Glutamate transporters contribute to the time course of synaptic transmission in cerebellar granule cells. J Neurosci *19*, 9663-9673.

Pan, Z.Z., Tong, G., and Jahr, C.E. (1993). A false transmitter at excitatory synapses. Neuron *11*, 85-91.

Partin, K.M., Bowie, D., and Mayer, M.L. (1995). Structural determinants of allosteric regulation in alternatively spliced AMPA receptors. Neuron *14*, 833-843.

Partin, K.M., Patneau, D.K., and Mayer, M.L. (1994). Cyclothiazide differentially modulates desensitization of alpha-amino-3-hydroxy-5-methyl-4-

isoxazolepropionic acid receptor splice variants. Mol Pharmacol *46*, 129-138.

Partin, K.M., Patneau, D.K., Winters, C.A., Mayer, M.L., and Buonanno, A. (1993). Selective modulation of desensitization at AMPA versus kainate receptors by cyclothiazide and concanavalin A. Neuron *11*, 1069-1082.

Patneau, D.K., and Mayer, M.L. (1991). Kinetic analysis of interactions between kainate and AMPA: evidence for activation of a single receptor in mouse hippocampal neurons. Neuron *6*, 785-798.

Priel, A., Kolleker, A., Ayalon, G., Gillor, M., Osten, P., and Stern-Bach, Y. (2005). Stargazin reduces desensitization and slows deactivation of the AMPA-type glutamate receptors. J Neurosci *25*, 2682-2686.

Quirk, J.C., Siuda, E.R., and Nisenbaum, E.S. (2004). Molecular determinants responsible for differences in desensitization kinetics of AMPA receptor splice variants. J Neurosci *24*, 11416-11420.

Robert, A., Armstrong, N., Gouaux, J.E., and Howe, J.R. (2005). AMPA receptor binding cleft mutations that alter affinity, efficacy, and recovery from desensitization. J Neurosci *25*, 3752-3762.

Robert, A., and Howe, J.R. (2003). How AMPA receptor desensitization depends on receptor occupancy. J Neurosci *23*, 847-858.

Rouach, N., Byrd, K., Petralia, R.S., Elias, G.M., Adesnik, H., Tomita, S., Karimzadegan, S., Kealey, C., Bredt, D.S., and Nicoll, R.A. (2005). TARP gamma-8 controls hippocampal AMPA receptor number, distribution and synaptic plasticity. Nat Neurosci *8*, 1525-1533.

Sargent, P.B., Saviane, C., Nielsen, T.A., DiGregorio, D.A., and Silver, R.A. (2005). Rapid vesicular release, quantal variability, and spillover contribute to the precision and reliability of transmission at a glomerular synapse. J Neurosci *25*, 8173-8187.

Schmid, S.M., Korber, C., Herrmann, S., Werner, M., and Hollmann, M. (2007). A domain linking the AMPA receptor agonist binding site to the ion pore controls gating and causes lurcher properties when mutated. J Neurosci *27*, 12230-12241.

Schnell, E., Sizemore, M., Karimzadegan, S., Chen, L., Bredt, D.S., and Nicoll, R.A. (2002). Direct interactions between PSD-95 and stargazin control synaptic AMPA receptor number. Proc Natl Acad Sci U S A *99*, 13902-13907.

Sekiguchi, M., Takeo, J., Harada, T., Morimoto, T., Kudo, Y., Yamashita, S., Kohsaka, S., and Wada, K. (1998). Pharmacological detection of AMPA receptor heterogeneity by use of two allosteric potentiators in rat hippocampal cultures. Br J Pharmacol *123*, 1294-1303.

Sheng, M., and Kim, M.J. (2002). Postsynaptic signaling and plasticity mechanisms. Science *298*, 776-780.

Shepherd, J.D., and Huganir, R.L. (2007). The cell biology of synaptic plasticity: AMPA receptor trafficking. Annu Rev Cell Dev Biol *23*, 613-643.

Shi, Y., Lu, W., Milstein, A.D., and Nicoll, R.A. (2009). The Stoichiometry of AMPA Receptors and TARPs Varies by Neuronal Cell Type. Neuron (submitted).

Silver, R.A., Colquhoun, D., Cull-Candy, S.G., and Edmonds, B. (1996). Deactivation and desensitization of non-NMDA receptors in patches and the time course of EPSCs in rat cerebellar granule cells. J Physiol *493 (Pt 1)*, 167-173.

Sommer, B., Keinanen, K., Verdoorn, T.A., Wisden, W., Burnashev, N., Herb, A., Kohler, M., Takagi, T., Sakmann, B., and Seeburg, P.H. (1990). Flip and flop: a cell-specific functional switch in glutamate-operated channels of the CNS. Science *249*, 1580-1585.

Soto, D., Coombs, I.D., Kelly, L., Farrant, M., and Cull-Candy, S.G. (2007). Stargazin attenuates intracellular polyamine block of calcium-permeable AMPA receptors. Nat Neurosci *10*, 1260-1267.

Soto, D., Coombs, I.D., Renzi, M., Zonouzi, M., Farrant, M., and Cull-Candy, S.G. (2009). Selective regulation of long-form calcium-permeable AMPA receptors by an atypical TARP, gamma-5. Nat Neurosci *12*, 277-285.

Stein, V., House, D.R., Bredt, D.S., and Nicoll, R.A. (2003). Postsynaptic density-95 mimics and occludes hippocampal long-term potentiation and enhances long-term depression. J Neurosci *23*, 5503-5506.

Sun, Y., Olson, R., Horning, M., Armstrong, N., Mayer, M., and Gouaux, E. (2002). Mechanism of glutamate receptor desensitization. Nature *417*, 245-253.

Swanson, G.T., Kamboj, S.K., and Cull-Candy, S.G. (1997). Single-channel properties of recombinant AMPA receptors depend on RNA editing, splice variation, and subunit composition. J Neurosci *17*, 58-69.

Takahashi, T. (2005). Postsynaptic receptor mechanisms underlying developmental speeding of synaptic transmission. Neurosci Res *53*, 229-240.

Taverna, F., Xiong, Z.G., Brandes, L., Roder, J.C., Salter, M.W., and MacDonald, J.F. (2000). The Lurcher mutation of an alpha-amino-3-hydroxy-5-methyl-4-isoxazolepropionic acid receptor subunit enhances potency of glutamate and converts an antagonist to an agonist. J Biol Chem *275*, 8475-8479.

Tomita, S., Adesnik, H., Sekiguchi, M., Zhang, W., Wada, K., Howe, J.R., Nicoll, R.A., and Bredt, D.S. (2005). Stargazin modulates AMPA receptor gating and trafficking by distinct domains. Nature *435*, 1052-1058.

Tomita, S., Chen, L., Kawasaki, Y., Petralia, R.S., Wenthold, R.J., Nicoll, R.A., and Bredt, D.S. (2003). Functional studies and distribution define a family of transmembrane AMPA receptor regulatory proteins. J Cell Biol *161*, 805-816.

Tomita, S., Sekiguchi, M., Wada, K., Nicoll, R.A., and Bredt, D.S. (2006). Stargazin controls the pharmacology of AMPA receptor potentiators. Proc Natl Acad Sci U S A *103*, 10064-10067.

Tomita, S., Shenoy, A., Fukata, Y., Nicoll, R.A., and Bredt, D.S. (2007). Stargazin interacts functionally with the AMPA receptor glutamate-binding module. Neuropharmacology *52*, 87-91.

Turetsky, D., Garringer, E., and Patneau, D.K. (2005). Stargazin modulates native AMPA receptor functional properties by two distinct mechanisms. J Neurosci *25*, 7438-7448.

Vandenberghe, W., Nicoll, R.A., and Bredt, D.S. (2005). Interaction with the unfolded protein response reveals a role for stargazin in biosynthetic AMPA receptor transport. J Neurosci *25*, 1095-1102.

Wall, M.J., Robert, A., Howe, J.R., and Usowicz, M.M. (2002). The speeding of EPSC kinetics during maturation of a central synapse. Eur J Neurosci *15*, 785-797.

Wang, Y.W., Ding, J.P., Xia, X.M., and Lingle, C.J. (2002). Consequences of the stoichiometry of Slo1 alpha and auxiliary beta subunits on functional properties of large-conductance Ca2+-activated K+ channels. J Neurosci *22*, 1550-1561.

Washburn, M.S., Numberger, M., Zhang, S., and Dingledine, R. (1997). Differential dependence on GluR2 expression of three characteristic features of AMPA receptors. J Neurosci *17*, 9393-9406.

Xu-Friedman, M.A., and Regehr, W.G. (2003). Ultrastructural contributions to desensitization at cerebellar mossy fiber to granule cell synapses. J Neurosci *23*, 2182-2192.

Yelshansky, M.V., Sobolevsky, A.I., Jatzke, C., and Wollmuth, L.P. (2004). Block of AMPA receptor desensitization by a point mutation outside the ligand-binding domain. J Neurosci *24*, 4728-4736.

Zamanillo, D., Sprengel, R., Hvalby, O., Jensen, V., Burnashev, N., Rozov, A., Kaiser, K.M., Koster, H.J., Borchardt, T., Worley, P.*, et al.* (1999). Importance of AMPA receptors for hippocampal synaptic plasticity but not for spatial learning. Science *284*, 1805-1811.

Zhang, W., Cho, Y., Lolis, E., and Howe, J.R. (2008). Structural and single-channel results indicate that the rates of ligand binding domain closing and opening directly impact AMPA receptor gating. J Neurosci *28*, 932-943.

Zhang, W., Robert, A., Vogensen, S.B., and Howe, J.R. (2006). The relationship between agonist potency and AMPA receptor kinetics. Biophys J *91*, 1336-1346.

Ziff, E.B. (2007). TARPs and the AMPA Receptor Trafficking Paradox. Neuron *53*, 627-633.

Publishing Agreement

It is the policy of the University to encourage the distribution of all theses, dissertations, and manuscripts. Copies of all UCSF theses, dissertations, and manuscripts will be routed to the library via the Graduate Division. The library will make all theses, dissertations, and manuscripts accessible to the public and will preserve these to the best of their abilities, in perpetuity.

Please sign the following statement:

I hereby grant permission to the Graduate Division of the University of California, San Francisco to release copies of my thesis, dissertation, or manuscript to the Campus Library to provide access and preservation, in whole or in part, in perpetuity.

Author Signature

5/5/09

Date